REPORT ON THE
SPECTRAL IP TEST SURVEY
OVER THE
GRUM DEPOSIT LINE 108W
FARO, YUKON TERRITORY
FOR
CYRUS ANVIL MINES LTD.

VOL. I

-001967

TABLE OF CONTENTS

PHOENIX GEOPHYSICS LIMITED

REPORT ON THE SPECTRAL IP TEST SURVEY OVER THE GRUM DEPOSIT LINE 108W FARO, YUKON TERRITORY FOR CYPRUS-ANVIL MINES LTD.

1. INTRODUCTION

At the request of Dr. David Jennings, Chief Geologist for Cyprus-Anvil Mines Ltd., we have completed a brief Spectral IP Test Survey over the Grum Deposit. The Grum Deposit is a known orebody on the company's property at Faro, Yukon Territory. Spectral IP measurements were made on Line 108W using X = 500'; n = 1,2,3,4,5,6 and X = 1000'; n = 1,2,3,4,5,6.

As shown on the enclosed plan map, Line 108W crosses over the west end of the Grum Deposit. At this location, the depth to the top of the sulphide mineralization is almost three hundred meters. It is necessary to use large electrode intervals and electrode separations to detect a source at this depth. Inductive coupling effects can distort the measurements, but the use of the Spectral IP Method permits coupling effects to be removed.

2. PRESENTATION OF RESULTS

The apparent resistivity and the apparent phase IP results at 1.0 Hz

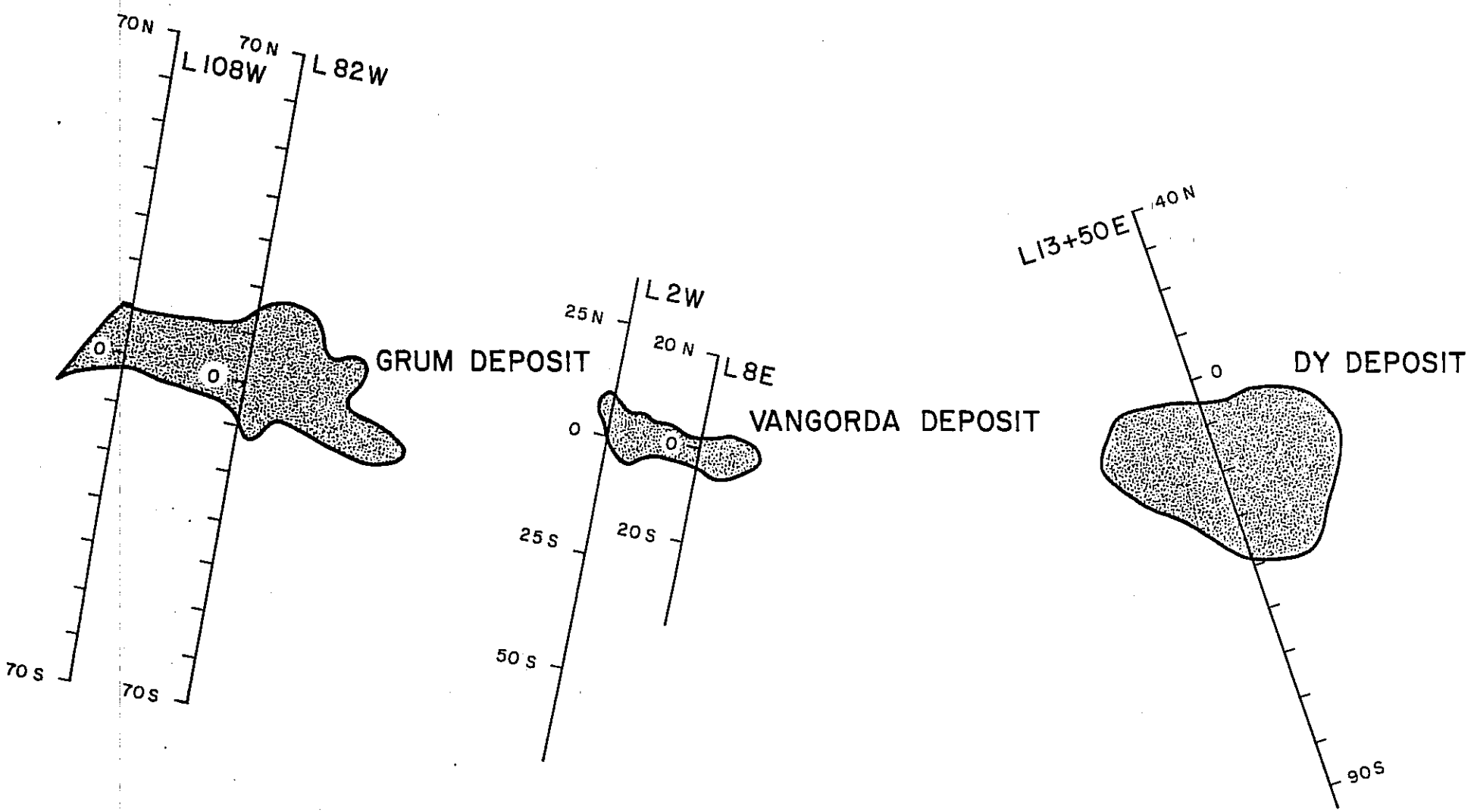

TEST LINE SURVEY POSITION

VANGORDA

Fig. – 1

are enclosed with this report. The field results have been plotted using the pseudosection format. A few of the complete spectral plots, with computer inversions, are also enclosed with this report, in order to clarify the interpretation.

All of the pseudosection plots that output from the computer interpretation of the Spectral IP data, as well as all of the spectral plots are included in Volume II of this report.

3. DISCUSSION OF RESULTS

For the measurements with both X = 500' and with X = 1000', the most obvious feature on the apparent resistivity pseudosection is the definite contact at about 25+00N. There is a high resistivity rock unit to the south and a lower resistivity rock unit to the north. The X = 1000' measurements show that the southern edge of the high resistivity (non-porous and dense) rock unit is at 50+00S.

The X = 500' measurements suggest that the lower resistivity rocks are present, at depth beneath the high resistivity rock unit, to the south of 25+00N. The pseudosection for the X = 1000' measurements confirm that the lower resistivity rock unit is present, at depth, at least as far south as 0+00 to 10+00S. It is possible that the lower resistivity rocks extend completely beneath the 7500 meter surface extent of the high resistivity rock unit.

The X = 500' measurements show that there is an increased background IP effect in the lower resistivity rocks to the north of 25+00N. In addition, there are slightly anomalous apparent IP effects for n = 5 and n = 6 in the region from 5+00N to 25+00N; these would correlate with the upper edge of the Grum Deposit.

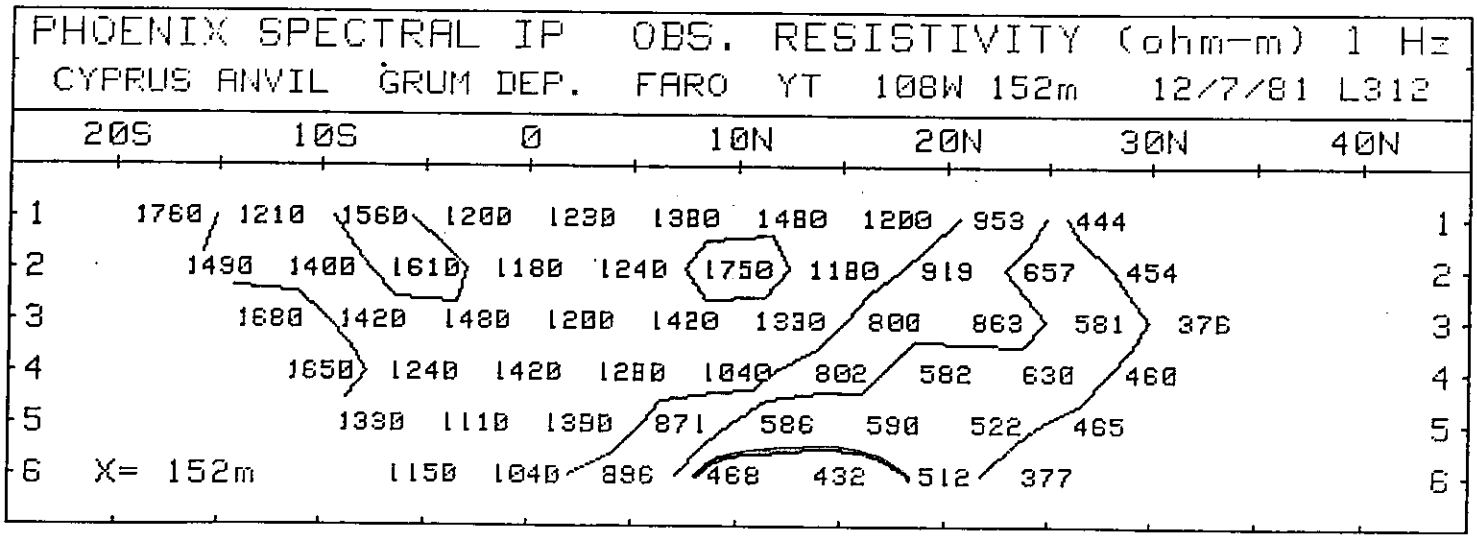
PHOENIX SPECTRAL IP OBS. RESISTIVITY (ohm-m) 1 Hz
CYPRUS ANVIL GRUM DEP. FARO YT 108W 152m 12/7/81 L312
20S 10S 0 10N 20N 30N 40N
1 1760 1210 1560 1200 1230 1380 1480 1200 953 444
2 1490 1400 1610 1180 1240 1750 1180 919 657 454
3 1680 1420 1480 1200 1420 1330 800 863 581 376
4 1650 1240 1420 1280 1040 802 582 630 460
5 1330 1110 1390 871 586 590 522 465
6 X= 152m 1150 1040 896 468 432 512 377

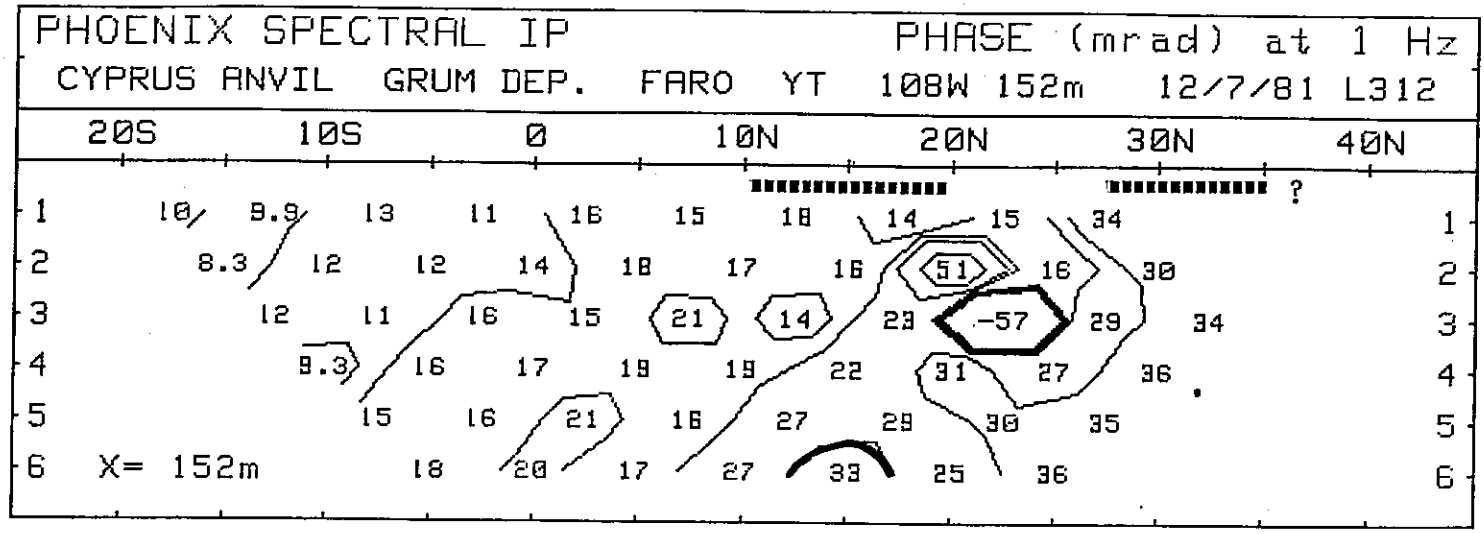
PHOENIX SPECTRAL IP PHASE (mrad) at 1 Hz
CYPRUS ANVIL GRUM DEP. FARO YT 108W 152m 12/7/81 L312
20S 10S 0 10N 20N 30N 40N
1 10 9.9 13 11 16 15 18 14 15 34
2 8.3 12 12 14 18 17 16 51 16 30
3 12 11 16 15 21 14 23 -57 29 34
4 9.3 16 17 18 19 22 31 27 36
5 15 16 21 16 27 28 30 35
6 X= 152m 18 20 17 27 33 25 36

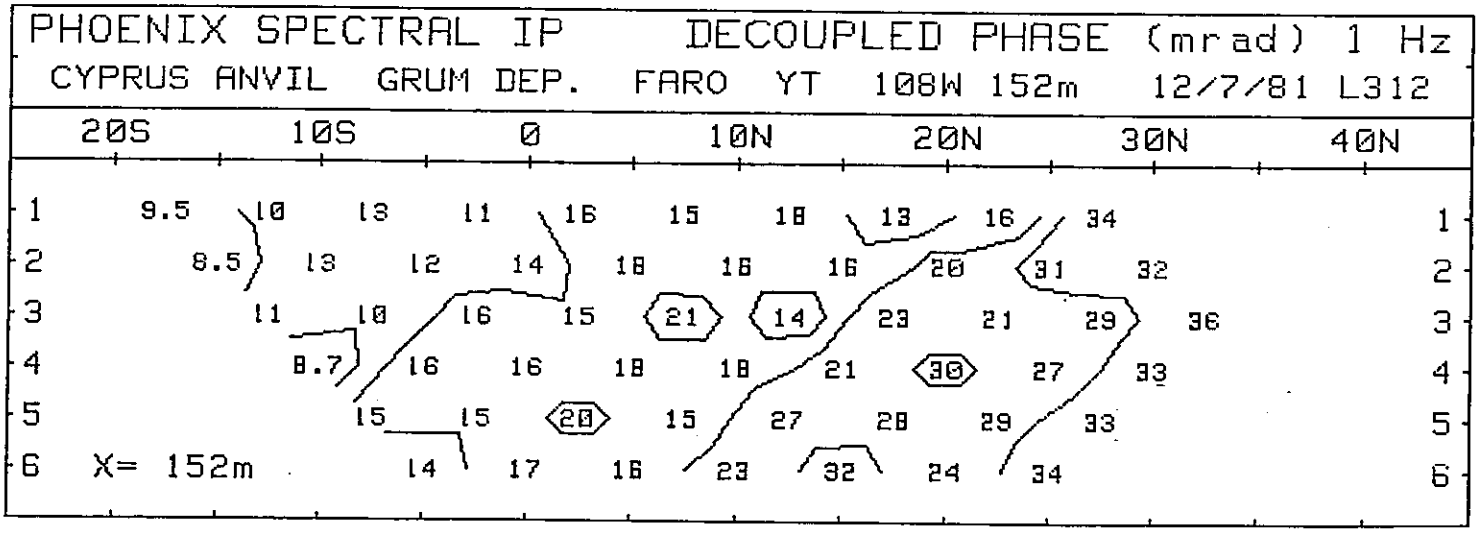
PHOENIX SPECTRAL IP DECOUPLED PHASE (mrad) 1 Hz
CYPRUS ANVIL GRUM DEP. FARO YT 108W 152m 12/7/81 L312
20S 10S 0 10N 20N 30N 40N
1 9.5 10 13 11 16 15 18 13 16 34
2 8.5 13 12 14 18 16 16 20 31 32
3 11 10 16 15 21 14 23 21 29 36
4 8.7 16 16 18 18 21 30 27 33
5 15 15 20 15 27 28 29 33
6 X= 152m 14 17 16 23 32 24 34

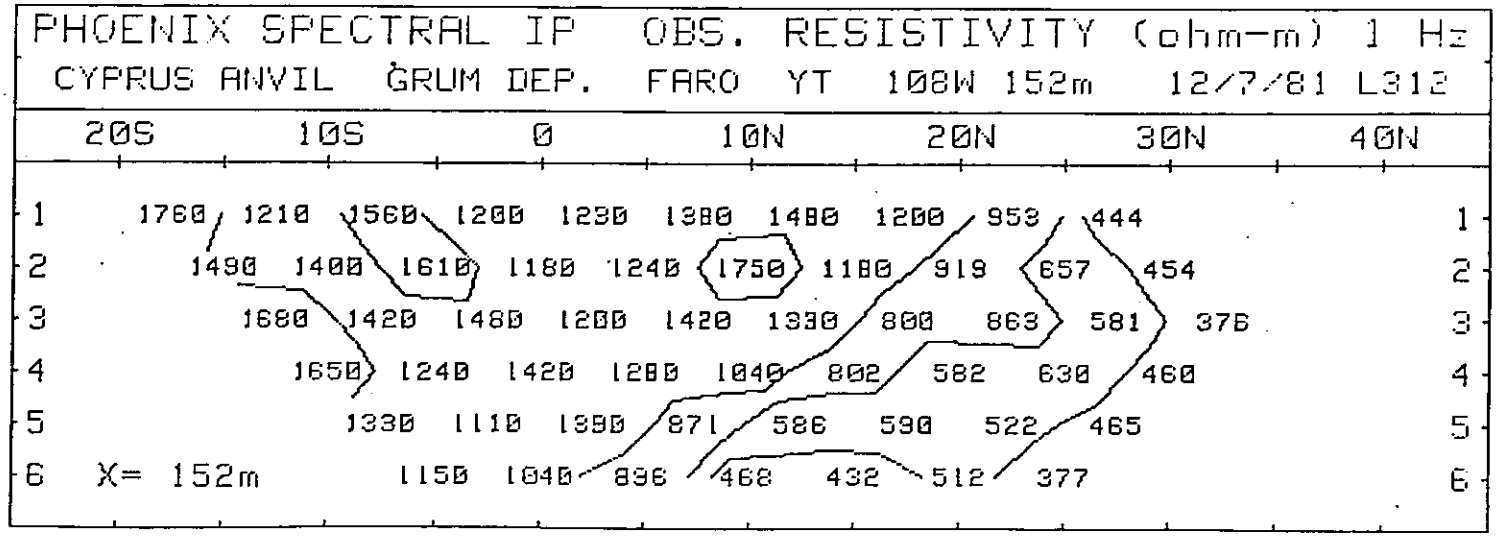
PHOENIX SPECTRAL IP OBS. RESISTIVITY (ohm-m) 1 Hz
CYPRUS ANVIL GRUM DEP. FARO YT 108W 152m 12/7/81 L312
20S 10S 0 10N 20N 30N 40N
1 1760 1210 1560 1200 1230 1380 1480 1200 953 444 1
2 1490 1400 1610 1180 1240 1750 1180 919 657 454 2
3 1680 1420 1480 1200 1420 1330 800 863 581 376 3
4 1650 1240 1420 1280 1040 802 582 630 460 4
5 1330 1110 1390 871 586 590 522 465 5
6 X= 152m 1150 1040 896 468 432 512 377 6

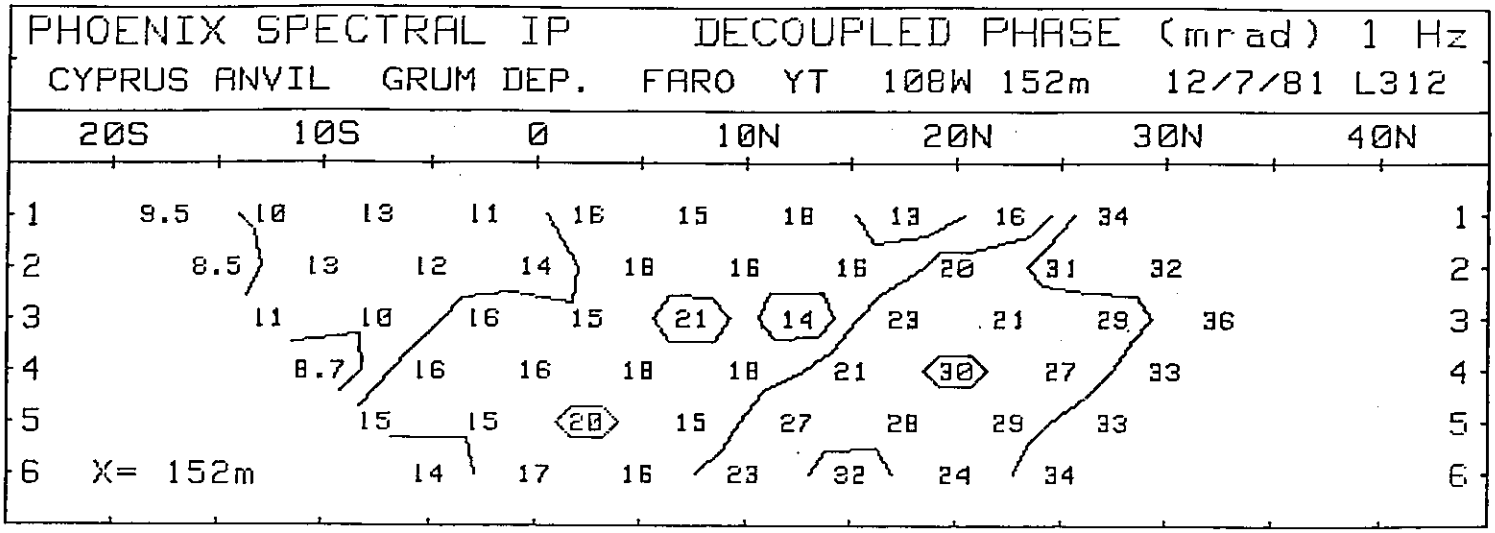
PHOENIX SPECTRAL IP DECOUPLED PHASE (mrad) 1 Hz
CYPRUS ANVIL GRUM DEP. FARO YT 108W 152m 12/7/81 L312
20S 10S 0 10N 20N 30N 40N
1 9.5 10 13 11 16 15 18 13 16 34 1
2 8.5 13 12 14 18 16 16 20 31 32 2
3 11 10 16 15 21 14 23 21 29 36 3
4 8.7 16 16 18 18 21 30 27 33 4
5 15 15 20 15 27 28 29 33 5
6 X= 152m 14 17 16 23 32 24 34 6

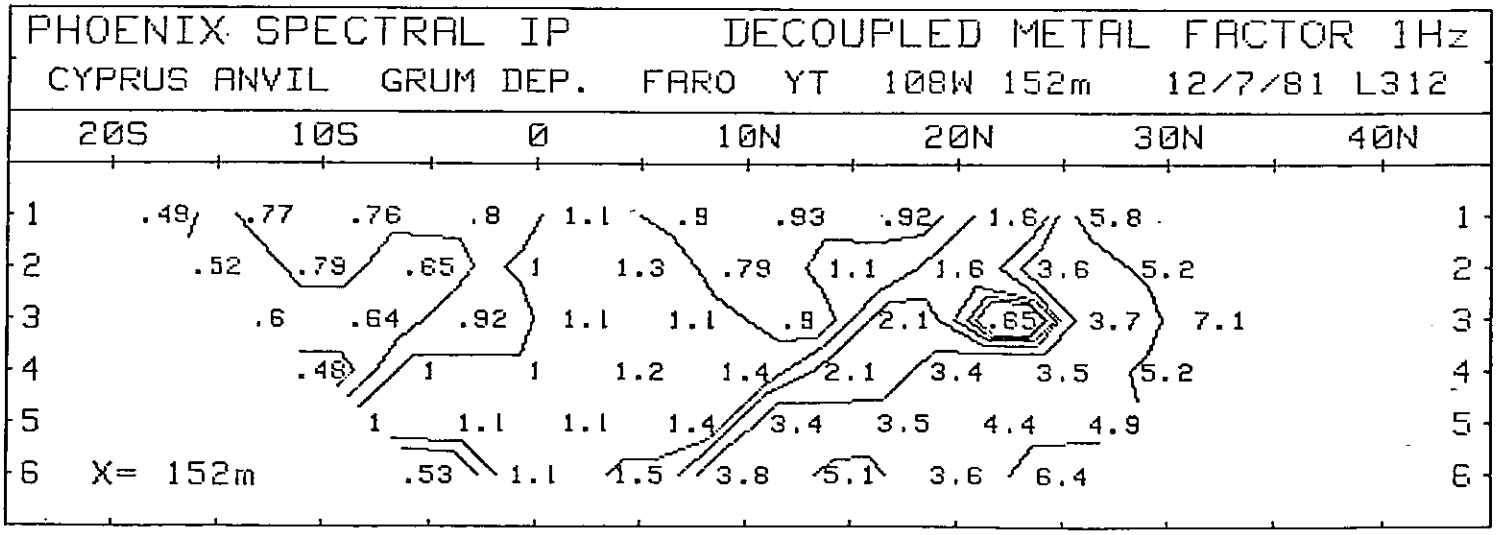
PHOENIX SPECTRAL IP DECOUPLED METAL FACTOR 1Hz
CYPRUS ANVIL GRUM DEP. FARO YT 108W 152m 12/7/81 L312
20S 10S 0 10N 20N 30N 40N
1 .49 .77 .76 .8 1.1 .9 .93 .92 1.6 5.8 1
2 .52 .79 .65 1 1.3 .79 1.1 1.6 3.6 5.2 2
3 .6 .64 .92 1.1 1.1 .9 2.1 .65 3.7 7.1 3
4 .48 1 1 1.2 1.4 2.1 3.4 3.5 5.2 4
5 1 1.1 1.1 1.4 3.4 3.5 4.4 4.9 5
6 X= 152m .53 1.1 1.5 3.8 5.1 3.6 6.4 6

CYPRUS ANVIL GRUM DEP. FARO, YT 108W 152m 12/7/81 L312 D= 5 N=6 X=152m

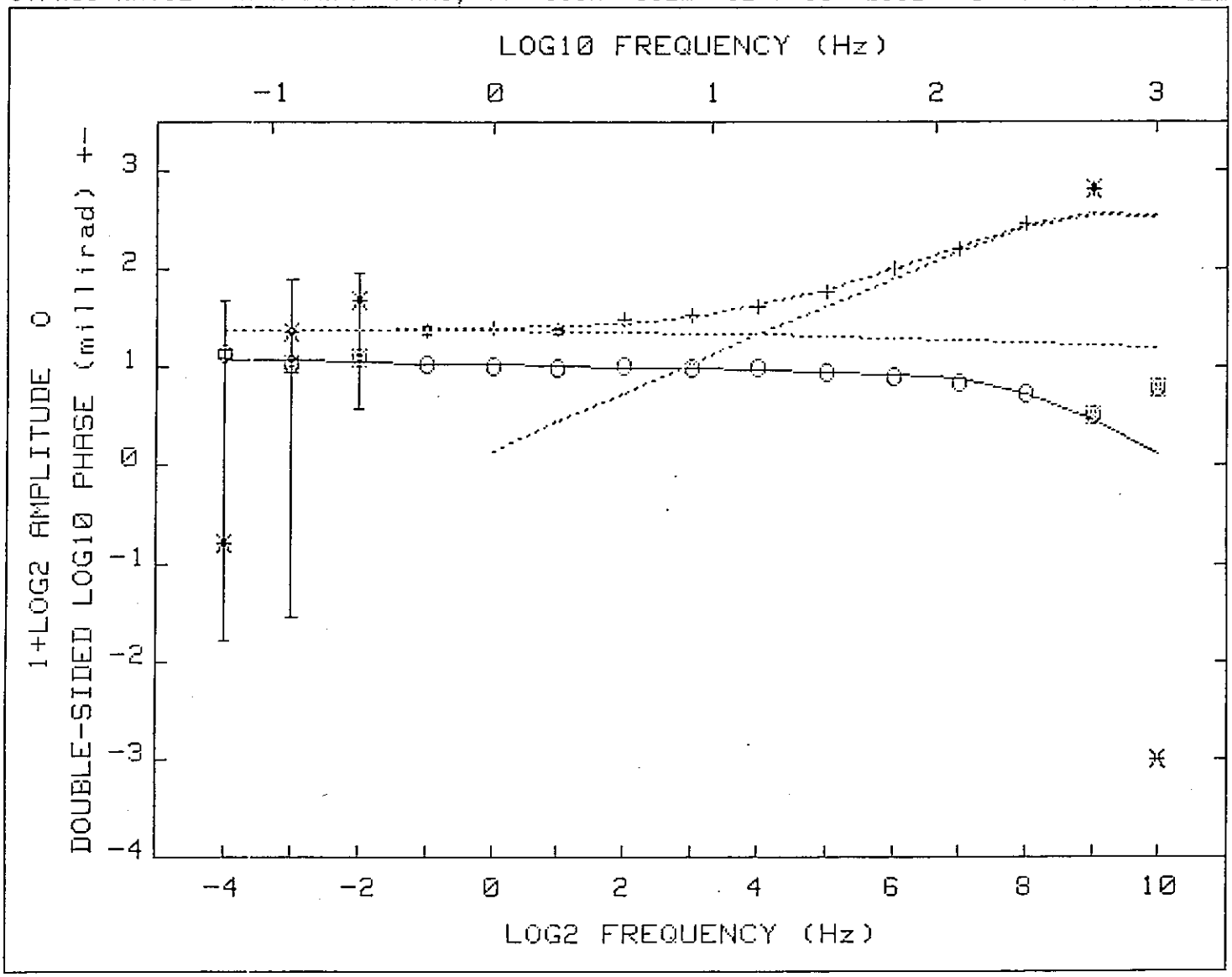

CRL: Number of dispersions= 2
C1=.15 M2=.39 T2=.00038 C2=.97 fixed

Iter	Lambda	Rchsq	R0	M1	T1
0	1.E-02	.00064	1.283	.336	3.9E+00
1	1.E-02	.00064	1.284	.336	3.9E+00

Pct Std Deviations 4.6 4.4 913.3

Correlation Matrix 1.000
.933 1.000
.984 .885 1.000

Apparent Resistivity Measured at 1 Hz is 511.7
Apparent Resistivity Calculated from Inductive Coupling is 1709

CYPRUS ANVIL GRUM DEP. FARO, YT 108W 152m 12/7/81 L312 D= 6 N=5 X=152m

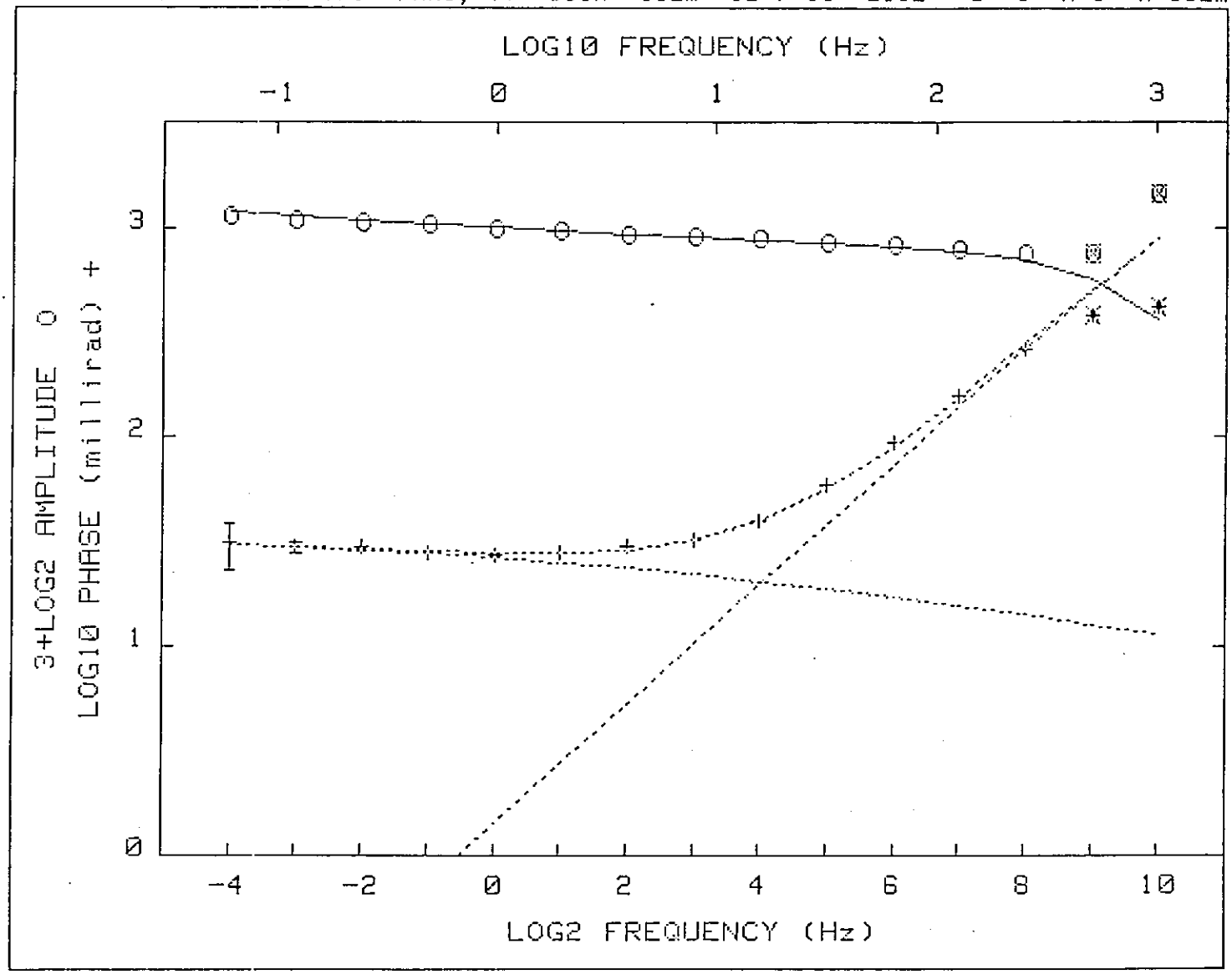

CRL: Number of dispersions= 2
M2=1 T2=.00011 C2=.94 fixed

Iter	Lambda	Rchsq	R0	M1	T1	C1
0	1.E-02	.00018	1.311	.324	2.0E+01	.198
1	1.E-02	.00018	1.312	.324	2.0E+01	.198
Pct Std Deviations			1.8	4.1	70.7	4.3

Correlation Matrix

1.000				
.943	1.000			
.969	.880	1.000		
-.637	-.833	-.535	1.000	

Apparent Resistivity Measured at 1 Hz is 586.2
Apparent Resistivity Calculated from Inductive Coupling is 1498

CYPRUS ANVIL GRUM DEP. FARO, YT 108W 152m 12/7/81 L312 D= 6 N=6 X=152m

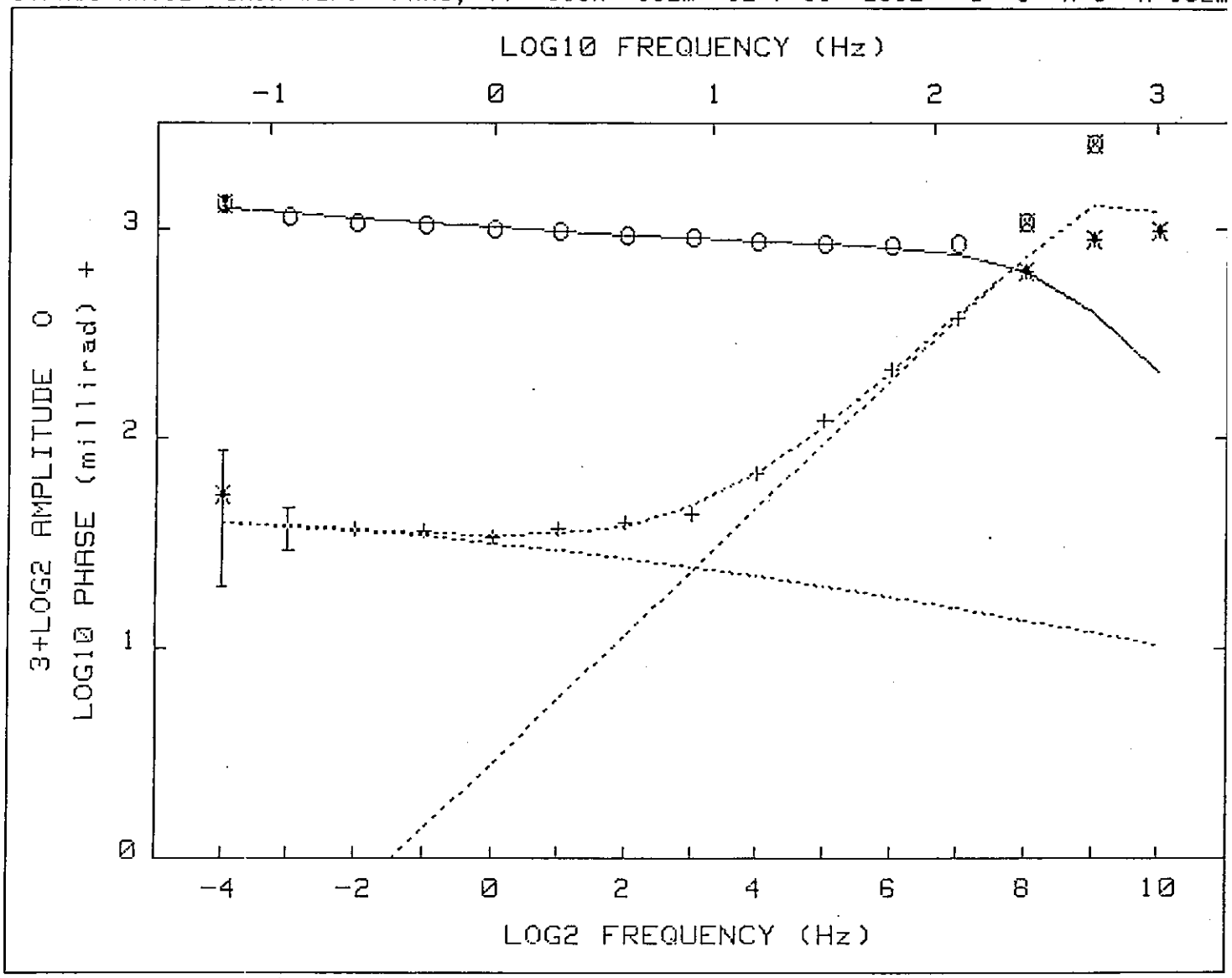

CRL: Number of dispersions= 2
M2=1 T2=.00031 C2=1 fixed

Iter	Lambda	Rchsq	R0	M1	T1	C1
0	1.E-02	.00043	1.431	.377	5.4E+01	.223
1	1.E-02	.00042	1.433	.378	5.6E+01	.223
Pct Std Deviations			3.1	5.0	96.0	6.7

Correlation Matrix

1.000				
.923	1.000			
.972	.899	1.000		
-.111	-.451	-.118	1.000	

Apparent Resistivity Measured at 1 Hz is 432.0
Apparent Resistivity Calculated from Inductive Coupling is 879.1

CYPRUS ANVIL GRUM DEP. FARO, YT 108W 152m 12/7/81 L312 D= 7 N=6 X=152m

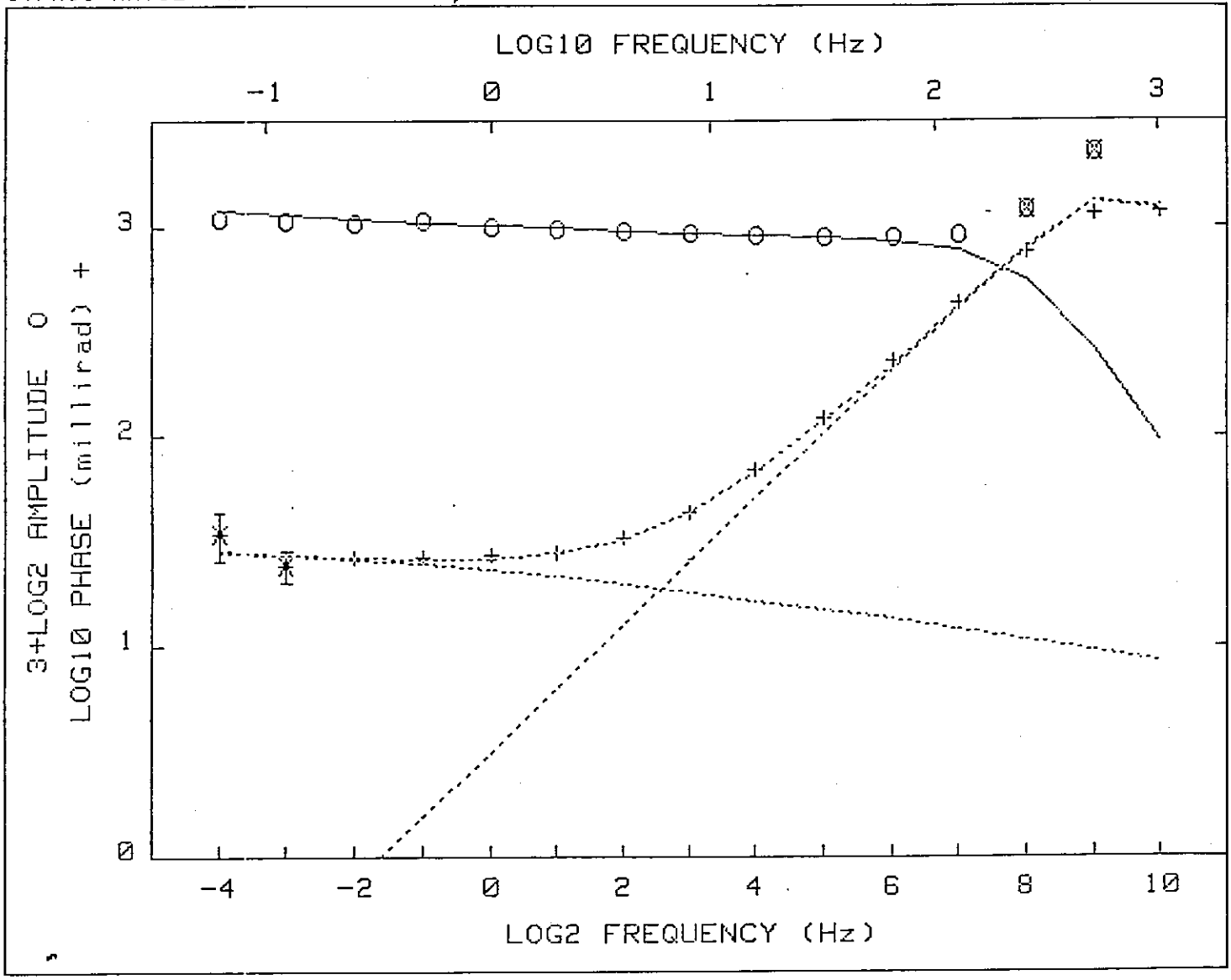

CRL: Number of dispersions= 2
M2=1 T2=.00038 C2=1 fixed

Iter	Lambda	Rchsq	R0	M1	T1	C1
0	1.E-02	.00080	1.238	.266	8.4E+00	.219
1	1.E-02	.00076	1.251	.280	9.3E+00	.203
2	1.E-03	.00071	1.271	.288	1.7E+01	.201
3	1.E-04	.00069	1.296	.294	3.9E+01	.210
4	1.E-05	.00068	1.300	.296	4.0E+01	.212

Pct Std Deviations	2.6	5.9	126.0	13.1	
Correlation Matrix	1.000				
	.748	1.000			
	.944	-.637	1.000		
	.134	-.516	.233	1.000	

Apparent Resistivity Measured at 1 Hz is 468.1
Apparent Resistivity Calculated from Inductive Coupling is 719.4

CYPRUS ANVIL GRUM DEP. FARO Y.T. LINE 108W 16/9/81 L330 D= 4 N=1 X=305m

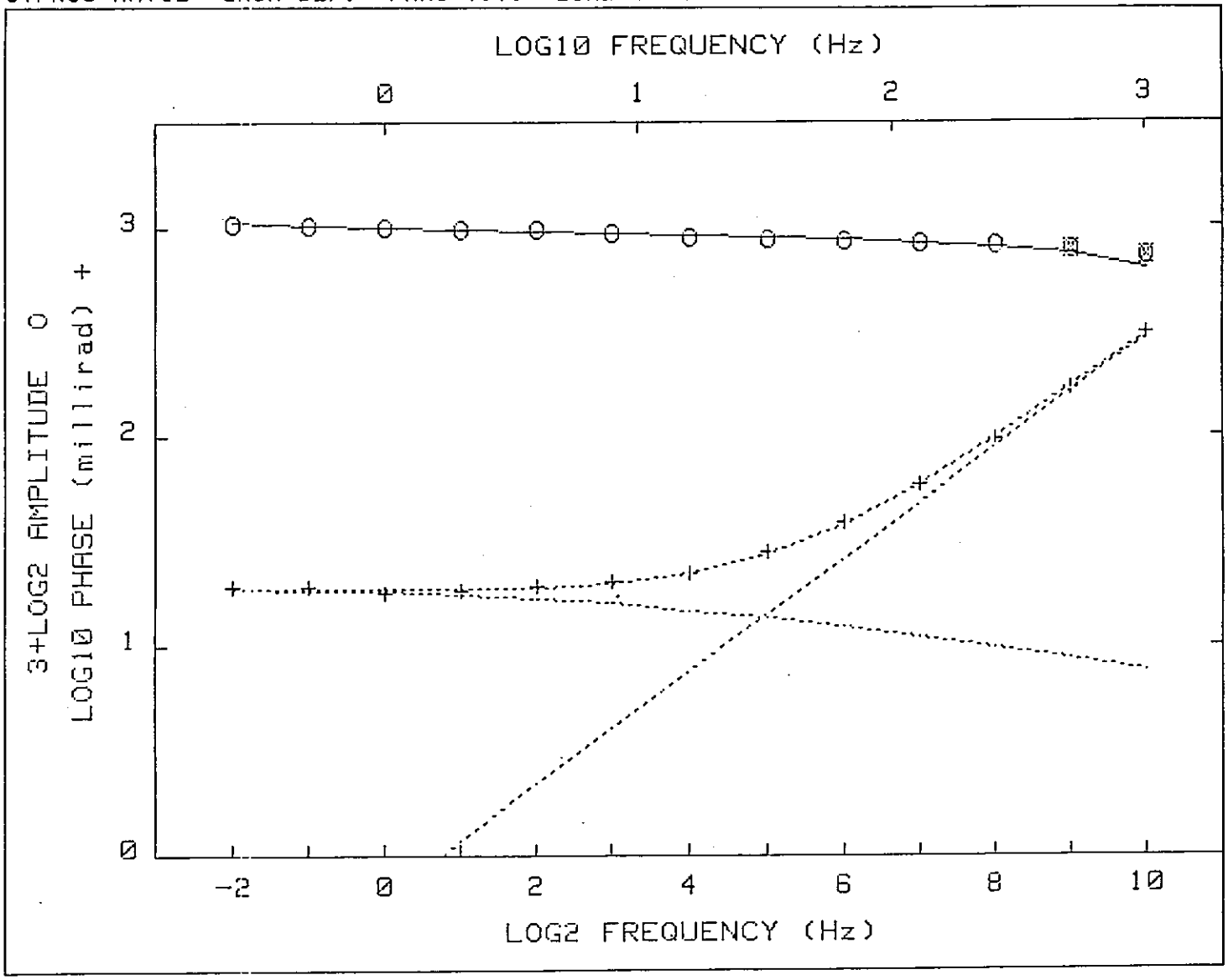

CRL: Number of dispersions= 2
C1=.25 M2=1 fixed

Iter	Lambda	Rchsq	R0	M1	T1	T2	C2
0	1.E-02	.03050	1.540	.367	4.8E+02	1.1E-05	.892
1	1.E-02	.00219	1.377	.318	4.0E+02	1.4E-05	.707
2	1.E-03	.00081	1.288	.269	1.7E+02	2.4E-05	.777
3	1.E-03	.00057	1.236	.237	6.3E+01	2.6E-05	.789
4	1.E-03	.00041	1.192	.211	2.1E+01	2.8E-05	.805
5	1.E-03	.00026	1.160	.192	7.7E+00	3.0E-05	.825
6	1.E-04	.00025	1.102	.162	8.2E-01	3.5E-05	.870
7	1.E-05	.00006	1.112	.171	7.2E-01	3.5E-05	.886
8	1.E-06	.00006	1.112	.171	7.1E-01	3.5E-05	.887

Pct Std Deviations	.4	1.1	29.9	2.7	1.2	

Correlation Matrix	1.000				
	.767	1.000			
	.896	.674	1.000		
	-.482	-.212	-.557	1.000	
	-.570	-.198	-.692	.906	1.000

CYPRUS ANVIL GRUM DEP. FARO Y.T. LINE 108W 16/9/81 L330 D= 4 N=2 X=305m

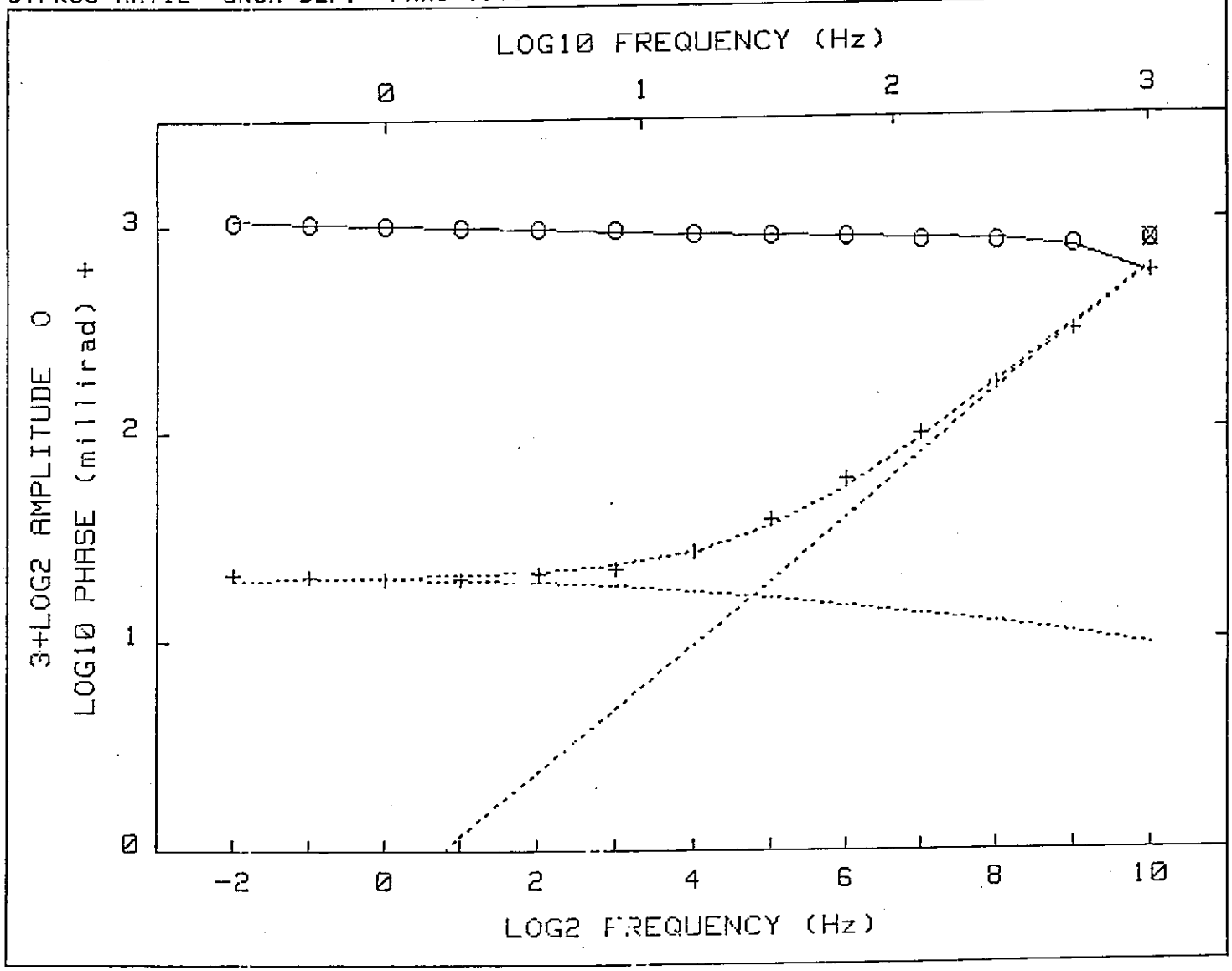

CRL: Number of dispersions= 2
C1=.25 M2=1 C2=1 fixed

Iter	Lambda	Rchsq	R0	M1	T1	T2
0	1.E-02	.00047	1.129	.187	5.6E-01	7.9E-05
1	1.E-02	.00035	1.118	.185	5.2E-01	8.3E-05
2	1.E-03	.00033	1.113	.183	4.0E-01	8.2E-05
3	1.E-04	.00033	1.111	.183	3.4E-01	8.2E-05

Pct Std Deviations	.8	1.9	53.7	2.3	
Correlation Matrix	1.000				
	.709	1.000			
	.825	.565	1.000		
	.084	-.189	.217	1.000	

Apparent Resistivity Measured at 1 Hz is 816.3
Apparent Resistivity Calculated from Inductive Coupling is 2216

CYPRUS ANVIL GRUM DEP. FARO Y.T. LINE 108W 16/9/81 L330 D= 4 N=3 X=305m

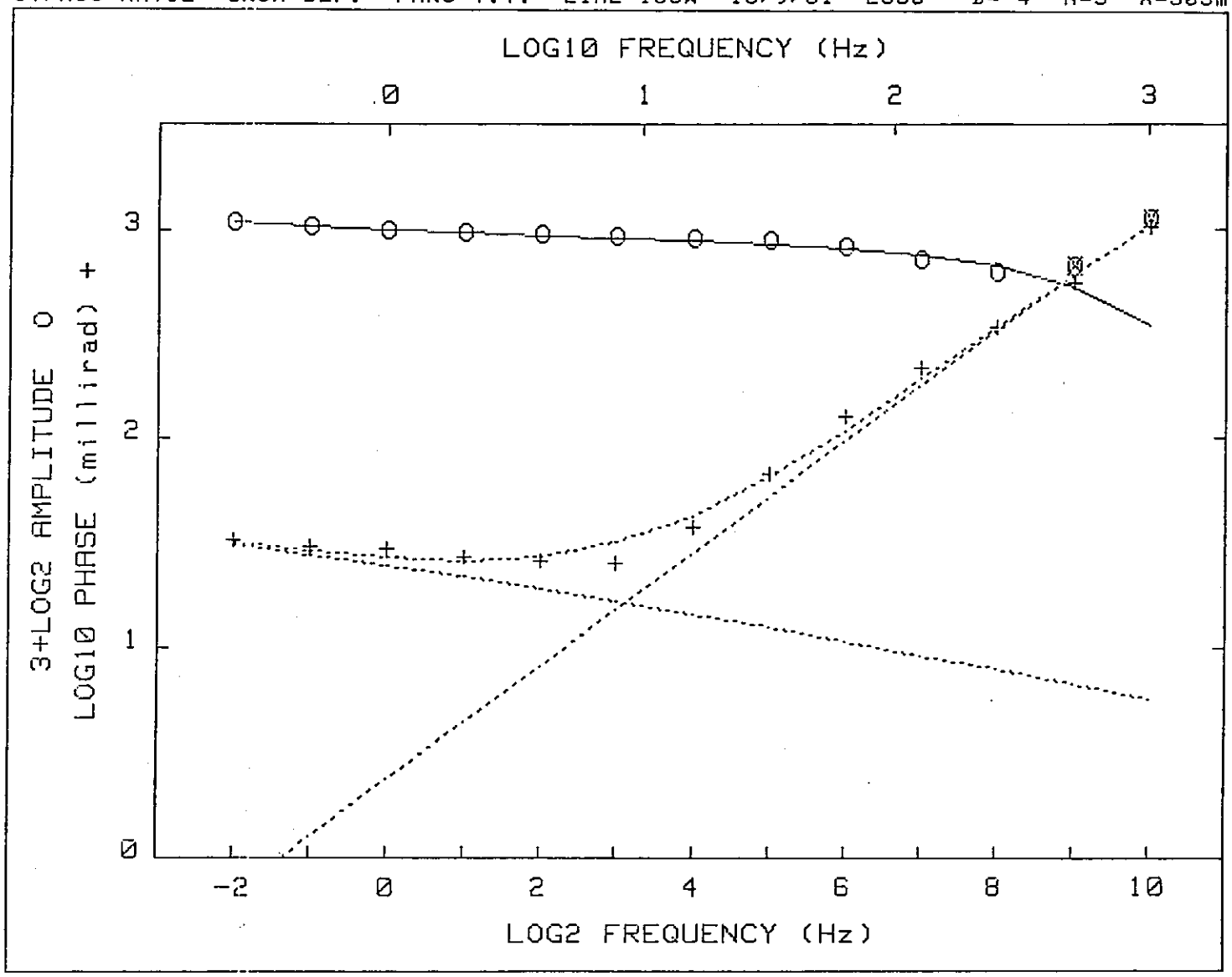

CRL: Number of dispersions= 2
C1=.25 M2=1 fixed

Iter	Lambda	Rchsq	R0	M1	T1	T2	C2
0	1.E-02	.00297	1.320	.283	4.2E+01	1.6E-04	.931
1	1.E-02	.00163	1.332	.309	4.5E+01	1.4E-04	.917
2	1.E-03	.00153	1.402	.341	1.3E+02	1.3E-04	.903
3	1.E-03	.00148	1.461	.366	2.3E+02	1.2E-04	.899
4	1.E-03	.00146	1.506	.384	3.6E+02	1.1E-04	.895
5	1.E-03	.00145	1.541	.397	4.8E+02	1.1E-04	.892

Pct Std Deviations	36.2	61.3	999.9	56.2	6.1	
Correlation Matrix	1.000					
	1.000	1.000				
	.998	.998	1.000			
	-.988	-.987	-.988	1.000		
	-.880	-.874	-.889	.923	1.000	

Apparent Resistivity Measured at 1 Hz is 404.8
Apparent Resistivity Calculated from Inductive Coupling is 2162

CYPRUS ANVIL GRUM DEP. FARO Y.T. LINE 108W 16/9/81 L330 D= 4 N=4 X=305m

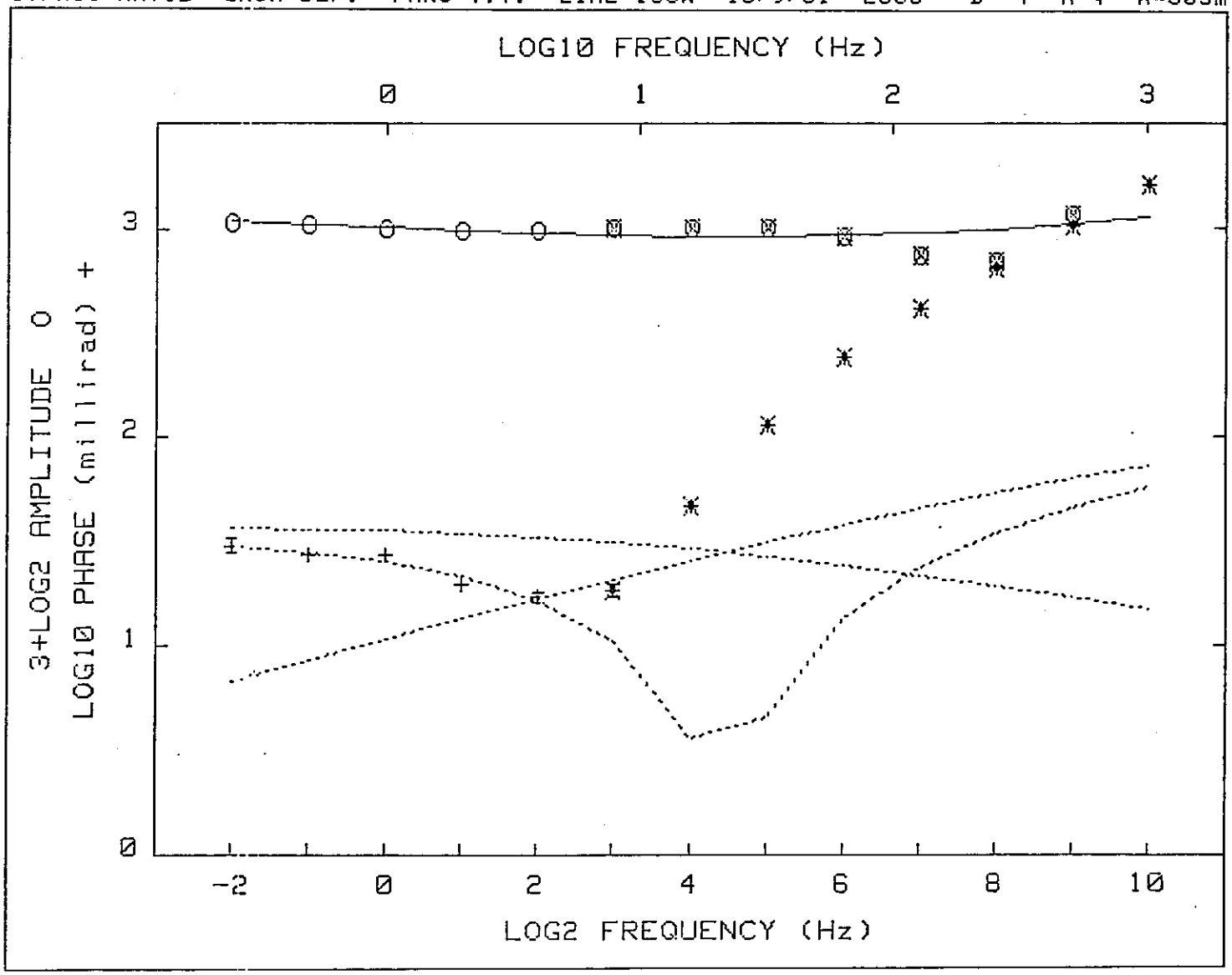

CRL: Number of dispersions= 2 Negative.
T1=1 C1=.25 M2=1 fixed

Iter	Lambda	Rchsq	R0	M1	T2	C2
0	1.E-02	.02618	1.310	.457	5.9E-05	.454
1	1.E-02	.00206	1.169	.272	4.9E-05	.660
2	1.E-03	.00067	1.197	.267	3.9E-05	.651
3	1.E-04	.00062	1.203	.278	8.8E-06	.500
4	1.E-04	.00056	1.207	.287	3.6E-06	.432
5	1.E-04	.00055	1.210	.294	1.9E-06	.391
6	1.E-04	.00054	1.212	.299	1.2E-06	.361
7	1.E-04	.00053	1.214	.304	7.7E-07	.339
8	1.E-04	.00053	1.215	.309	5.5E-07	.320

Pct Std Deviations 2.8 41.3 999.9 . 296.7

Correlation Matrix

1.000				
.954	1.000			
-.916	-.985	1.000		
-.928	-.992	.999	1.000	

CYPRUS ANVIL GRUM DEP. FARO Y.T. LINE 108W 16/9/81 L330 D= 4 N=5 X=305m

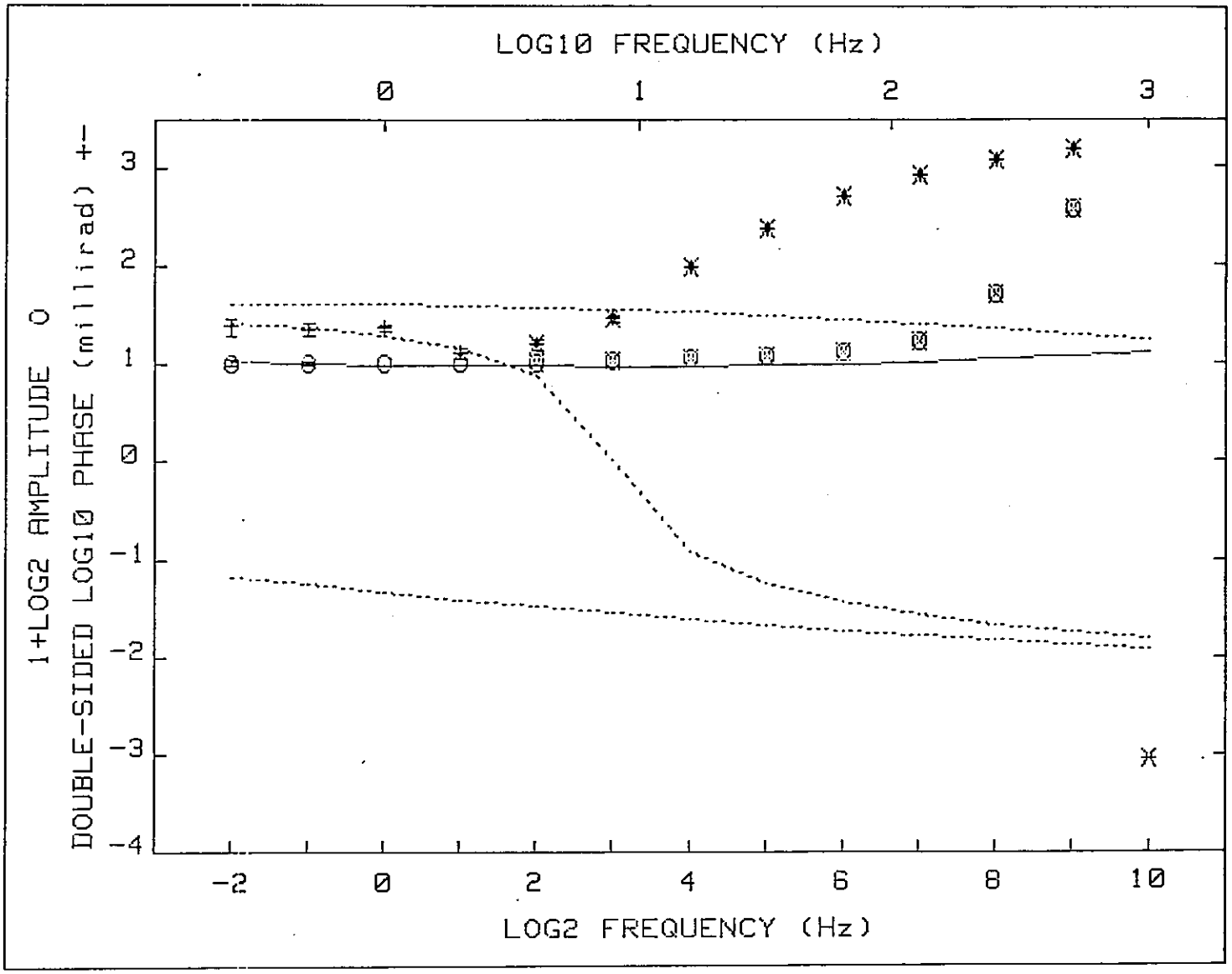

CRL: Number of dispersions= 2 Negative.
T1=1 C1=.25 M2=1 fixed

Iter	Lambda	Rchsq	R0	M1	T2	C2
0	1.E-02	.00944	1.210	.309	8.5E-07	.320
1	1.E-02	.00290	1.205	.332	8.8E-07	.260
2	1.E-03	.00232	1.211	.353	1.1E-06	.256
3	1.E-03	.00230	1.211	.345	1.3E-06	.267

Pct Std Deviations	6.6	956.7	999.9	999.9

Correlation Matrix	1.000			
	.931	1.000		
	-.898	-.994	1.000	
	-.916	-.999	.998	1.000

Apparent Resistivity Measured at 1 Hz is 155.6
Apparent Resistivity Calculated from Inductive Coupling is 176.6

CYPRUS ANVIL GRUM DEP. FARO Y.T. LINE 108W 16/9/81 L330 D= 4 N=6 X=305m

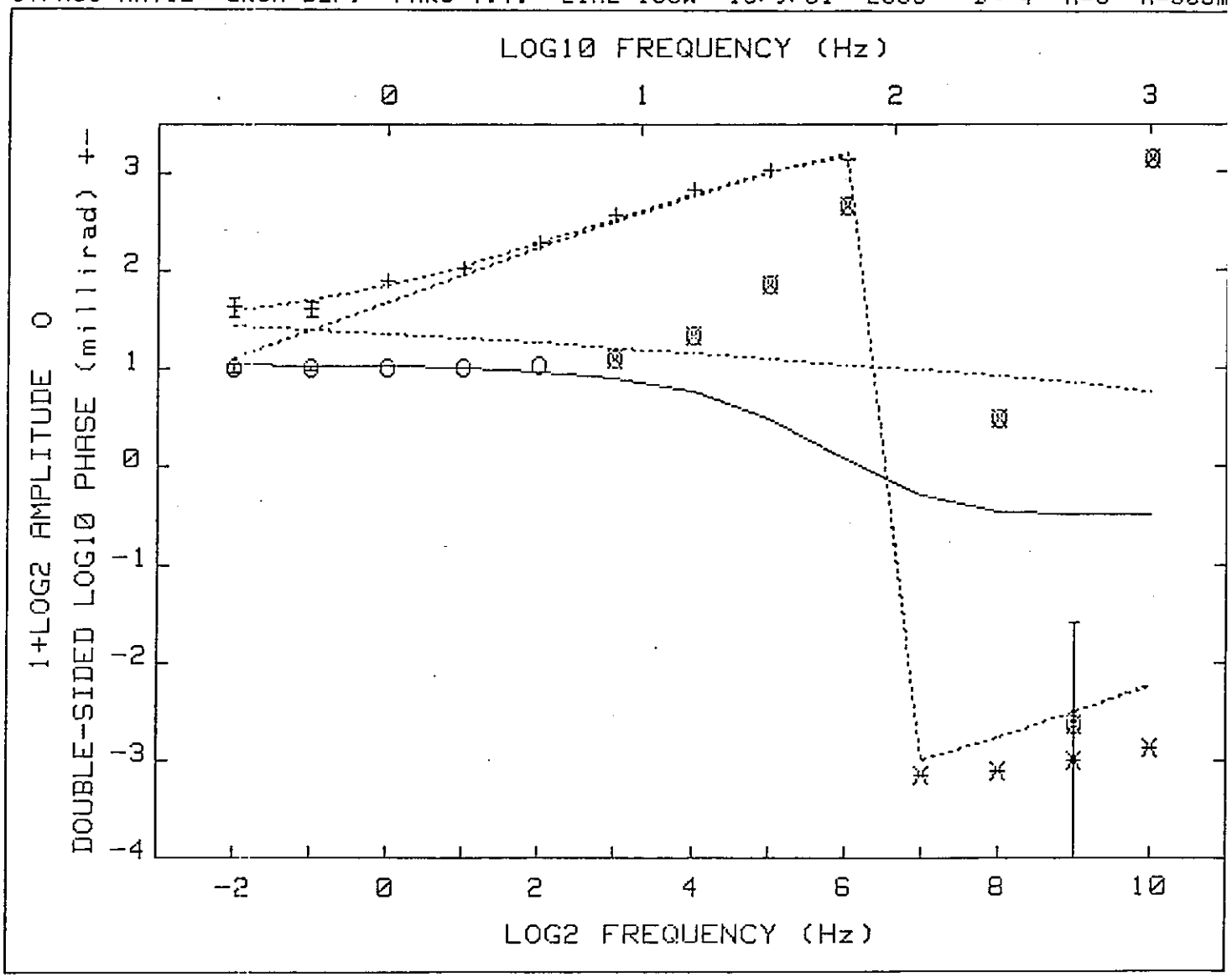

CRL: Number of dispersions= 2
C1=.25 M2=1 fixed

Iter	Lambda	Rchsq	R0	M1	T1	T2	C2
0	1.E-02	.00302	1.345	.281	4.1E+01	4.6E-03	.933
1	1.E+01	.00247	1.330	.282	4.1E+01	4.6E-03	.931
2	1.E+01	.00234	1.323	.283	4.1E+01	4.6E-03	.931
3	1.E+03	.00234	1.323	.283	4.1E+01	4.6E-03	.931

Pct Std Deviations	73.6	187.8	999.9	104.4	18.5	
Correlation Matrix	1.000					
	.997	1.000				
	.997	.991	1.000			
	-.994	-.994	-.990	1.000		
	-.960	-.944	-.971	.960	1.000	

Apparent Resistivity Measured at 1 Hz is 87.69
Apparent Resistivity Calculated from Inductive Coupling is 190.5

As expected, the measurements with X = 1000' (305 meters) show a more clearly defined anomaly at depth. For these deep measurements the apparent IP effects within the anomaly at depth are greater than the high background IP effects to the north. In addition, there are a few, shallow, above background IP effects at the south edge of the measured data (50+00S to 60+00S).

No useful spectral interpretation can be made from the n = 5 or n = 6 measurements for either X = 500' or X = 1000'. As the enclosed examples show, the voltage levels were low in magnitude and the electrical noise levels were high in magnitude. The parameters for the IP dispersion for the deep anomalous source can not be determined from the present data.

The higher background IP effects to the north and the slightly anomalous IP effects at the south edge of the data (for X = 1000') were both detected for n = 1 and n = 2. For these measurements, the measurements were more reliable; the standard deviations for the data were much smaller.

For both of these anomalies (D1, N1; D1,N2) and (D10, N1; D10, N2), the spectral IP data plots can be accurately inverted. The attached data plots show the accuracy with which the data can be approximated by two Cole-Cole Dispersions.

For both anomalies, the time-constants (T_1) for the IP dispersion are in the range from ten seconds to one hundred seconds. Our field tests elsewhere in the Faro Area indicates that these large time-constant dispersions are due to large grain-sized sources, usually graphite.

4. CONCLUSIONS AND RECOMMENDATIONS

The Spectral IP Test Survey on Line 108W, over the Grum Deposit has shown that the deep source in the Faro Area can be detected if the

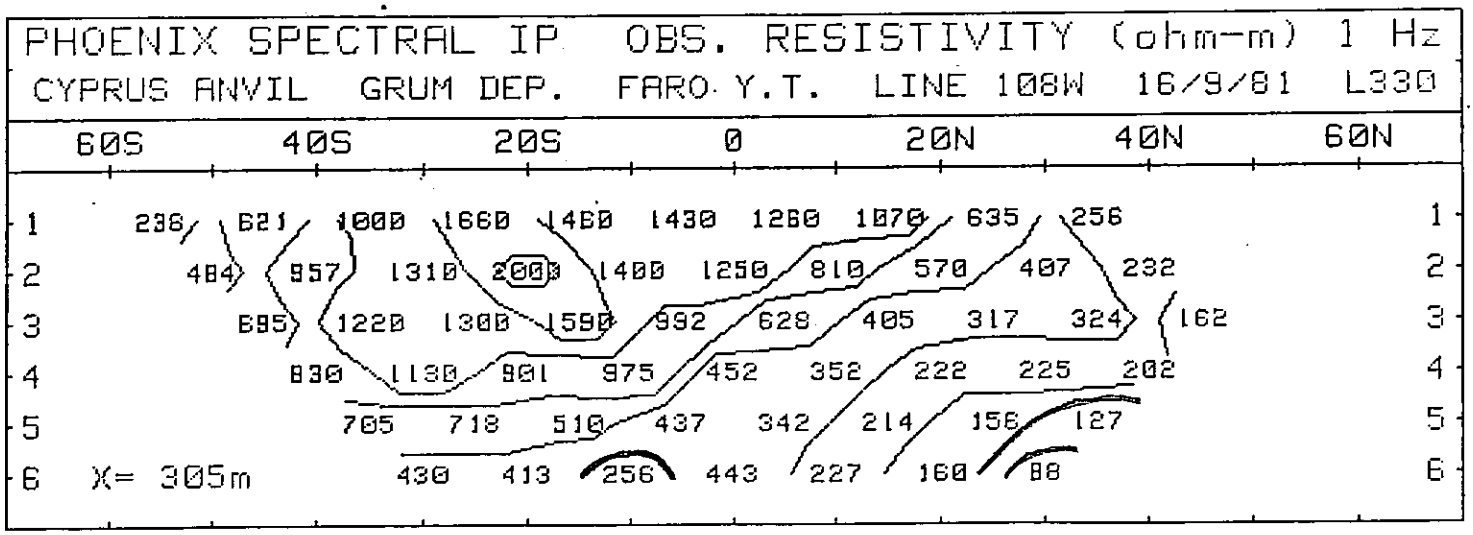
PHOENIX SPECTRAL IP OBS. RESISTIVITY (ohm-m) 1 Hz
CYPRUS ANVIL GRUM DEP. FARO Y.T. LINE 108W 16/9/81 L330
60S 40S 20S 0 20N 40N 60N
X= 305m

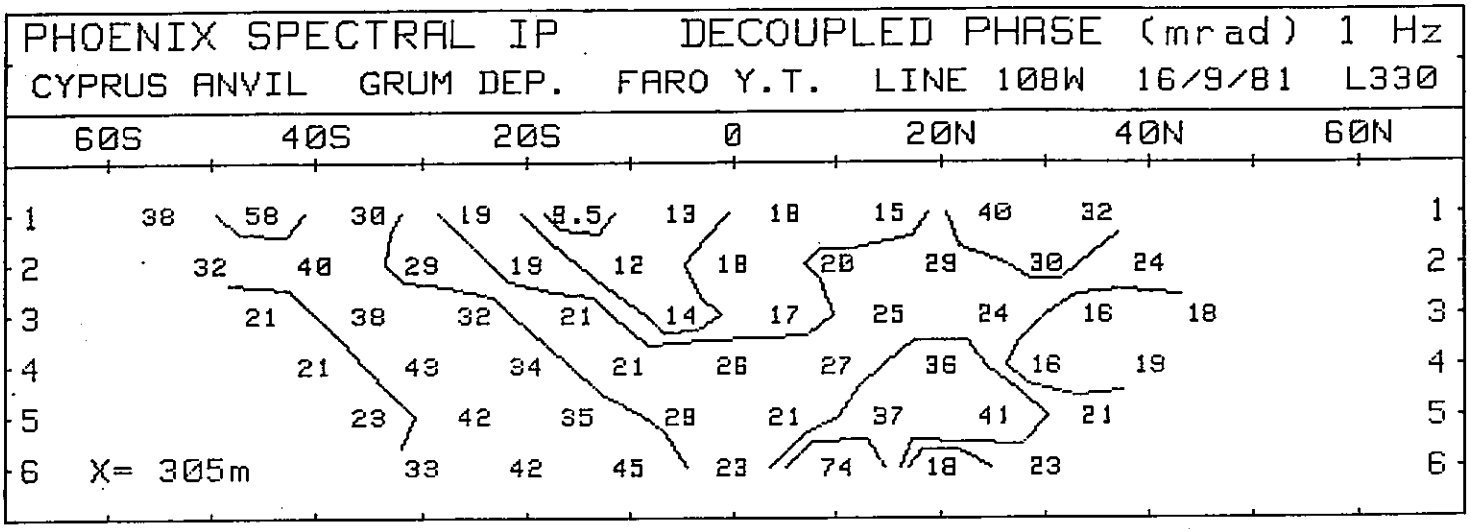
PHOENIX SPECTRAL IP DECOUPLED PHASE (mrad) 1 Hz
CYPRUS ANVIL GRUM DEP. FARO Y.T. LINE 108W 16/9/81 L330
60S 40S 20S 0 20N 40N 60N
X= 305m

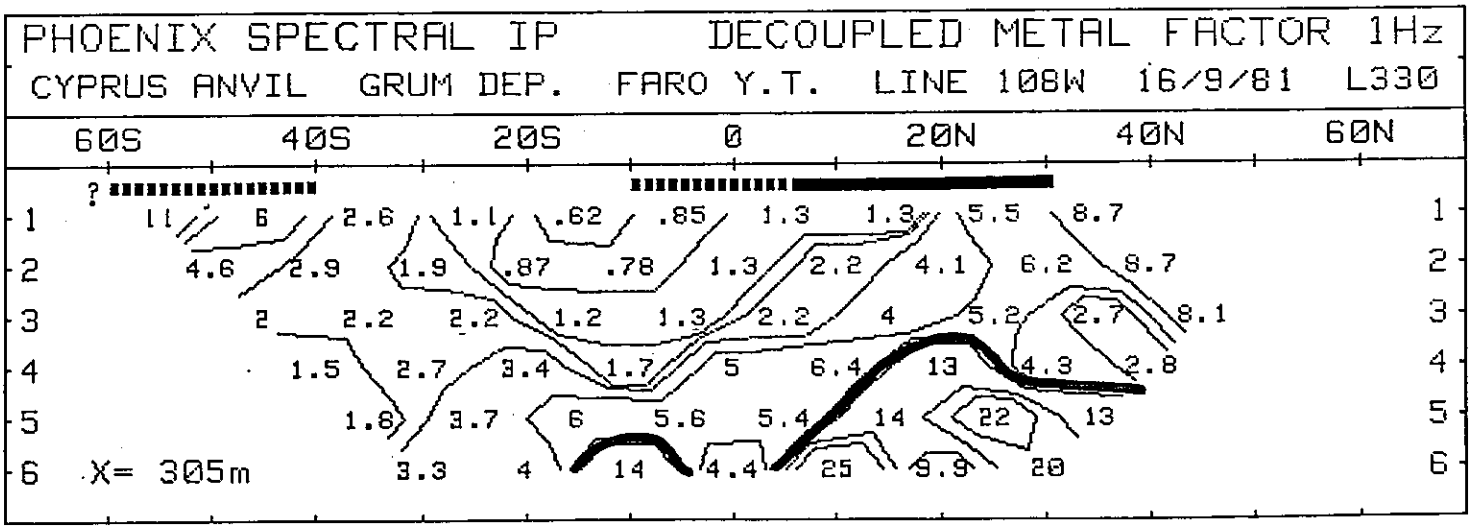
PHOENIX SPECTRAL IP DECOUPLED METAL FACTOR 1Hz
CYPRUS ANVIL GRUM DEP. FARO Y.T. LINE 108W 16/9/81 L330
60S 40S 20S 0 20N 40N 60N
X= 305m

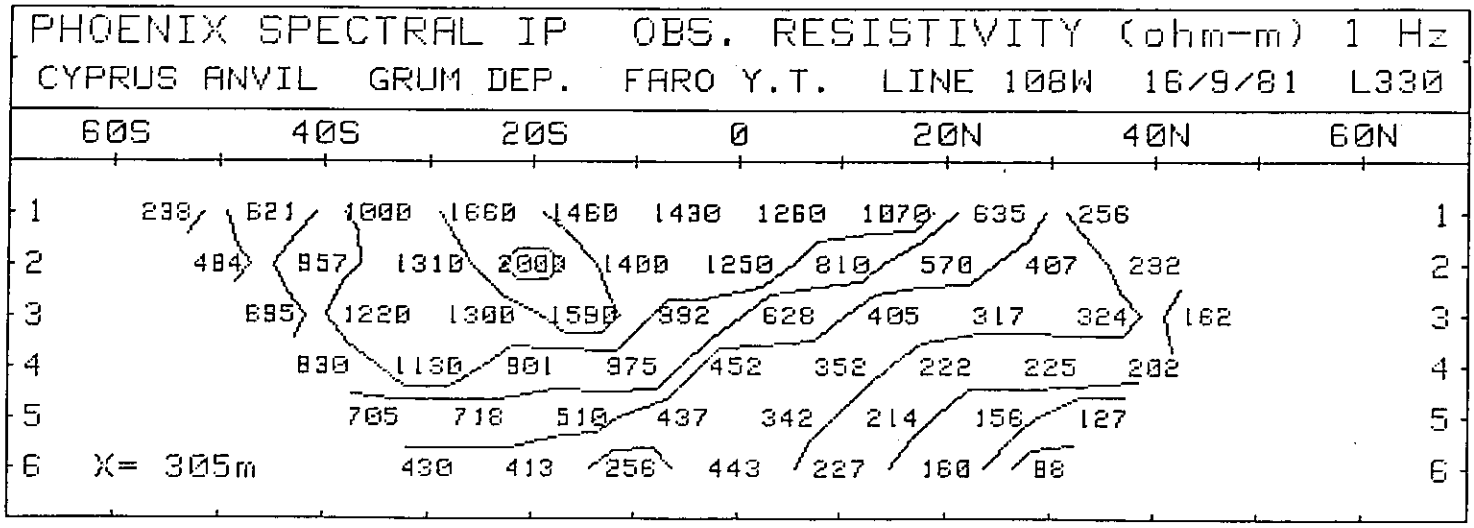
PHOENIX SPECTRAL IP OBS. RESISTIVITY (ohm-m) 1 Hz
CYPRUS ANVIL GRUM DEP. FARO Y.T. LINE 108W 16/9/81 L330
60S 40S 20S 0 20N 40N 60N
1 238 621 1000 1660 1460 1430 1260 1070 635 256
2 484 857 1310 2000 1400 1250 810 570 407 232
3 685 1220 1300 1590 992 628 405 317 324 162
4 830 1130 901 975 452 352 222 225 202
5 705 718 510 437 342 214 156 127
6 X= 305m 430 413 256 443 227 160 88

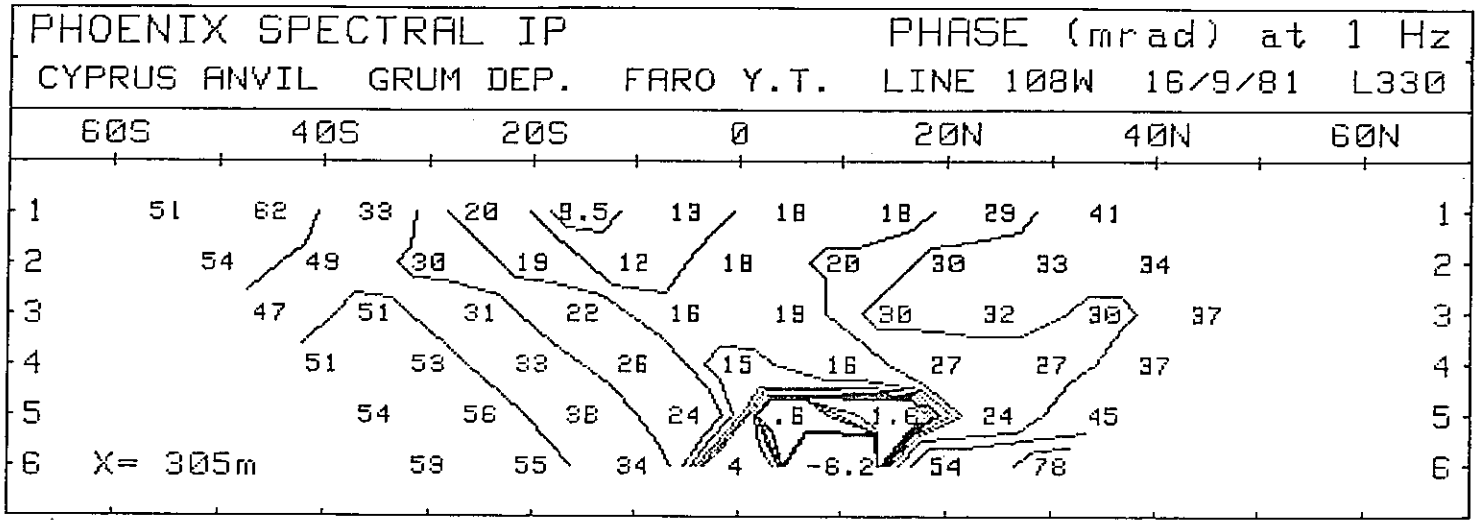
PHOENIX SPECTRAL IP PHASE (mrad) at 1 Hz
CYPRUS ANVIL GRUM DEP. FARO Y.T. LINE 108W 16/9/81 L330
60S 40S 20S 0 20N 40N 60N
1 51 62 33 20 9.5 13 18 18 29 41
2 54 49 30 19 12 18 20 30 33 34
3 47 51 31 22 16 19 30 32 30 37
4 51 53 33 26 15 16 27 27 37
5 54 56 38 24 .6 1.6 24 45
6 X= 305m 58 55 34 4 -6.2 54 78

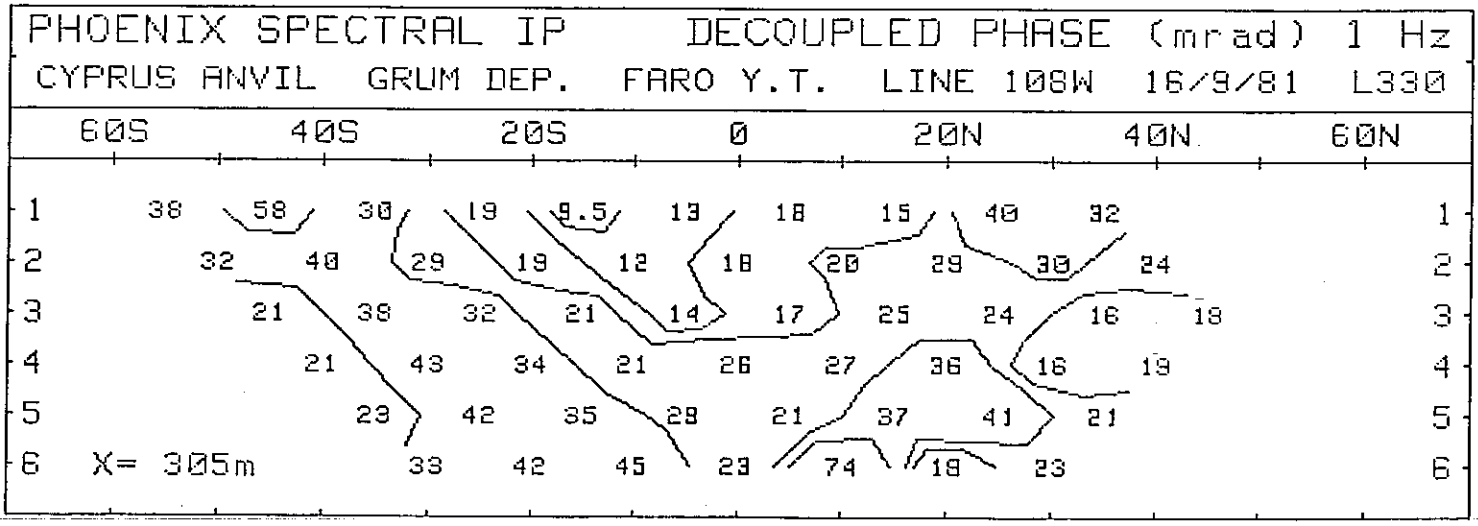
PHOENIX SPECTRAL IP DECOUPLED PHASE (mrad) 1 Hz
CYPRUS ANVIL GRUM DEP. FARO Y.T. LINE 108W 16/9/81 L330
60S 40S 20S 0 20N 40N 60N
1 38 58 30 19 9.5 13 18 15 40 32
2 32 40 29 19 12 18 20 29 30 24
3 21 38 32 21 14 17 25 24 16 18
4 21 43 34 21 26 27 36 16 19
5 23 42 35 28 21 37 41 21
6 X= 305m 33 42 45 23 74 18 23

CYPRUS ANVIL GRUM DEP. FARO Y.T. LINE 108W 16/9/81 L330 D= 1 N=1 X=305m

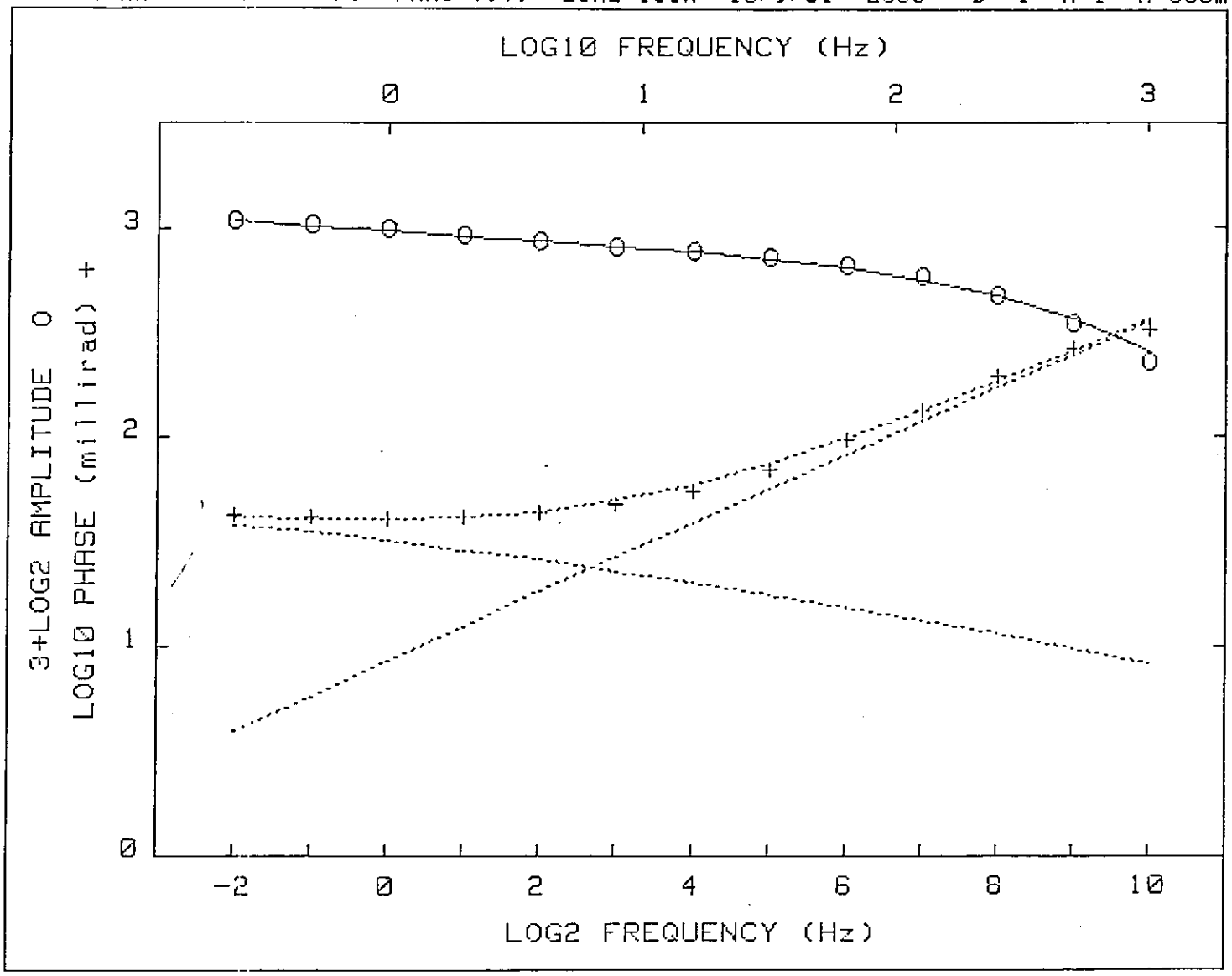

CRL: Number of dispersions= 2
C1=.25 M2=1 fixed

Iter	Lambda	Rchsq	R0	M1	T1	T2	C2
0	1.E-02	.00762	1.517	.411	4.5E+01	2.0E-05	.497
1	1.E-02	.00056	1.410	.368	4.6E+01	2.0E-05	.542
2	1.E-03	.00047	1.422	.368	4.8E+01	2.0E-05	.543
3	1.E-04	.00047	1.441	.375	6.1E+01	1.9E-05	.540

Pct Std Deviations	14.8	21.9	999.9	44.0	7.1	
Correlation Matrix	1.000					
	.997	1.000				
	.997	.990	1.000			
	-.979	-.972	-.980	1.000		
	-.902	-.876	-.920	.952	1.000	

Apparent Resistivity Measured at 1 Hz is 255.5
Apparent Resistivity Calculated from Inductive Coupling is 289.7

CYPRUS ANVIL GRUM DEP. FARO Y.T. LINE 108W 16/9/81 L330 D= 1 N=2 X=305m

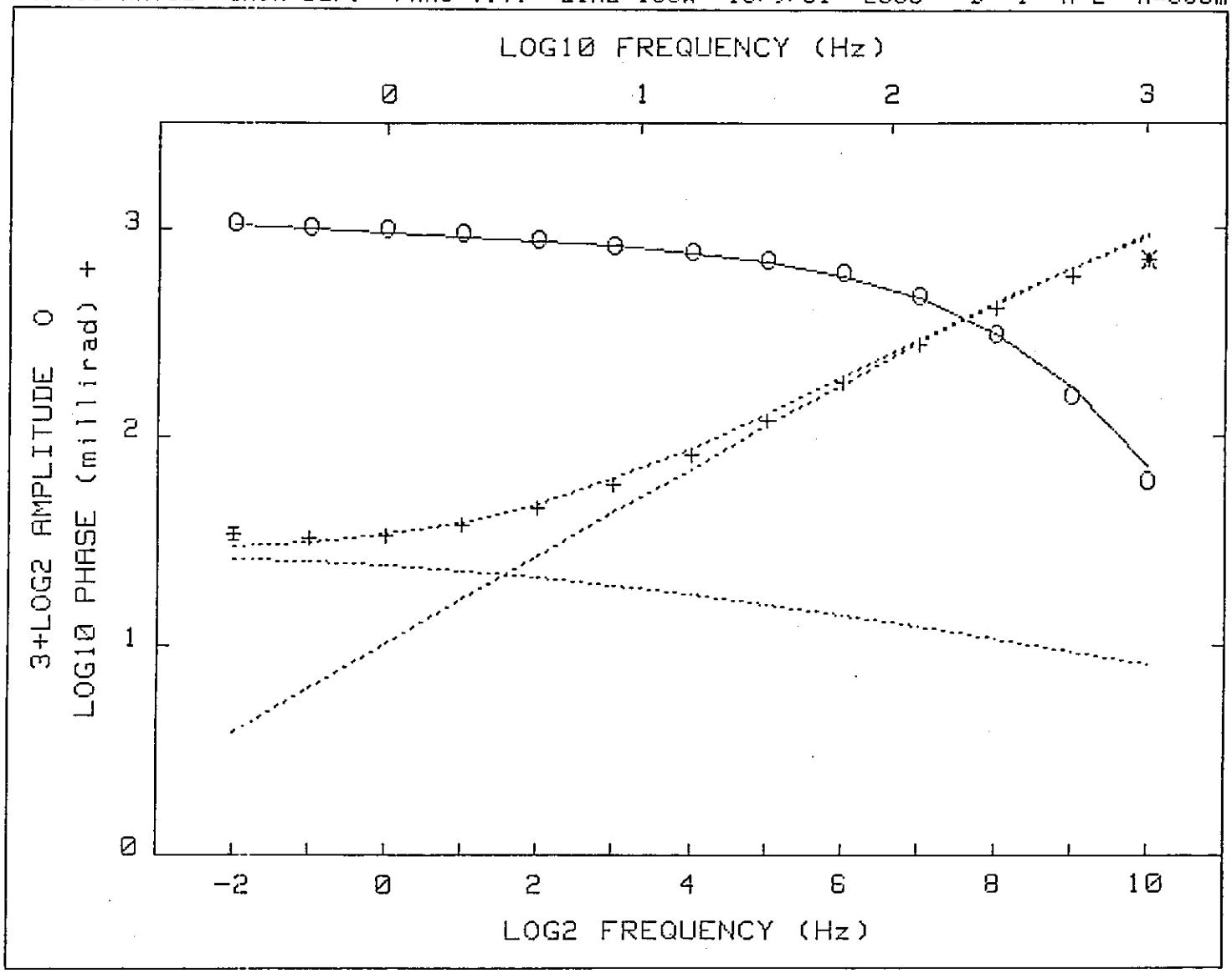

CRL: Number of dispersions= 2
C1=.25 M2=1 fixed

Iter	Lambda	Rchsq	R0	M1	T1	T2	C2
0	1.E-02	.00510	1.180	.225	1.0E+02	1.8E-04	.662
1	1.E-02	.00175	1.297	.293	7.8E+01	1.7E-04	.660
2	1.E-03	.00129	1.190	.235	9.6E+00	1.9E-04	.671
3	1.E-03	.00100	1.193	.239	4.7E+00	1.9E-04	.690
4	1.E-03	.00099	1.183	.235	3.4E+00	1.9E-04	.692

Pct Std Deviations	6.9	12.8	999.9	9.8	5.1	
Correlation Matrix	1.000					
	.947	1.000				
	.987	.910	1.000			
	-.821	-.777	-.825	1.000		
	-.799	-.621	-.831	.862	1.000	

Apparent Resistivity Measured at 1 Hz is 232.4
Apparent Resistivity Calculated from Inductive Coupling is 252.7

CYPRUS ANVIL GRUM DEP. FARO Y.T. LINE 108W 16/9/81 L330 D=10 N=1 X=305m

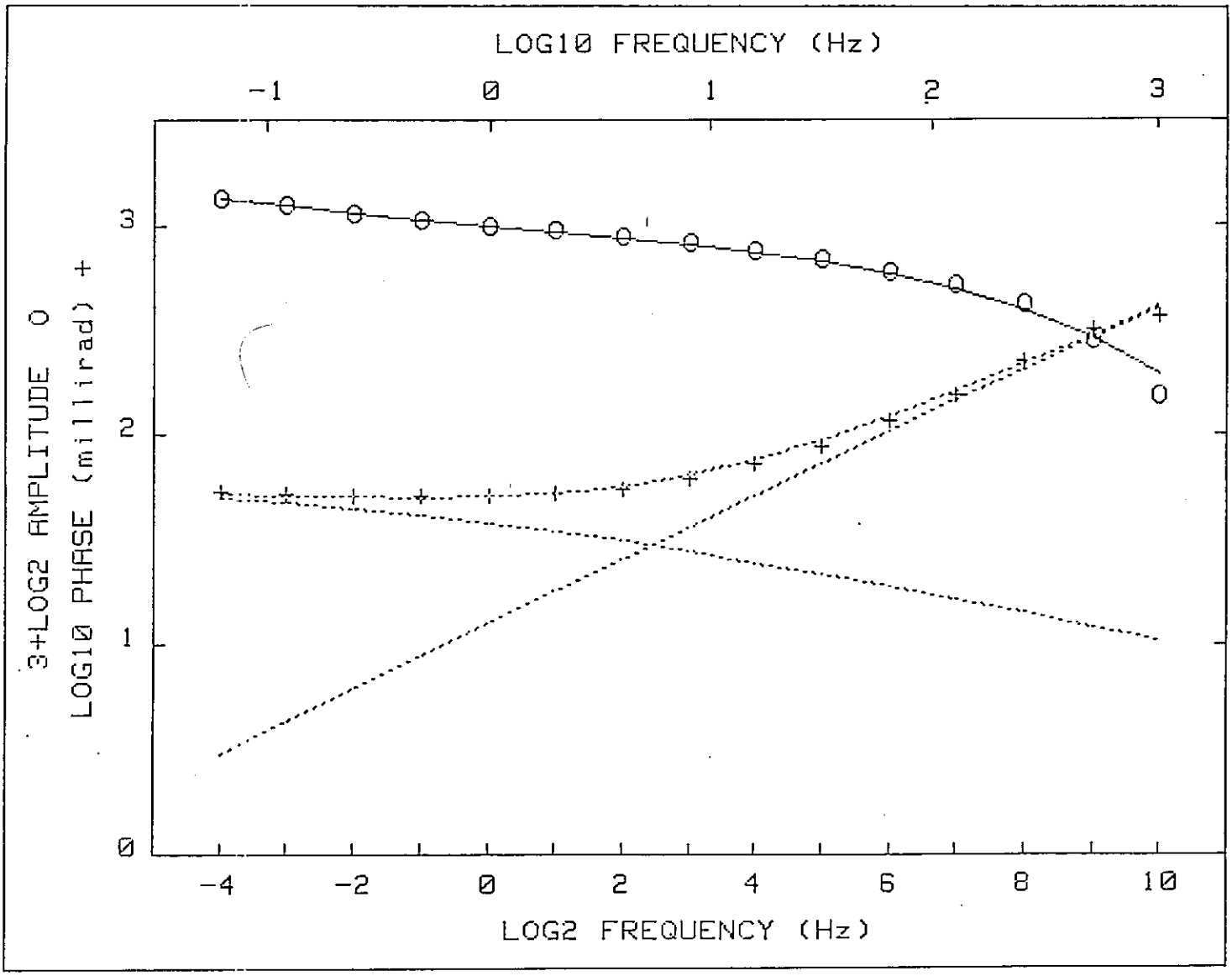

CRL: Number of dispersions= 2
C1=.25 M2=1 fixed

Iter	Lambda	Rchsq	R0	M1	T1	T2	C2
0	1.E-02	.02755	1.453	.365	4.2E+01	7.6E-05	.489
1	1.E-02	.00181	1.469	.388	3.5E+01	2.4E-05	.471
2	1.E-03	.00081	1.502	.409	3.6E+01	2.0E-05	.501
3	1.E-04	.00079	1.544	.418	6.4E+01	1.9E-05	.490
4	1.E-05	.00079	1.517	.411	4.5E+01	2.0E-05	.497

Pct Std Deviations	11.0	11.6	539.4	36.5	7.4	
Correlation Matrix	1.000					
	.988	1.000				
	.992	.967	1.000			
	-.952	-.929	-.951	1.000		
	-.849	-.777	-.880	.927	1.000	

Apparent Resistivity Measured at 1 Hz is 237.9
Apparent Resistivity Calculated from Inductive Coupling is 169.5

CYPRUS ANVIL GRUM DEP. FARO Y.T. LINE 108W 16/9/81 L330 D=10 N=2 X=305m

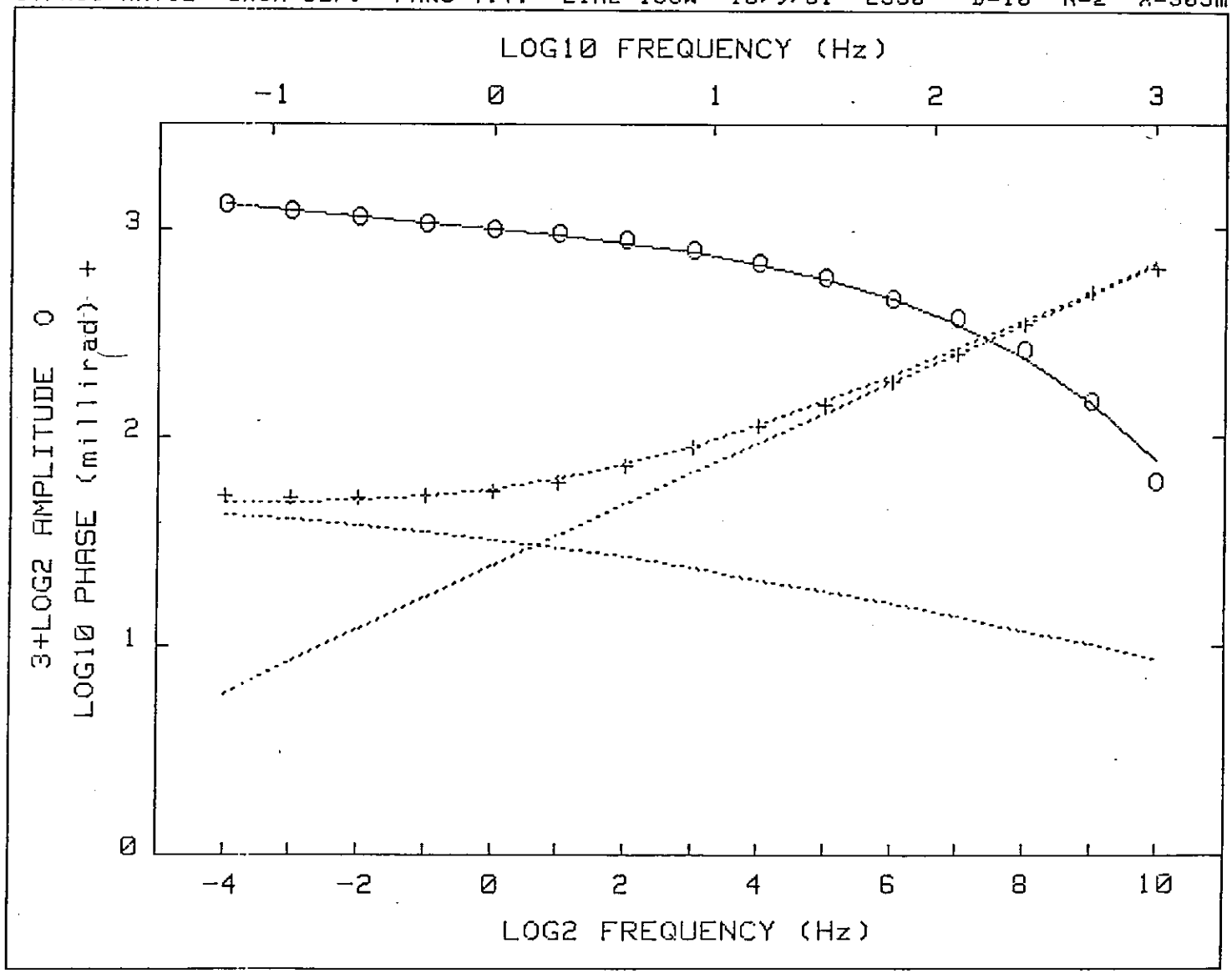

CRL: Number of dispersions= 2
C1=.25 M2=1 fixed

Iter	Lambda	Rchsq	R0	M1	T1	T2	C2
0	1.E-02	.01336	1.394	.311	1.5E+02	2.1E-04	.541
1	1.E-02	.00179	1.480	.362	1.1E+02	8.7E-05	.467
2	1.E-03	.00079	1.471	.370	5.5E+01	7.3E-05	.483
3	1.E-03	.00079	1.453	.365	4.2E+01	7.6E-05	.489

Pct Std Deviations	12.8	14.5	999.9	33.4	8.2	
Correlation Matrix	1.000					
	.985	1.000				
	.994	.966	1.000			
	-.976	-.972	-.966	1.000		
	-.930	-.868	-.945	.933	1.000	

Apparent Resistivity Measured at 1 Hz is 483.9
Apparent Resistivity Calculated from Inductive Coupling is 105.9

proper electrode interval is used. However, the measurements are difficult to make due to the low signal voltage levels and the high electrical noise levels.

These spectral plots are too unreliable to permit accurate inversions to be made to determine the electrical parameters of the IP dispersion. This is one of the more useful features of the Spectral IP Method and steps have been taken to assure better low frequency data. In further work in the Faro Area, a high-power IP transmitter will be used (15KVA to 30KVA). The higher current levels this power will permit will give higher voltage levels and smaller standard deviations.

A further step that would aid with the interpretation of deep, indistinct anomalies, would be to double the density of the data on the pseudosection plotter. This can be accomplished by, for instance, repeating the X = 1000' measurements with the electrode positions shifted by 500'.

With these extra steps, the deep anomalies expected from the deep sources in the Faro Area should be more easily interpreted.

PHOENIX GEOPHYSICS LIMITED

Philip G. Hallof, Ph.D.
Geophysicist

PROFESSIONAL ENGINEER PROVINCE OF BRITISH COLUMBIA P.G. HALLOF

Expiry Date: February 25, 1982

Dated: February 2, 1982

CERTIFICATE

I, Philip George Hallof, of the City of Toronto, Province of Ontario, do hereby certify that:

1. I am a geophysicist residing at Suite 3505, 2045 Lakeshore Blvd. W., Toronto, Ontario.

2. I am a graduate of the Massachusetts Institute of Technology with a B.Sc. Degree (1952) in Geology and Geophysics, and a Ph.D. Degree (1957) in Geophysics.

3. I am a member of the Society of Exploration Geophysicists and the European Association of the Exploration Geophysicists.

4. I am a Professional Geophysicist, registered in the Province of Ontario, the Province of British Columbia and the State of Arizona.

5. I have no direct or indirect interest, nor do I expect to receive any interest directly or indirectly, in the property or securities of Cyprus-Anvil Mines Ltd., or any affiliate.

6. The statements made in this report are based on a study of published geological literature and unpublished private reports.

7. Permission is granted to use in whole or in part for assessment and qualification requirements but nor for advertising purposes.

Dated at Toronto

This 2nd day of February, 1982

Philip G. Hallof, Ph.D.

PROFESSIONAL ENGINEER
P. HALLOF
BRITISH COLUMBIA
ENGINEER

Expiry Date: February 25, 1982

RECENT AND FUTURE ADVANCES IN THE INDUCED POLARIZATION METHOD

by

Philip G. Hallof, Ph.D., and William H. Pelton, Ph.D.

Prepared for Presentation
at the Prospectors and Developers Convention
Royal York Hotel, Toronto
March 8th to March 11th, 1981

- -

RECENT AND FUTURE ADVANCES IN THE INDUCED POLARIZATION METHOD

BY

Philip G. Hallof, Ph.D., and William H. Pelton, Ph.D.

INTRODUCTION

The induced polarization (IP) method was introduced into Canadian exploration practice in the period from 1955 to 1960. Two measurement techniques were widely used, the pulse-transient method (time domain) and the variable frequency method (frequency domain). In the fifteen years following 1960, striking improvements were made in both frequency domain and time domain IP equipment, but only limited progress was made in a better understanding of the IP phenomenon, its source, and how to use it.

However, in the five year period since 1975, considerable progress has been made in our understanding of the IP method. Beginning with an understanding of the exact equivalence of the IP measurements in the phase-domain, the frequency-domain and the time-domain (see Figure 1), we have progressed to the study of the IP effect over the entire frequency range of interest. These studies have led to a greatly advanced understanding of the IP method in at least three important areas:-

i) Our understanding of the IP phenomenon itself has been vastly increased. A greater knowledge of the source of the IP effect and its detailed behavior has suggested additional uses for the method, beyond the simple detection of anomalies.

ii) A better idea of what we wanted to measure, and modern solid-state electronics, have resulted in greatly improved measurement techniques and instrumentation.

iii) The advent of smaller, less expensive digital computers has greatly helped with the interpretation of IP field data. Rapid forward problem solutions and the possibility of direct inversion of IP field data have made it possible for the geophysicists to give the exploration geologist a much better picture of just what the source of a particular IP anomaly might be.

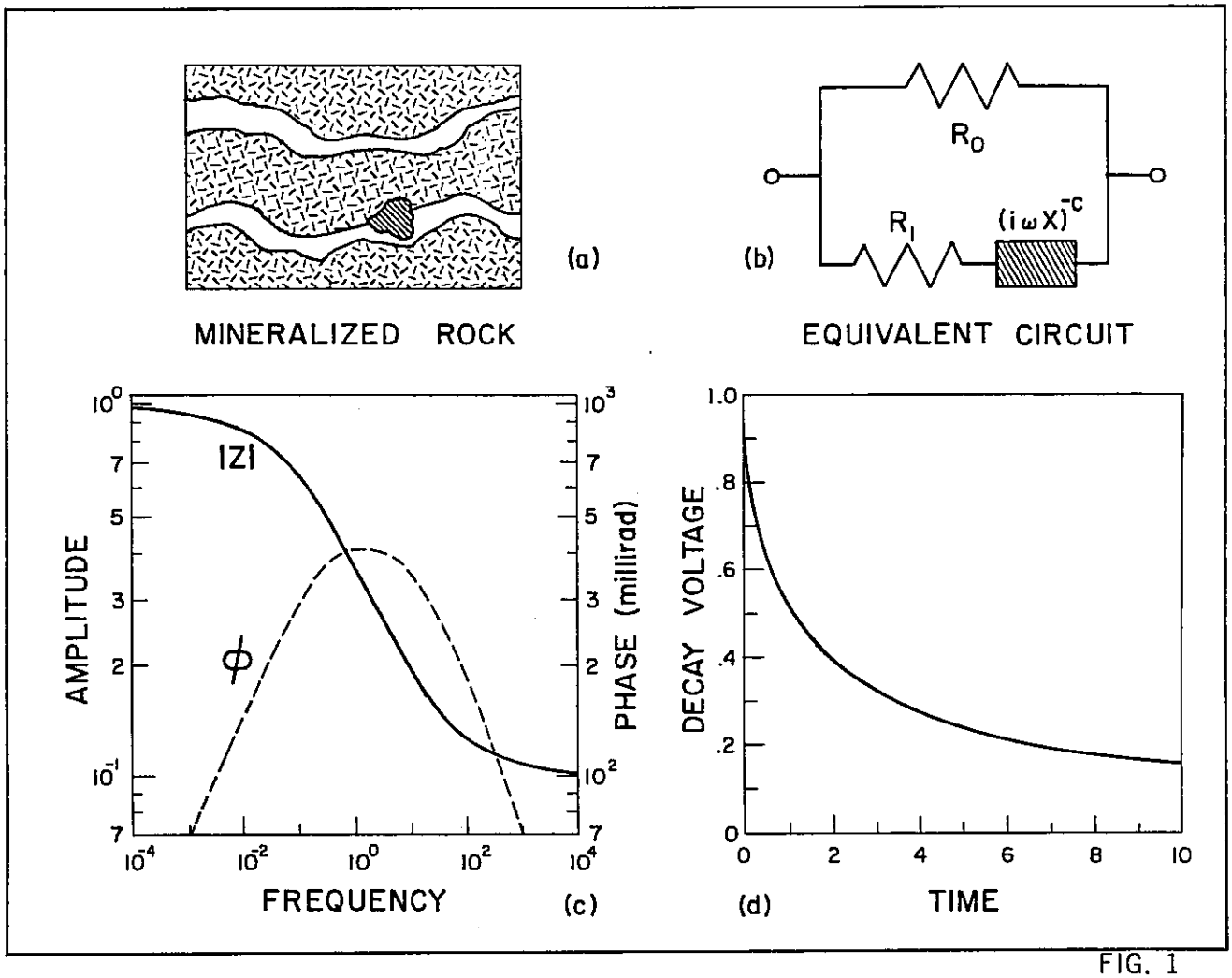

FIG. 1

WHAT IS THE NATURE OF THE IP EFFECT

Spectral induced polarization measurements (the measurement of the phase shifts over a wide frequency range) in open-pit mines, gave the first information concerning the detailed nature of the IP phenomenon. It became clear that four parameters, not just two (resistivity and IP

effect) were necessary to completely describe the IP effect.

The equation shown on Figure 2 and Figure 3 is formally known as the Cole-Cole Dispersion Equation; the four electrical parameters are:

Ro - the dc resistivity value

m - the IP effect (in non-dimensional form)

τ - the time constant of the IP effect

c - the exponent of the frequency (ω)

Since the very beginning of our experience with spectral IP measurements, we have found that these four parameters, and the Cole-Cole equation will adequately describe any IP effect that has been measured. The first measurements were made using one meter electrode intervals, within open-pit mines. The circles on Figure 4 and Figure 5 show the data points measured over massive graphite and massive sulphides at the Anvil Mine. As the solid line curves on the drawings show, the measured data points can be almost exactly replaced using a Cole-Cole Dispersion.

The four parameters obtained by the computer inversion of the graphite data are typical of those that have been measured over all graphite deposits. The IP effect is very large and the time constant (τ) is much greater than 1.0 seconds.

Large IP effects are also measured over massive sulphide sources. However, invariably the time constant value for (τ) is less than 1.0 seconds. The measurements shown on Figure 6 are for a massive sulphide source at the Kidd Creek Mine; again there is a large IP effect, and a small time constant.

The critical frequency (Fc) for a Cole-Cole Dispersion is defined as that frequency for which the maximum phase-shift is measured. An examination of the equation and curves in Figure 2 shows that as the time-constant (τ) is increased by a factor of ten, the critical frequency (Fc) will decrease by a factor of ten. Therefore, we can expect that for the spectral IP response of polarizable sources (Fc) will be inversely proportional to (τ).

An understanding of the physical parameters that affect the time-constant (τ) of a spectral IP response has come from two areas of research. One is the study of the spectral IP response from artificial rocks; these samples are prepared using metallic particles of known material and size (see Figure 8 for example). The second line of attack has been to formulate the mathematical expressions that might describe the macro-characteristics of conduction in a mineralized rock, with certain simplifying assumptions. Initially spherical particles were assumed for this work and an example of the predicted spectral results is shown on Figure 7.

We have shown these two different sets of data, because they are very similar in character. Further, they show the same result that all of

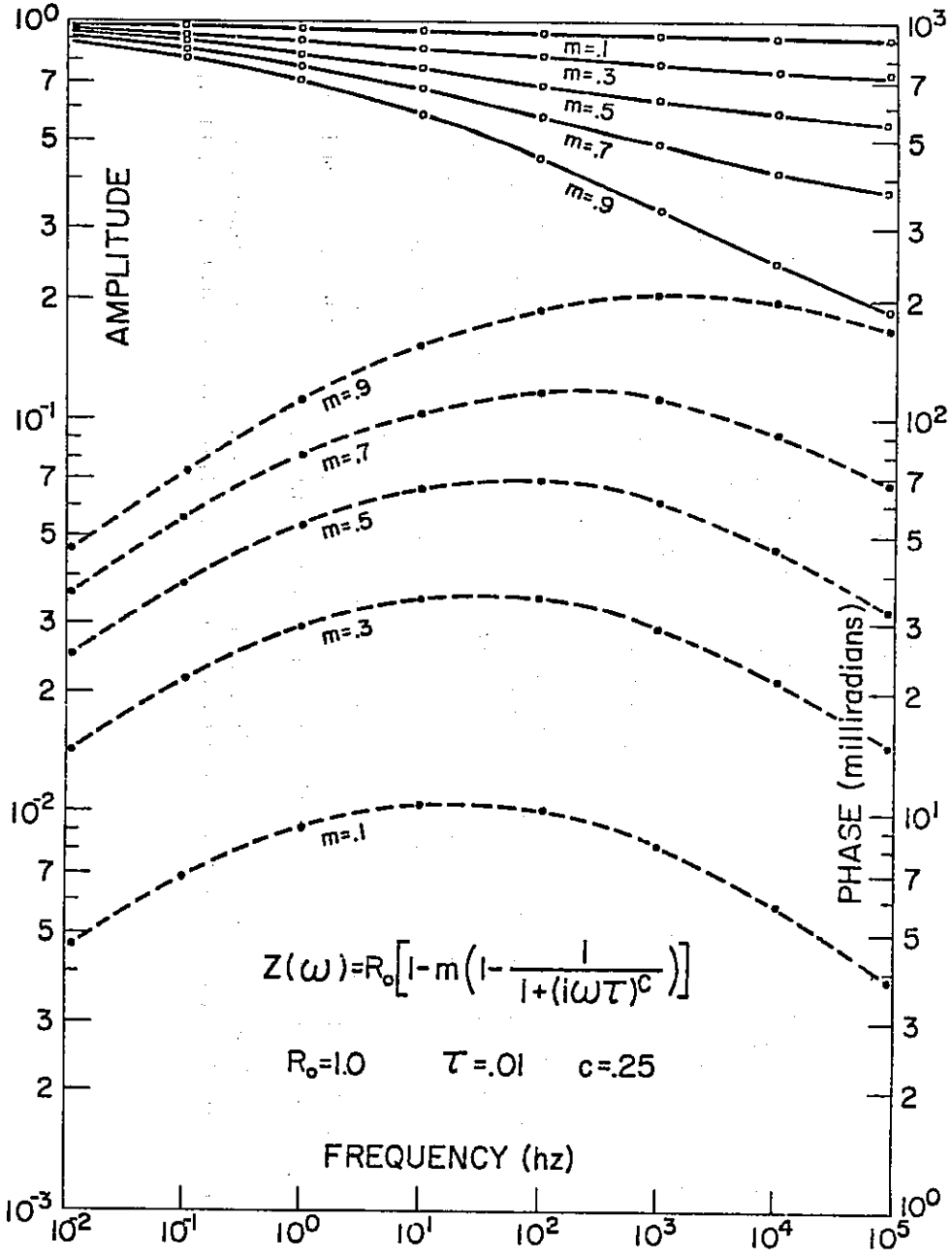
AMPLITUDE
PHASE (milliradians)
m=.1
m=.3
m=.5
m=.7
m=.9
$Z(\omega)=R_o\left[1-m\left(1-\frac{1}{1+(i\omega\tau)^c}\right)\right]$
R_o=1.0 τ=.01 c=.25
FREQUENCY (hz)

FIG. 2

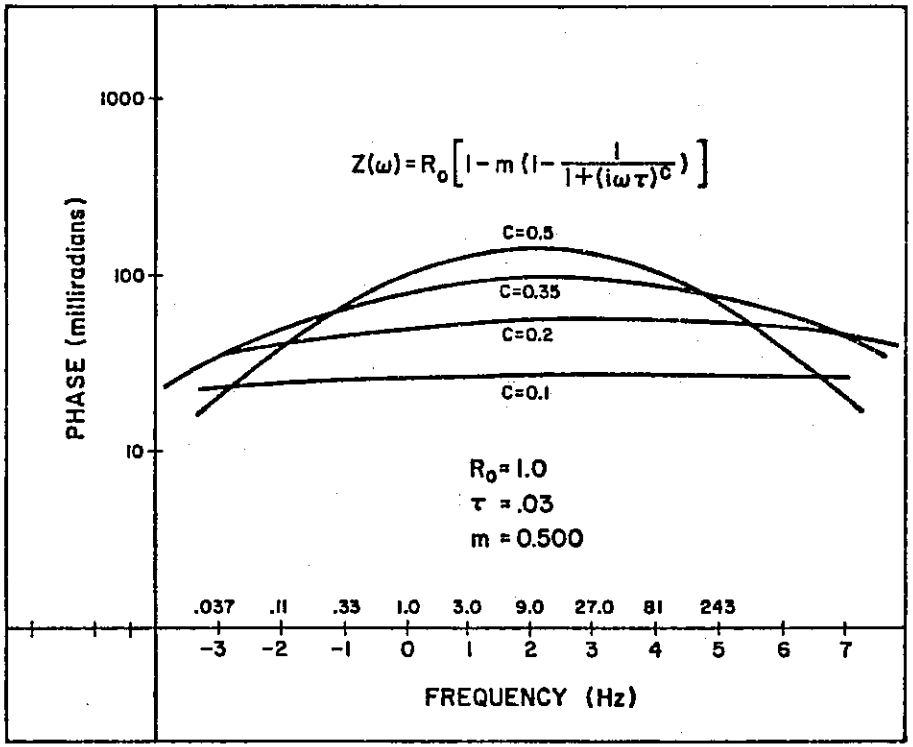
PHASE (milliradians)
$Z(\omega)=R_o\left[1-m\left(1-\frac{1}{1+(i\omega\tau)^c}\right)\right]$
C=0.5
C=0.35
C=0.2
C=0.1
R_o=1.0
τ=.03
m=0.500
.037 .11 .33 1.0 3.0 9.0 27.0 81 243
FREQUENCY (Hz)

FIG. 3

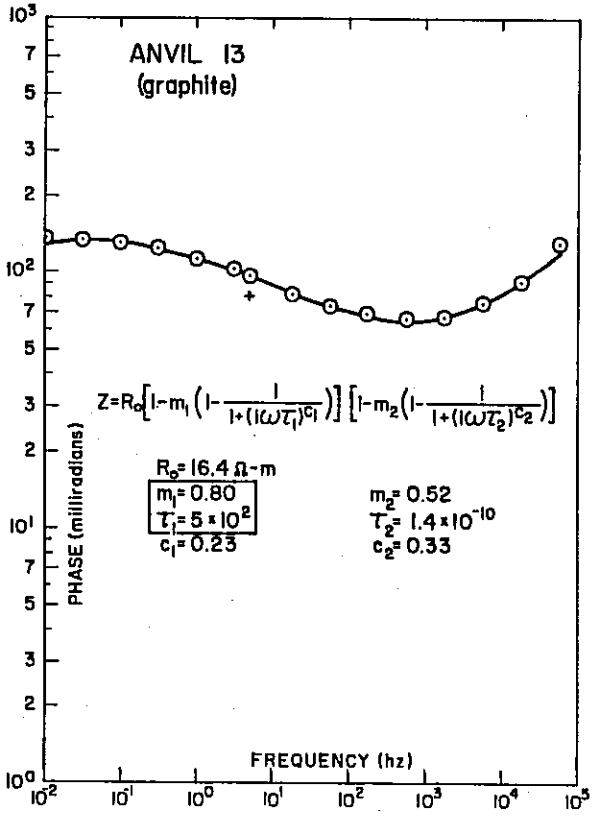

FIG. 4

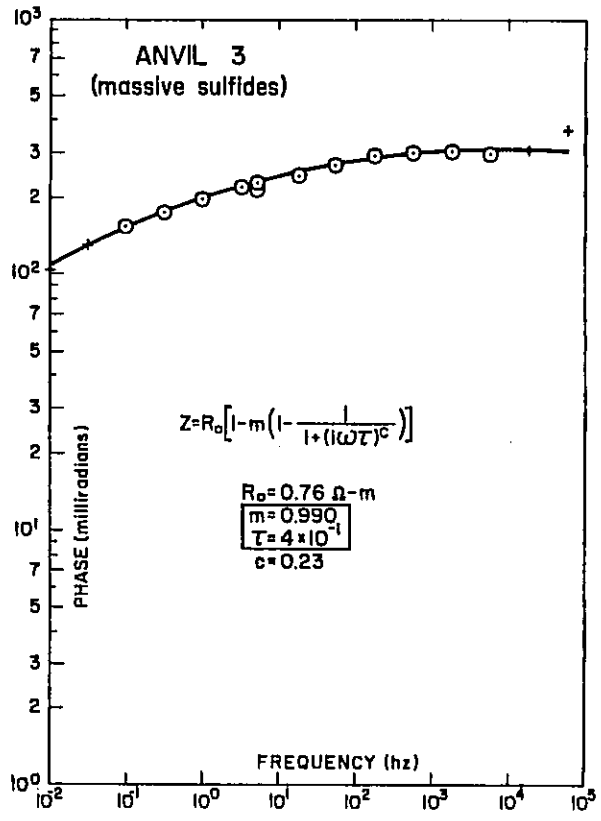

FIG. 5

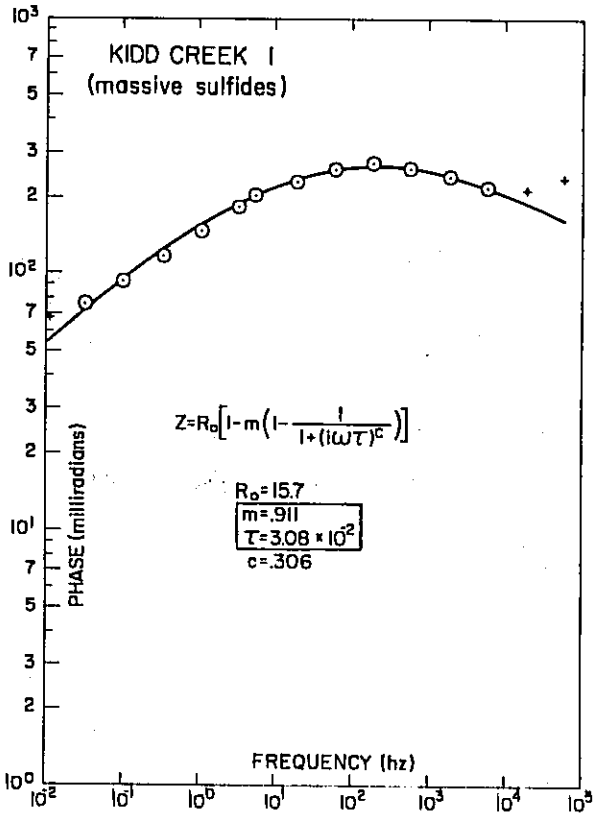

FIG. 6

THEORETICAL RESULTS FOR VARIATION IN GRAIN SIZE OF POLARIZABLE PARTICLE

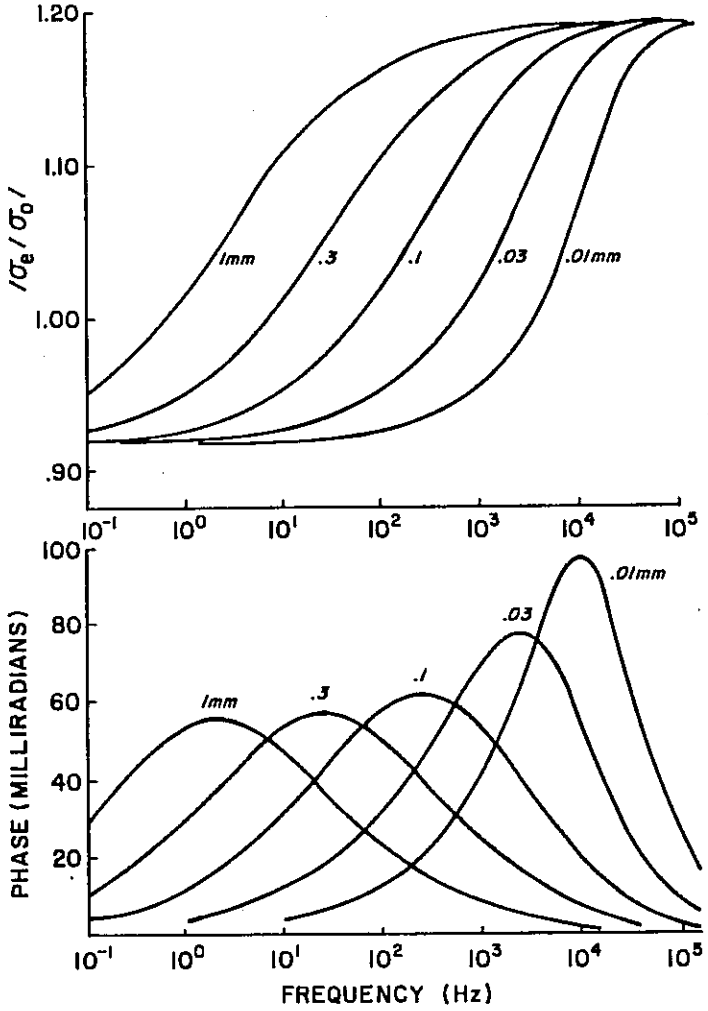

from Wong

FIG. 7

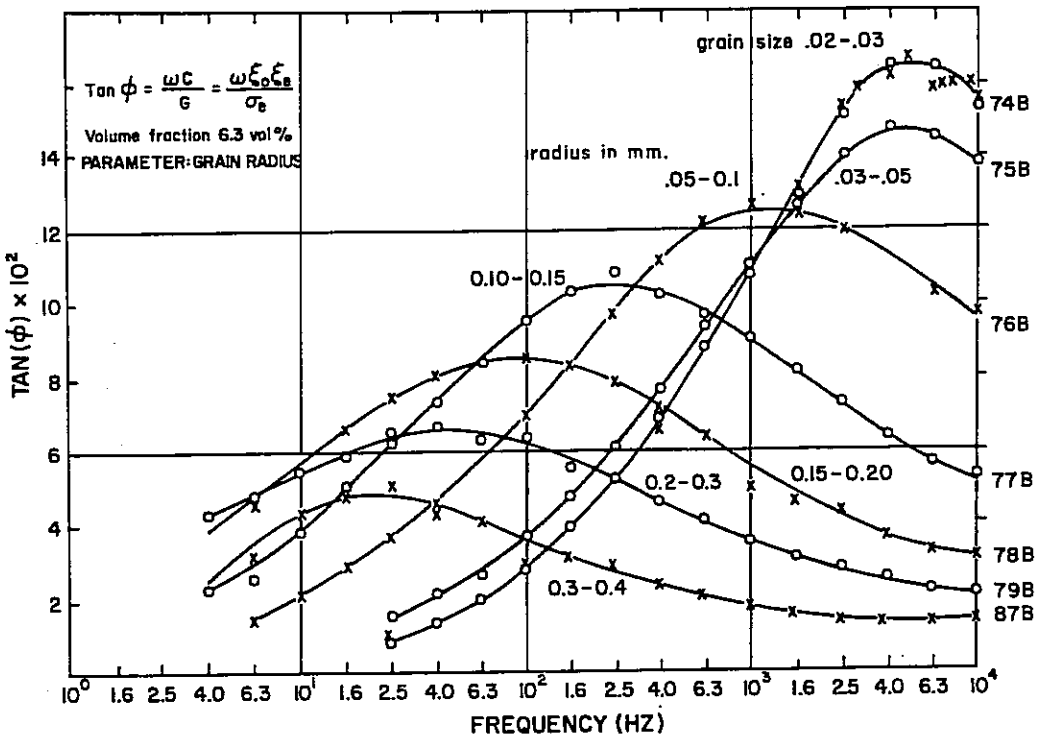

from Wong
data by Grissemann

FIG. 8

our research has shown. The time-constant (τ) of a spectral IP dispersion curve is directly related to the physical size of the metallic particles that are the source of the IP effect. The critical (Fc) is therefore inversely related to the grain-size. Thus, for all of the massive sulphide deposits for which we have spectral measurements, the effective grain-size of the polarizable particles is appreciably smaller than that for graphite sources.

There is one additional test we have devised to confirm the validity of the electrochemical model we have developed to describe the detailed nature of the IP phenomenon. The spectral IP results for a single mineral electrode (pyrite, chalcopyrite, bornite, galena, etc.) immersed in distilled water can be measured, and then inverted using the computer. This inversion determines the various electrical parameters that describe the electrical transfer function for that particular mineral. These electrical parameters, and the analytically determined concentrations of the metal cation in the solution after steady-state current flow has been achieved, can be used to calculate the reaction valence (total number of electrons involved) of the chemical reaction at the interface. This measured value of the reaction valence can be compared to the various values that would be possible from various chemical reactions.

In past research, these measured numbers have not agreed within an order of magnitude with those predicted by the commonly accepted dissolution reaction equations for the various sulphide minerals. The results we have achieved for galena (Figure 10) and chalcopyrite (Figure 9) are typical of the work that has been done recently. The measured values of the reaction valence give much closer agreement to the predicted valence than was previously the case. For chalcopyrite, the predicted reaction varies with the copper ion concentration, and the agreement is still quite acceptable.

With the success of the above described research, has come the implication that we may now understand the IP phenomenon well enough to use some of our knowledge in a predictive way. The resistivity and phase-shift data plotted in the pseudo-section format on Figure 11 are from the Kennedy Property near Winnemucca, Nevada. The results suggest a broad, weak IP anomaly that might be due to a "porphyry copper" type source containing a small concentration of metallic mineralization. However, one notices immediately that the phase-shifts measured at 9.0 Hz are the same magnitude as those measured at 0.11 Hz (a factor of 3^{-4} lower in frequency). This is the same Spectral IP characteristic that was previously measured at the Brenda Mine in British Columbia.

This unusual circumstance is confirmed by the spectral plots for two typical dipole pairs, shown in Figure 12 and Figure 13. With the inductive coupling effects removed by computer inversion, the phase-shift vs. frequency curve is very flat over a frequency range of 3^{8}Hz. This requires a very low (c_1) value of 0.125 (see Figure 3); more importantly, a value of IP effect (m) in excess of 0.500 is necessary. Therefore, although the measured phase-shifts are low in magnitude, the true IP effect within the source material must be large. This should not be considered to be a weak anomaly.

CHALCOPYRITE

$[CuSO_4]$ 0	10^{-5}	10^{-4}	10^{-3}	Reaction Valence
4.6 3.5 3.6	1.5	.95	.53	Measured
4.0	1.33	1.33		Actual

$$CuFeS_2 \longleftrightarrow Cu^{2+} + Fe^{2+} + 2S + 4e^-$$

$$\frac{2}{3}\,CuFeS_2 + Cu^{2+} + \frac{4}{3}e^- \longleftrightarrow \frac{1}{3}\,Cu_5FeS_4 + \frac{1}{3}\,Fe^{2+}$$

(Wadsworth, 1980)

FIG. 9

GALENA

[NaCl] 0.10	Reaction Valence
1.6 1.6	Measured
2.0	Actual

$$PbS \longleftrightarrow Pb^{2+} + S^0 + 2e^-$$

(Sato, 1960)

FIG. 10

E-T

W A BOWES KENNEDY AREA WINNEMUCCA NEVADA X=200 JUNE 1979

Apparent Resistivity(ohm-m)

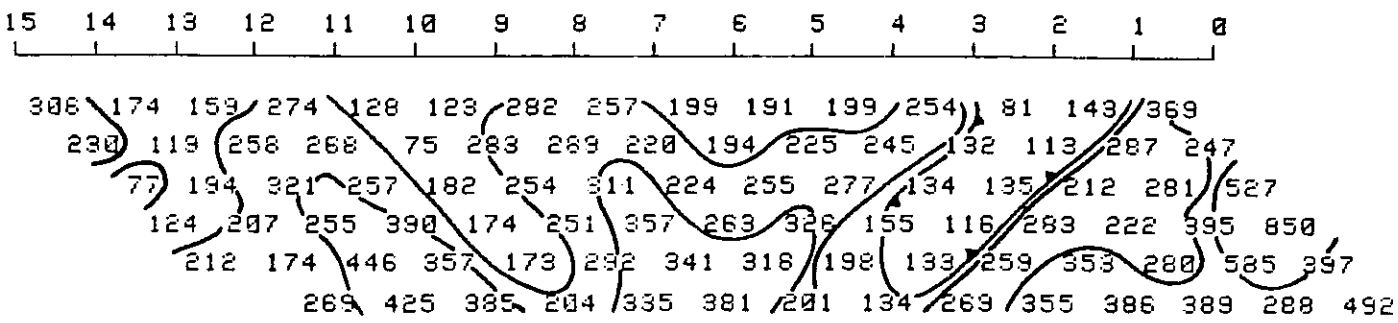

Decoupled Phase(mrad) 9 Hz

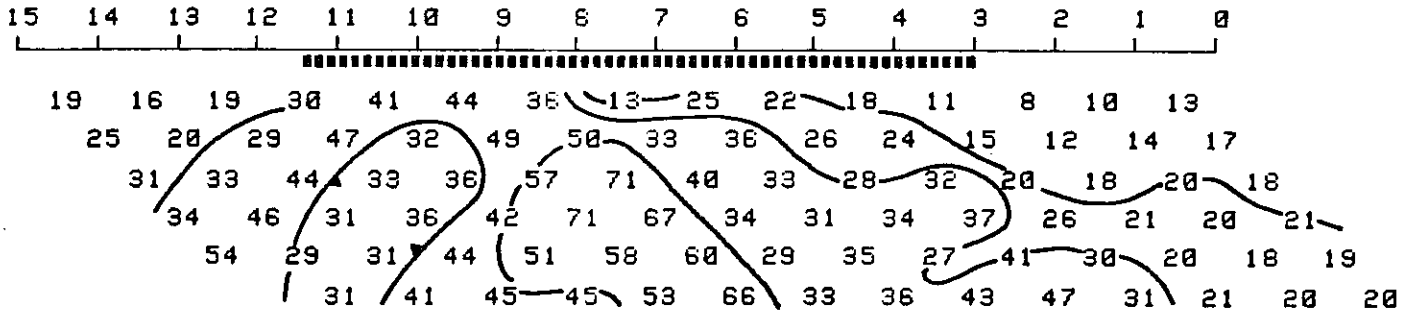

Decoupled Phase(mrad) .1111 Hz

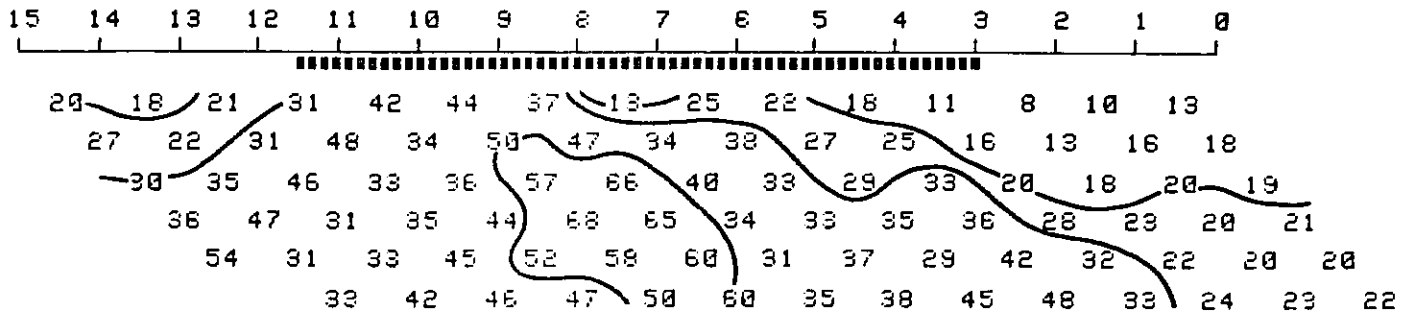

FIG. 11

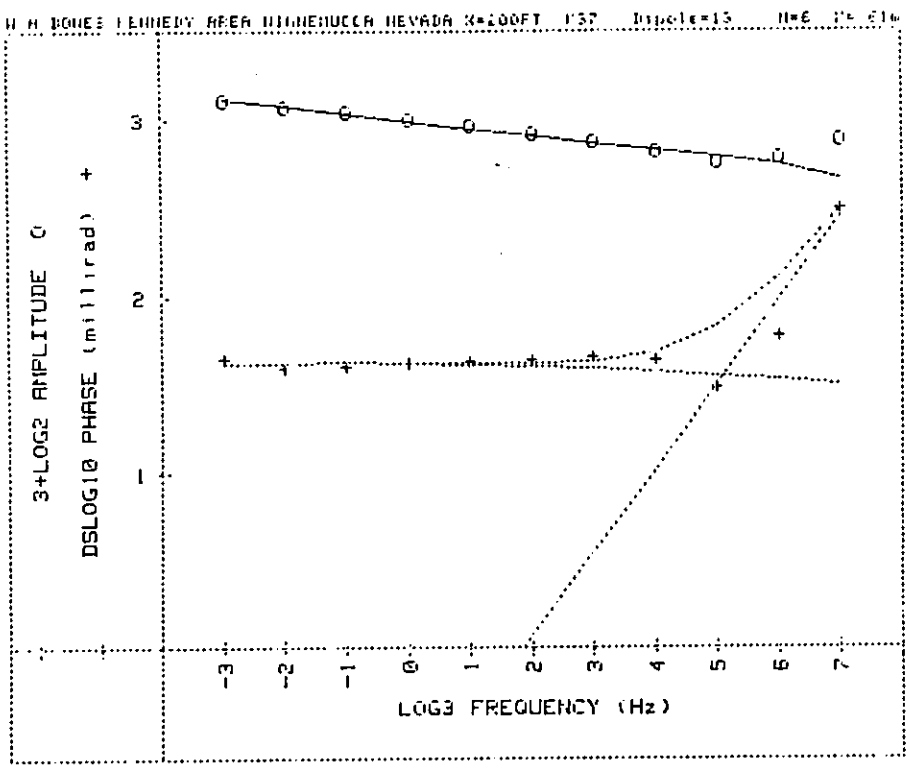

Iter	Lambda	Rchsq	P0	M1	T1	C1	M2	T2	C2
0	1.E-02	.00068	1.599	.567	2.0E+01	.125	1.000	2.0E-05	.992
1	1.E-01	.00064	1.599	.566	2.0E+01	.125	1.000	2.1E-05	1.000
2	1.E+00	.00063	1.596	.564	2.0E+01	.125	1.000	2.1E-05	1.000
3	1.E+00	.00063	1.595	.563	2.0E+01	.125	1.000	2.1E-05	1.000

Pct Std Deviations	5.4	1.6	499.4	0.0	0.0	10.5	9.8	
Correlation Matrix	1.0000							
	.5235	1.0000						
	.9782	.3667	1.0000					
	0.0000	0.0000	0.0000	0.0000				
	0.0000	0.0000	0.0000	0.0000	0.0000			
	-.3604	.0864	-.3990	0.0000	0.0000	1.0000		
	-.6447	.0924	-.7125	0.0000	0.0000	.7305	1.0000	

Apparent Resistivity Measured at 1 Hz is 425

Apparent Resistivity Calculated from Inductive Coupling is 2117

FIG. 12

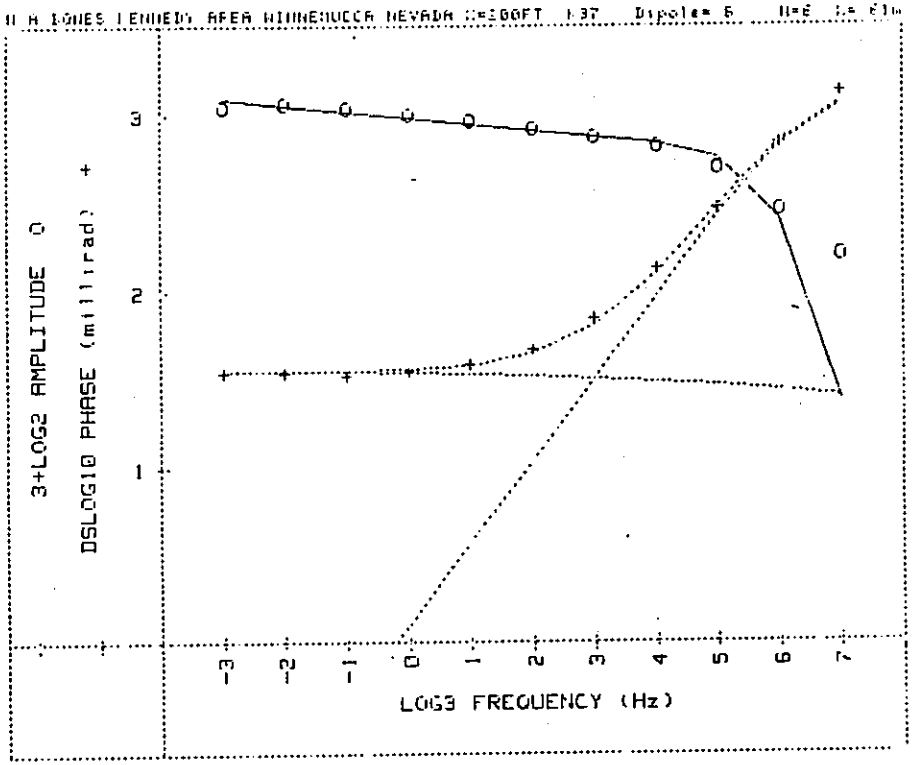

Iter	Lambda	Rchsq	P0	M1	T1	C1	M2	T2	C2
0	1.E-02	.00102	1.482	.517	2.0E+01	.125	1.000	1.8E-04	.977
1	1.E-01	.00162	1.481	.518	1.9E+01	.125	1.000	1.8E-04	.978

Pct Std Deviations	6.7	2.6	1243.0	0.0	0.0	5.4	2.8	
Correlation Matrix	1.0000							
	.6234	1.0000						
	.9788	.4657	1.0000					
	0.0000	0.0000	0.0000	0.0000				
	0.0000	0.0000	0.0000	0.0000	0.0000			
	.1989	.0726	.2067	0.0000	0.0000	1.0000		
	-.4224	.0478	-.4586	0.0000	0.0000	.4189	1.0000	

Apparent Resistivity Measured at 1 Hz is 201

Apparent Resistivity Calculated from Inductive Coupling is 235

FIG. 13

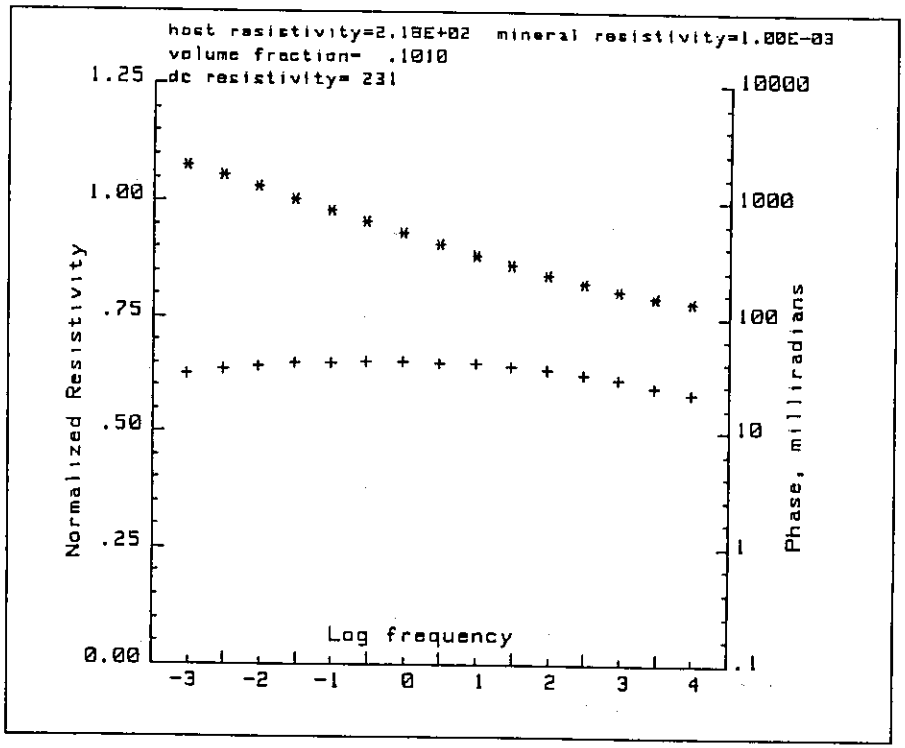
host resistivity=2.18E+02 mineral resistivity=1.00E-03
volume fraction= .1010
dc resistivity= 231
Normalized Resistivity
Phase, milliradians
Log frequency
1.25
1.00
.75
.50
.25
0.00
10000
1000
100
10
1
.1
-3
-2
-1
0
1
2
3
4

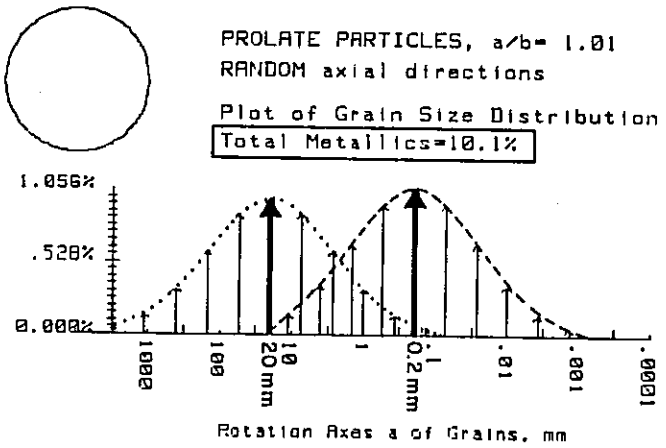
PROLATE PARTICLES, a/b= 1.01
RANDOM axial directions
Plot of Grain Size Distribution
Total Metallics=10.1%
Volume %
1.056%
.528%
0.000%
1000
100
20mm
10
1
0.2mm
.1
.01
.001
.0001
Rotation Axes a of Grains, mm

FIG. 14

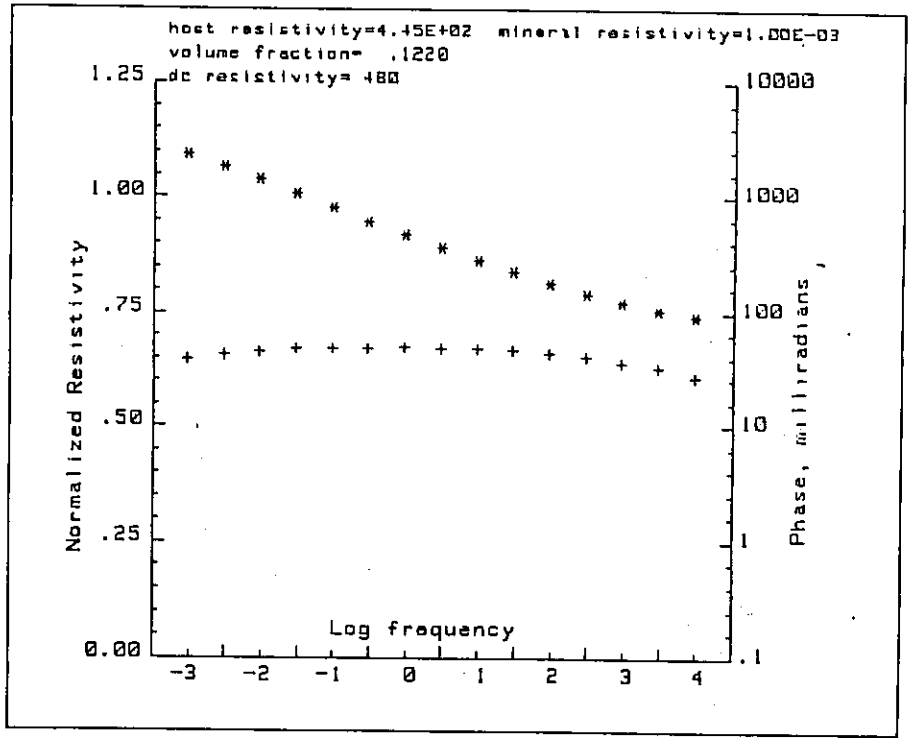
host resistivity=4.45E+02 mineral resistivity=1.00E-03
volume fraction= .1220
dc resistivity= 480
Normalized Resistivity
Phase, milliradians
Log frequency
1.25
1.00
.75
.50
.25
0.00
10000
1000
100
10
1
.1
-3
-2
-1
0
1
2
3
4

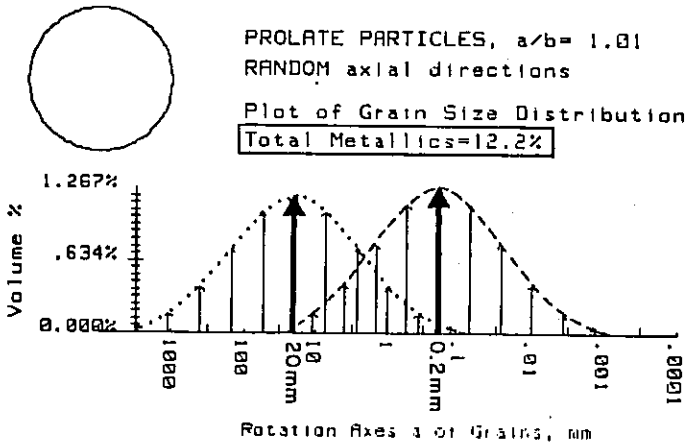
PROLATE PARTICLES, a/b= 1.01
RANDOM axial directions
Plot of Grain Size Distribution
Total Metallics=12.2%
Volume %
1.267%
.634%
0.000%
1000
100
20mm
10
1
0.2mm
.1
.01
.001
.0001
Rotation Axes a of Grains, mm

FIG. 15

We used these results in our first attempt to predict the nature of the mineralization that is the source of the "weak" anomaly shown in Figure 11. The mathematical formula used to predict the spectra shown in Figure 7 has been expanded to include prolate and oblate spheroids, as well as spheres, of metallic material. By a trial and error process, the spectra shown in Figure 14 and Figure 15 were generated as being a "good fit" to the measured data.

The chosen parameters for the sources are probably not unique; however, some valid points can be drawn from the calculation presented.

i) the flat spectrum (small c value) cannot be obtained from a single grain-size (time-constant) population. There must be at least two different grain-size populations present.

ii) Although the two grain-size distributions, with mean values of 20mm and 0.2mm, are probably not exactly correct, a difference of at least two orders of magnitude is necessary to produce the value c = 0.125.

iii) Despite the low magnitude for the IP field anomaly, the true IP effect within the source is large ($m_1 > 0.500$) and this results in a fairly high concentration of metallic mineralization predicted for the source (10 - 12% total metallic mineralization).

The first drill hole at the Kennedy Project is now nearing completion; it was collared at approximately station No. 5 along the line of data shown in Figure 11. There was metallic mineralization throughout the drill hole, with an increase below about 75-80 meters of depth.

Throughout the entire length of the drill hole (in excess of 250 meters), there were two different types of mineralization present. There were veinlets (large grain-size) that might, or might not, contain quartz. All of the veinlets contained chalcopyrite or molybdenite or chalcopyrite with molybdenite; some pyrite was also present. There was also fine-grained disseminated metallic magnetite throughout the hole (the small grain-sized source). The magnetite contains appreciable gold value; there is enough gold present to give detectable assays throughout the length of the hole.

We do not have enough information to determine if the total concentration of metallic mineralization approaches 10 to 12 percent. However, in other respects the source of the IP anomaly does seem to approximate that predicted by the spectral IP analysis.

IMPROVED MEASUREMENT TECHNIQUES AND INSTRUMENTATION

The much publicized "explosion" in solid-state, semi-conductor

electronic components has produced as many changes in the geophysical instrumentation industry as it has in other phases of modern life. Beginning with diodes and transistors and now including complex microprocessor chips, there has been a bewildering number of improvements in this industry. They have resulted in a major reduction in the size of, and the power requirements of (smaller battery packs), geophysical field instruments; at the same time the reliability, digital data storage capability and analysis capability have been almost infinitely increased.

The Phoenix IPV-2, Prospecting Phase IP system is an example of one of the least complicated units that can be engineered with modern electronics. The types of features that can now be made available are:

i) Microprocessor-controlled signal stacking of each measurement to give almost infinite noise rejection through coherent detection.

ii) Matched, heated crystal clocks give phase stability between current source and voltmeter without connecting cable.

iii) Dual-channel electronics permits two separate voltages to be measured simultaneously.

iv) Digital readout of magnitude and phase-shift of measured voltage at either channel.

v) Five frequency capability (0.11, 0.33, 1.0, 3.0, 9.0 Hz) permits limited analysis of spectral character of any anomaly.

vi) Appreciable increase in survey speed over either frequency-domain or time-domain IP systems.

By completing a reconnaissance survey with a single frequency (typically 0.33 Hz or 1.0 Hz) it is possible to achieve the lowest cost possible for IP field surveys. However, once an anomaly is detected, the IPV-2 can be used to make detailed measurements that give some feeling for the character of the spectral response of the source.

If detailed measurements are made at only two frequencies, it is possible to make some statement about the critical frequency (Fc) of the IP spectrum from the source. On Figure 17 and Figure 18 are shown the detailed phase-IP measurements made using X = 100' and 0.33 Hz over two anomalies previously located by a reconnaissance IP survey using larger electrode intervals. On both Line 18E and Line 15E the anomalous pattern indicates a relatively narrow source, with some depth to the top.

During the detailed survey with X = 100', several of the anomalous values in each anomalous pattern were measured at both 0.33 Hz and 3.0 Hz.

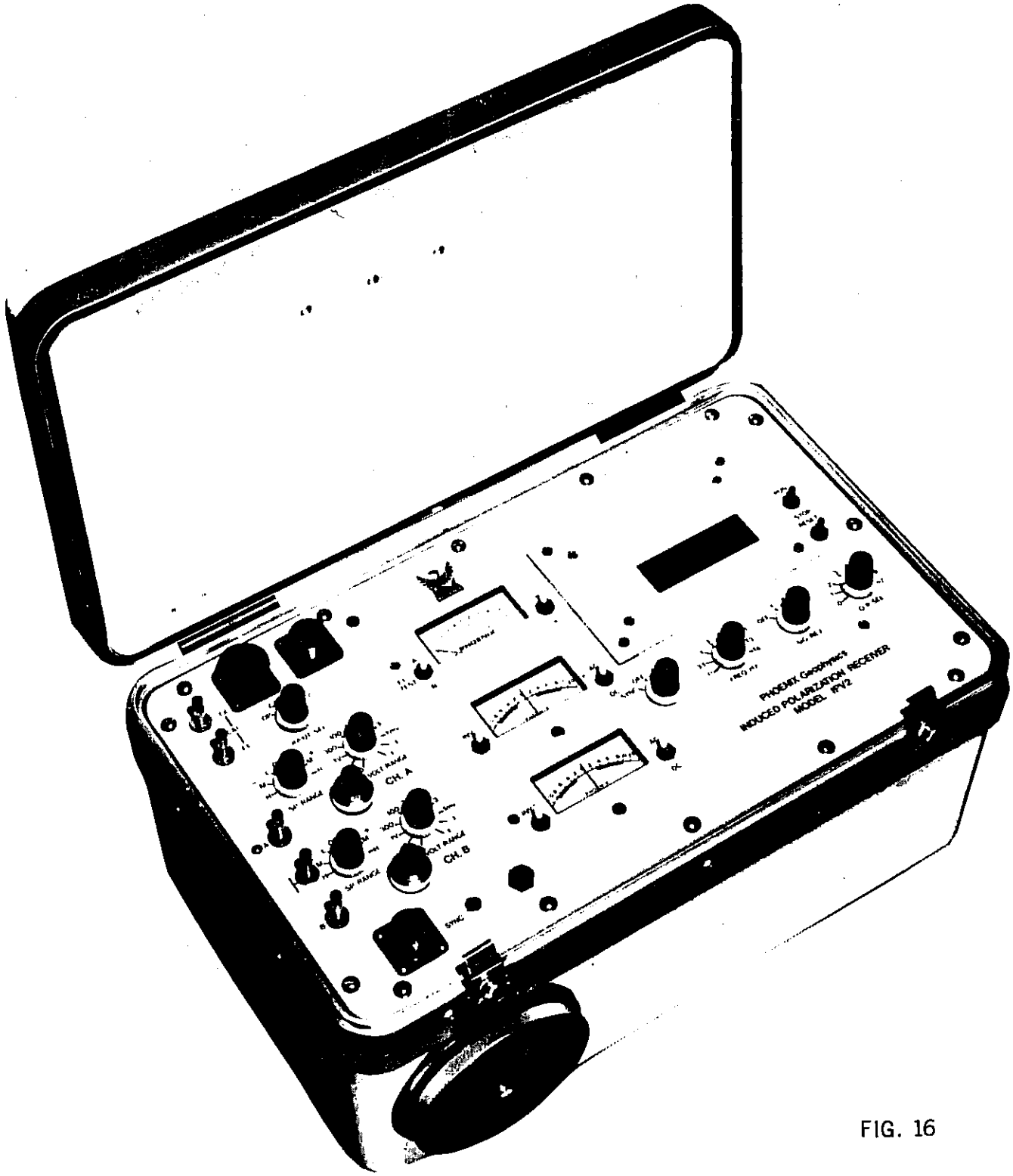
PHOENIX GEOPHYSICS
INDUCED POLARIZATION RECEIVER
MODEL IPV2
CH. A
CH. B
SYNC

FIG. 16

PRICE COMPANY BLOCK NO.8 PROPERTY
IPV-2 PHASE IP TEST

LINE-18E

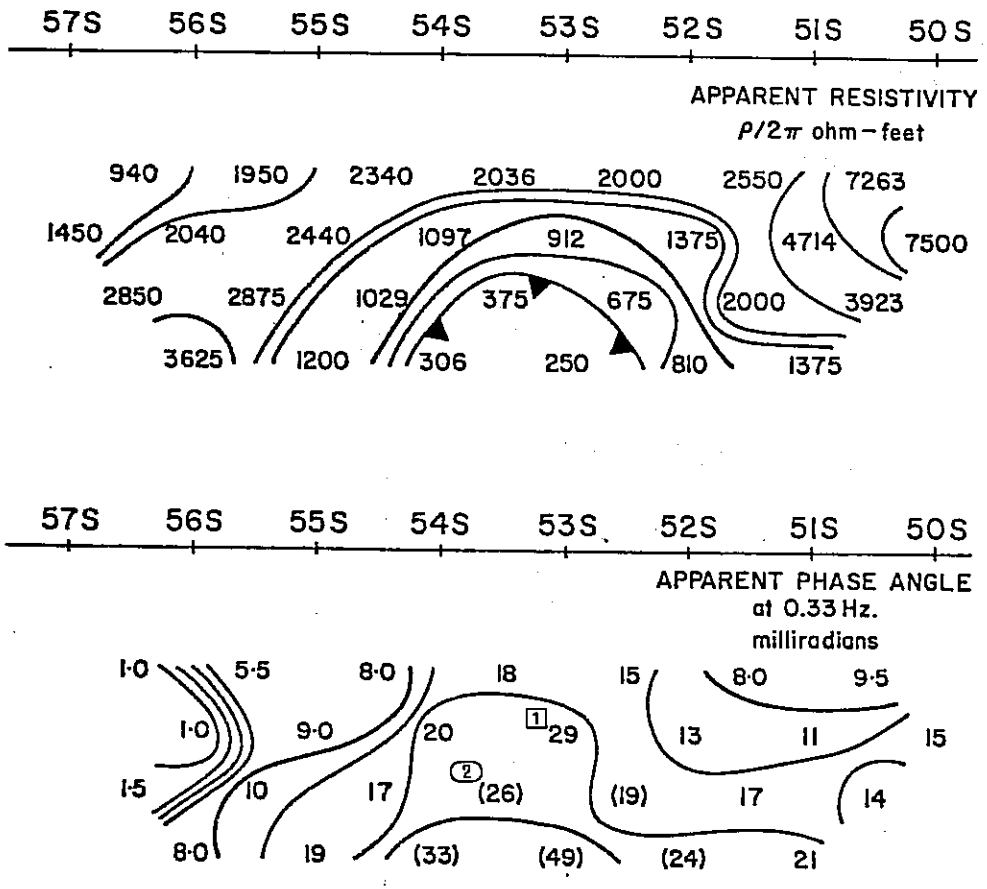

FIG. 17

PRICE COMPANY BLOCK NO.8 PROPERTY
IPV-2 PHASE IP TEST

LINE-15E

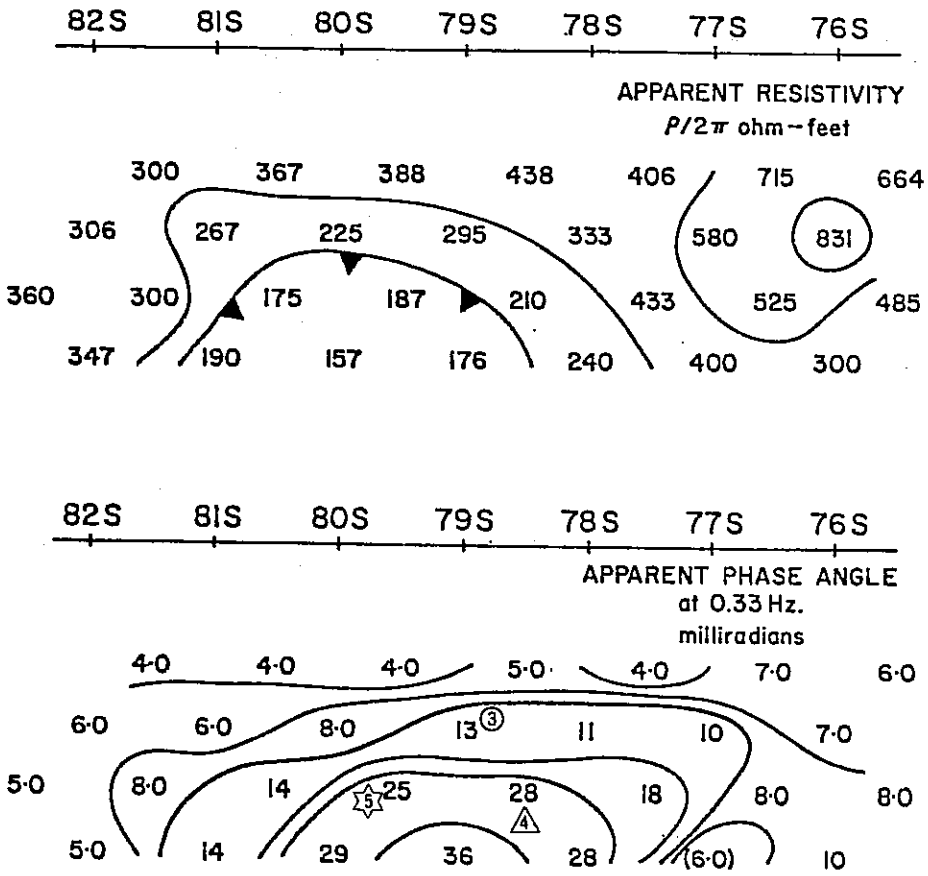

FIG. 18

The results are shown on Figure 19 and Figure 20. On Line 18E, the apparent phase values measured increase with frequency, indicating a value for Fc above 3.0 Hz. On Line 15E the apparent phase values were decreasing with frequency, indicating a value for Fc that is below 0.33 Hz.

The relationship we have established between the critical frequency (Fc) - the time constant (τ) - and the grain-size of the polarizable particles, coupled with our experience over known zones suggests that the grain-size of the source of the anomaly on Line 18E is appreciably smaller than the grain-size of the source of the anomaly on Line 15E.

Our expectation that the large grain-size source is more likely to be graphite is confirmed by the drilling of the two anomalies. The anomaly on Line 18E was found to be due to massive sulphide mineralization; the source of the anomaly located on Line 15E was a graphitic tuff zone, with small concentrations of pyrite.

If field time is taken to make measurements at all five frequencies, it is possible to make a more formal presentation of the spectral characteristics of two anomalies. On Figure 21, is shown a computer-plotted pseudo-section of a single line of phase IP data. The plot shows the apparent resistivity value and the apparent phase value (1.0 Hz) measured for each dipole pair. At the lower part of the data plot is shown the short (five frequency) spectrum (normalized to the value at 1.0 Hz) for each dipole pair.

In this case, the two anomalous zones had a considerable strike length, in an area where the surface was largely covered. The electrical parameters of the two sources were much the same; however, as shown on Figure 21, the source of Zone I is clearly different from the source of Zone II. From drilling, it is known that Zone I is due to a broad, irregular zone of pyrite and sphalerite (with appreciable silver) in a tuffaceous rock unit. The source of Zone II is pyrrhotite in an adjoining andesite rock unit.

Another example of a difference in spectral character is shown in Figure 22. In this location, the source of Zone A had been traced for a considerable distance along strike. Zone B was detected only on two adjacent lines. The difference in spectral character strongly suggests that Zone B is not merely a greater width to the mineralized zone that is the source of Zone A.

The Phoenix IPV-3, Spectral IP Receiver is the most advanced induced polarization receiver ever put into field operation (Figure 23). It completely replaces a truck-mounted system that was assembled largely from off-the-shelf computers, voltmeters, oscilloscopes, etc. The entire system is controlled by the Phoenix CP-1, geophysical computer, that was designed especially for this function. Through an FM-modulated link, the CP-1 also controls the spectral IP current source. Some of the more important features of the IPV-3 are:

i) Six simultaneous voltage channels plus current monitor.

LINE-18E $R\Phi_{0.3-3.0}$ TEST

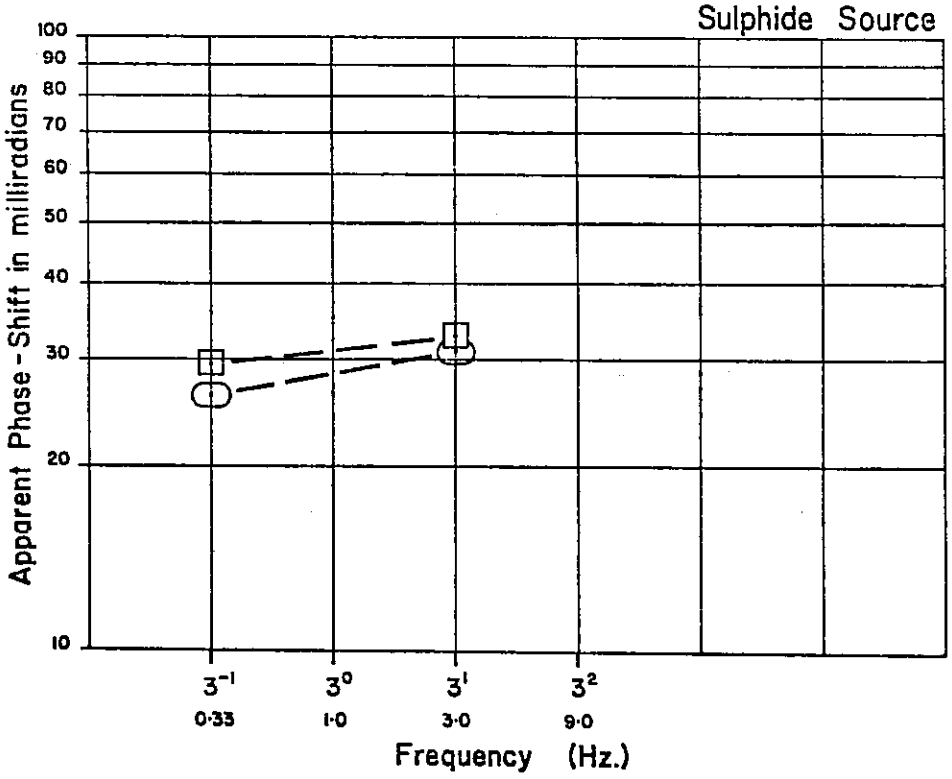

FIG. 19

LINE-15E $R\Phi_{0.3-3.0}$ TEST

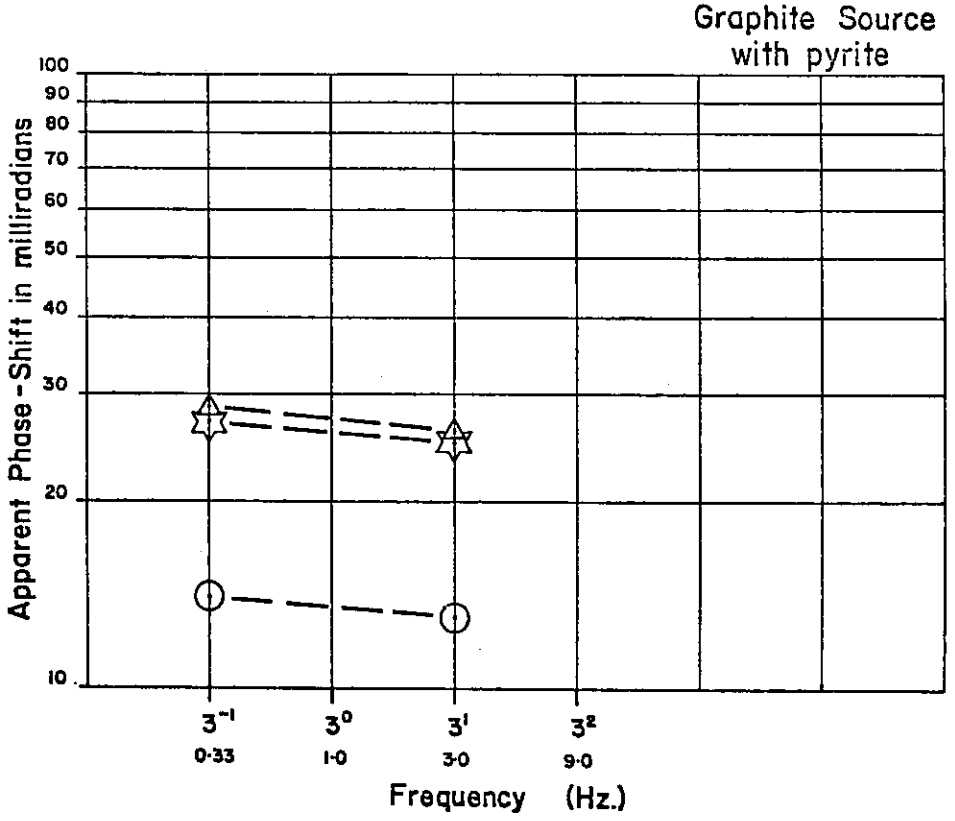

FIG. 20

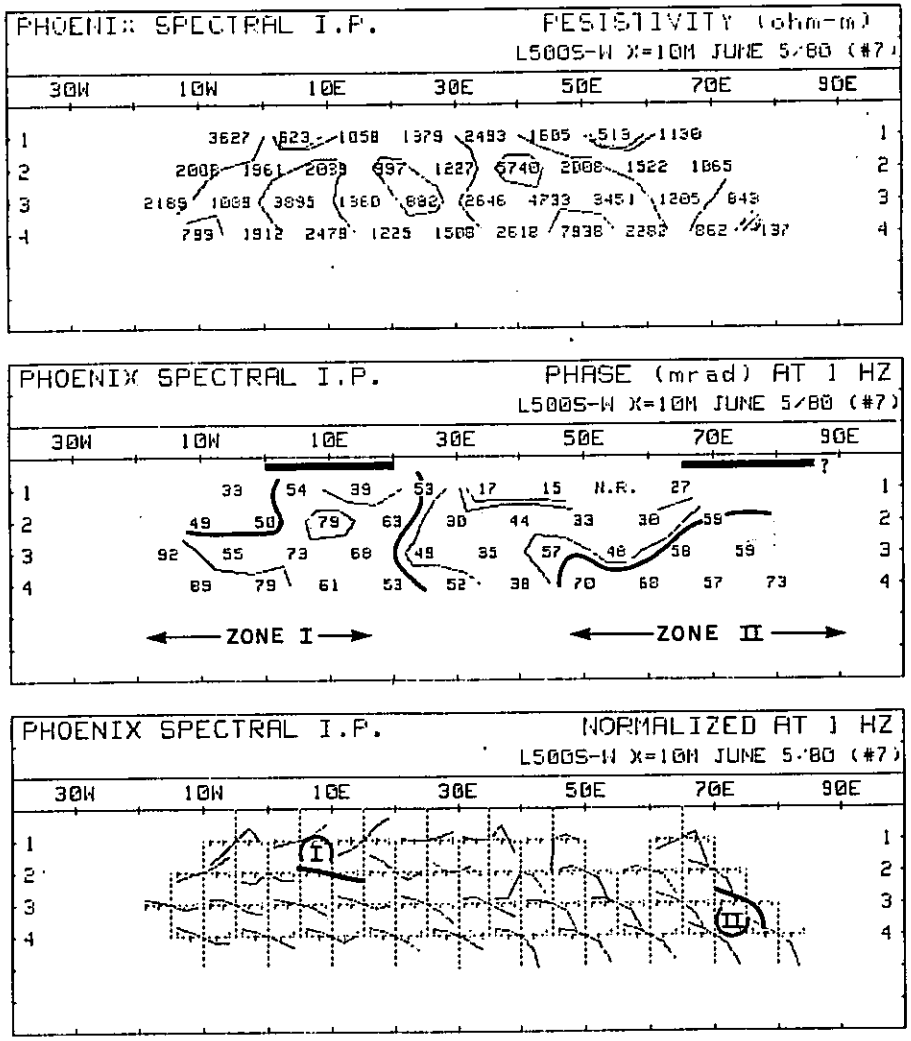
PHOENIX SPECTRAL I.P.
RESISTIVITY (ohm-m)
L500S-W X=10M JUNE 5/80 (#7)
30W 10W 10E 30E 50E 70E 90E
PHOENIX SPECTRAL I.P.
PHASE (mrad) AT 1 HZ
L500S-W X=10M JUNE 5/80 (#7)
30W 10W 10E 30E 50E 70E 90E
ZONE I
ZONE II
PHOENIX SPECTRAL I.P.
NORMALIZED AT 1 HZ
L500S-W X=10M JUNE 5/80 (#7)
30W 10W 10E 30E 50E 70E 90E
I
II

FIG. 21

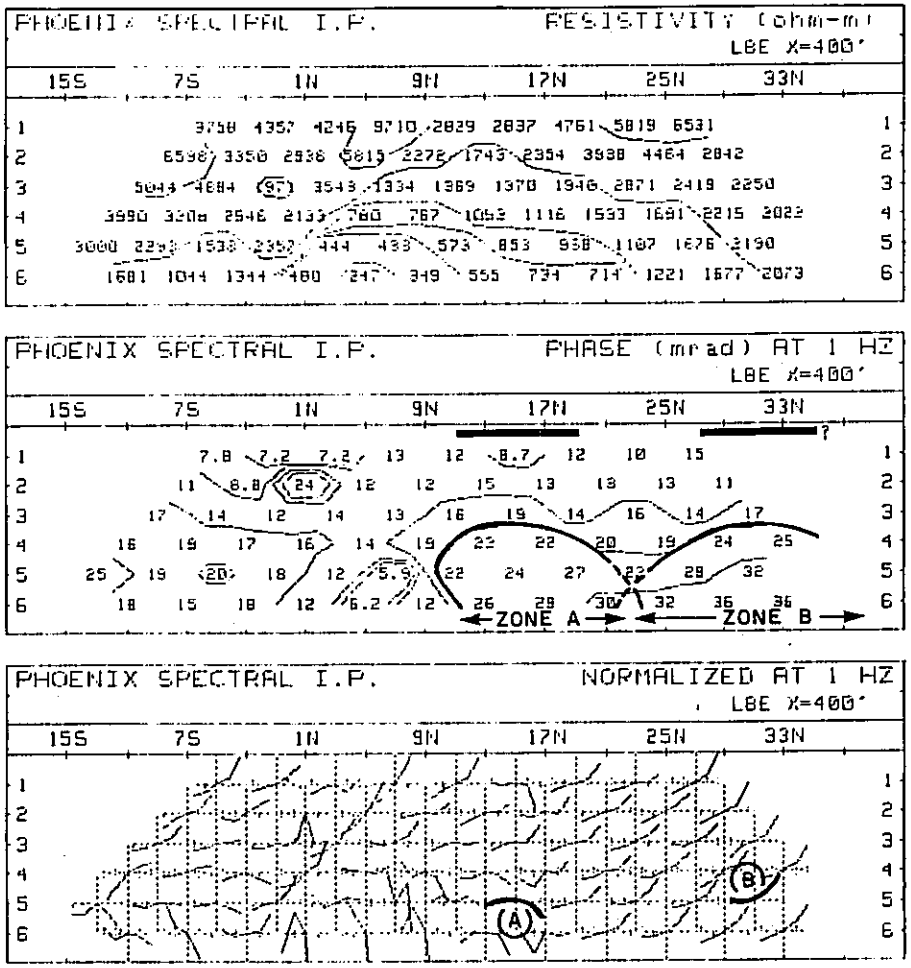
PHOENIX SPECTRAL I.P.
RESISTIVITY (ohm-m)
L8E X=400'
15S 7S 1N 9N 17N 25N 33N
PHOENIX SPECTRAL I.P.
PHASE (mrad) AT 1 HZ
L8E X=400'
15S 7S 1N 9N 17N 25N 33N
ZONE A
ZONE B
PHOENIX SPECTRAL I.P.
NORMALIZED AT 1 HZ
L8E X=400'
15S 7S 1N 9N 17N 25N 33N
A
B

FIG. 22

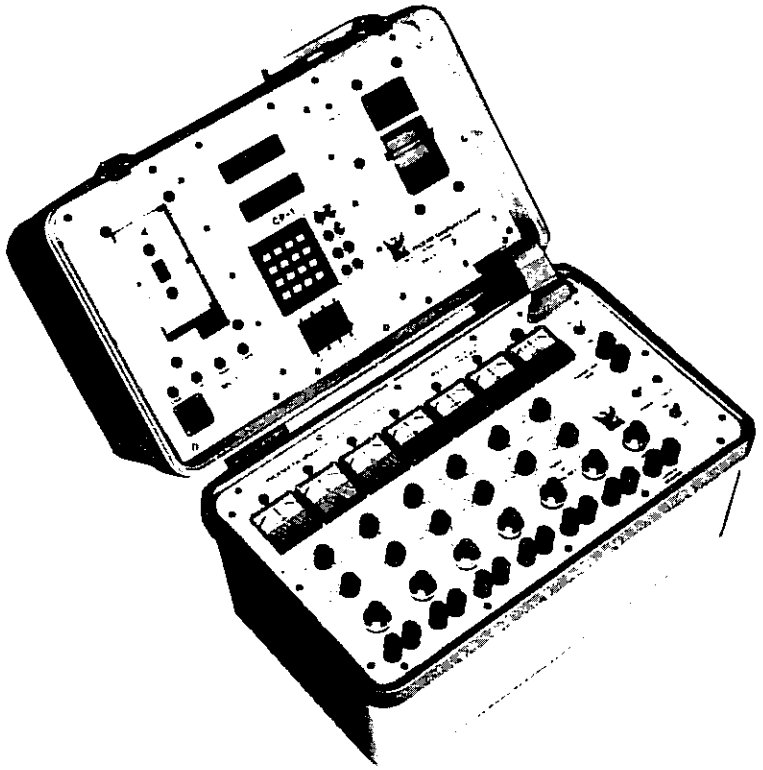

FIG. 23

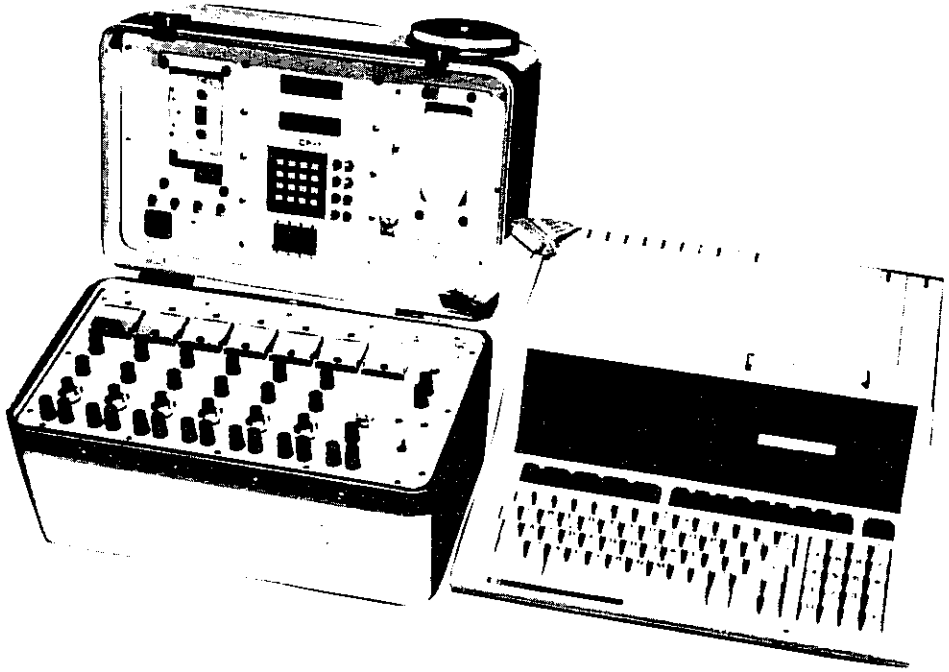

FIG. 24

ii) Frequency range from 2^{-14} Hz (0.00006 Hz) to 2^{+16} Hz (65,536 Hz) with automatic scanning programmable through CP-1.

iii) Real time de-convolution and coherent filtering via use of CP-1.

iv) Field Data available through digital read-out and recorded on paper tape and tape cassette.

v) Field results directly transferrable from tape cassette through CP-1 and interface to computer for analysis and interpretation. (Figure 24).

By using the IPV-3 and the HP=85 computer in the field, the geophysicist has at his disposal all of the interpretational power of the spectral IP method. As shown on Figure 25 it is possible to remove the inductive coupling effects from the broad-band spectral IP results. When this information is removed, it is possible to invert the remaining, decoupled IP spectra and determine the apparent values of Ro, m, τ, c for that particular dipole-pair measurement.

For the spectra shown in Figure 25, the values are m = 0.172; c = 0.376; τ = 0.044 sec.; these parameters suggest a small grain-size, and in fact the source is a massive sulphide zone in New Brunswick. The parameter values obtained by inverting the spectral curve from all of the anomalous dipole pairs were essentially the same; we have found this to be universally true if the anomaly is due to a single, more-or-less uniform source.

For the spectral curve shown in Figure 26, the parameter values of the source are m = 0.509; c = 0.180; τ = 540 seconds. The large time-constant confirms the large grain-size for the graphite zone that is the source of the anomaly.

For IP measurements with large electrode intervals in areas of low resistivity (high conductivity) inductive coupling effects will completely distort IP field data. This can happen even for low frequency measurements (in the variable frequency method) or long time delay measurements (in the time domain technique). When the inductive coupling effects are removed from the spectral curve for each dipole pair (as in Figure 12 and Figure 25) the pseudo-section can be reconstructed using the decoupled data.

The data pseudo-section shown in Figure 27 is from the Elura Deposit near Cobar, New South Wales. The resistivity results show a deep, variable high conductivity surface layer. The phase IP measurements at 3.0 Hz with X = 100 meters are completely dominated by inductive coupling effects that essentially depend only upon the electrode separation (n). However, when the inductive effects are removed from the data for each dipole pair, the pseudo-section clearly shows the presence of the massive sulphide zone, at depth, at approximately station 2500E.

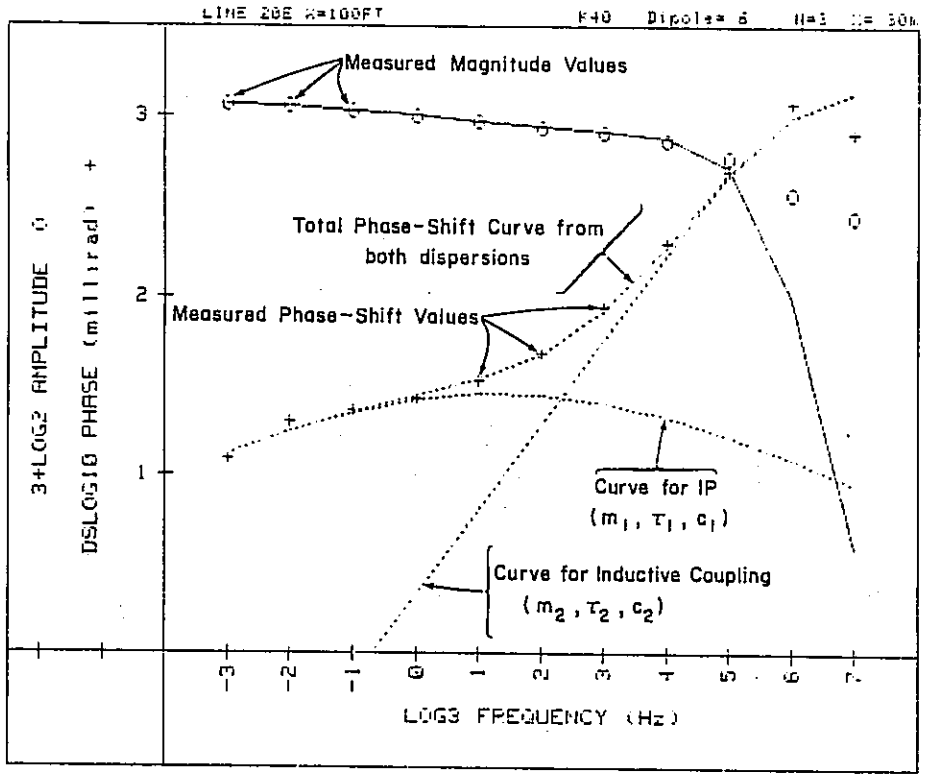

				IP EFFECT			INDUCTIVE COUPLING EFFECT		
Iter	Lambda	Rchsq	R0	M1	T1	C1	M2	T2	C2
9	1.E-02	.03406	1.089	.221	4.0E-02	.329	1.000	1.1E-04	1.000
1	1.E-01	.00168	1.063	.196	2.5E-02	.373	1.000	3.6E-04	1.000
2	1.E-03	.00053	1.072	.186	3.1E-02	.355	1.000	3.3E-04	1.000
3	1.E-04	.00067	1.071	.174	4.3E-02	.375	1.000	3.4E-04	1.000
4	1.E-05	.00066	1.071	.173	4.4E-02	.376	1.000	3.4E-04	1.000
Pct Std Deviations			.6	16.4	84.2	13.5	0.0	5.5	0.0

Correlation Matrix

1.0000							
.5173	1.0000						
-.4239	-.9715	1.0000					
-.5302	-.9438	.8971	1.0000				
0.0000	0.0000	0.0000	0.0000	0.0000			
-.2093	-.6596	.6657	.5343	0.0000	1.0000		
0.0000	0.0000	0.0000	0.0000	0.0000	0.0000	0.0000	

Apparent Resistivity Measured at 1 Hz is 78

Apparent Resistivity Calculated from Inductive Coupling is 10

FIG. 25

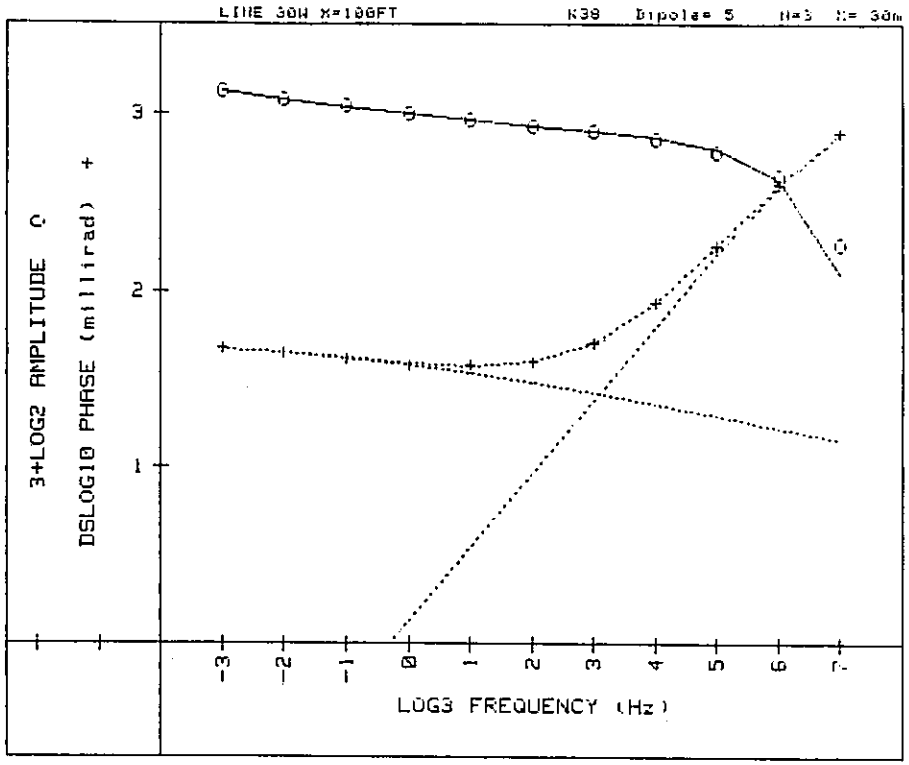

				IP EFFECT			INDUCTIVE COUPLING EFFECT		
Iter	Lambda	Rchsq	R0	M1	T1	C1	M2	T2	C2
0	1.E-02	.01496	1.776	.571	1.2E+02	.180	1.000	1.5E-04	.970
1	1.E-02	.00083	1.569	.483	1.3E+02	.180	1.000	9.3E-05	.893
2	1.E-03	.00009	1.616	.487	1.9E+02	.180	1.000	8.6E-05	.891
3	1.E-04	.00006	1.677	.502	4.0E+02	.180	1.000	8.7E-05	.882
4	1.E-05	.00005	1.704	.508	5.3E+02	.180	1.000	8.7E-05	.879
5	1.E-06	.00005	1.707	.509	5.4E+02	.180	1.000	8.7E-05	.879
Pct Std Deviations			2.4	2.0	53.1	0.0	0.0	2.0	1.0

Correlation Matrix

1.0000							
.9916	1.0000						
.5885	.9710	1.0000					
0.0000	0.0000	0.0000	0.0000				
0.0000	0.0000	0.0000	0.0000	0.0000			
-.1166	-.0989	-.1282	0.0000	0.0000	1.0000		
-.4909	-.4268	-.5273	0.0000	0.0000	.7128	1.0000	

Apparent Resistivity Measured at 1 Hz is 231

Apparent Resistivity Calculated from Inductive Coupling is 26

FIG. 26

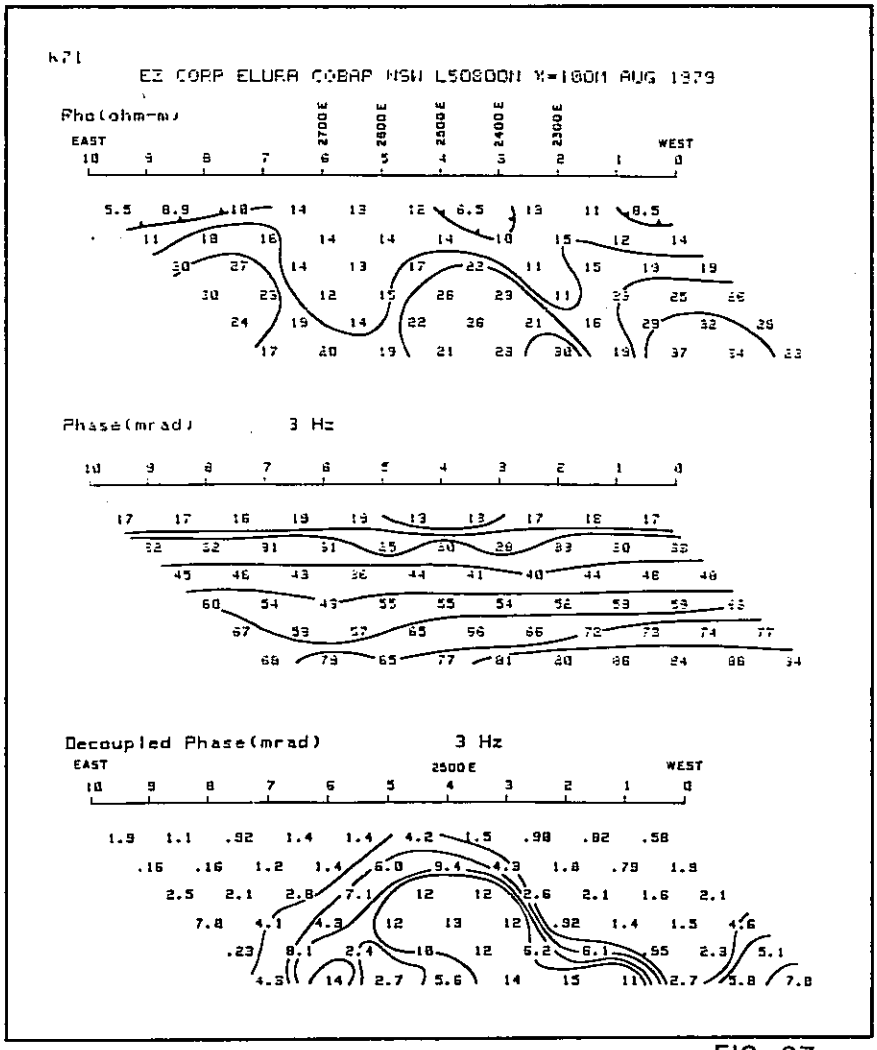

FIG. 27

COMPUTER ASSISTED INTERPRETATION OF IP DATA

The increased size, storage capability and speed of the modern digital computer has been a big boon to the exploration geophysicist. Forward problem solutions for potential methods (gravity, magnetics, etc.) have been available for some time. Recently, numerical modelling methods and large, very fast computers have made similar forward problem solutions available for applied field geophysics such as resistivity and induced polarization.

The forward problem solution shown in Figure 28 is for a fairly normal, dipping source. (The geometry is Two-Dimensional). The patterns of the induced polarization and resistivity pseudo-sections are similar to those we have previously seen from field data over dipping sources.

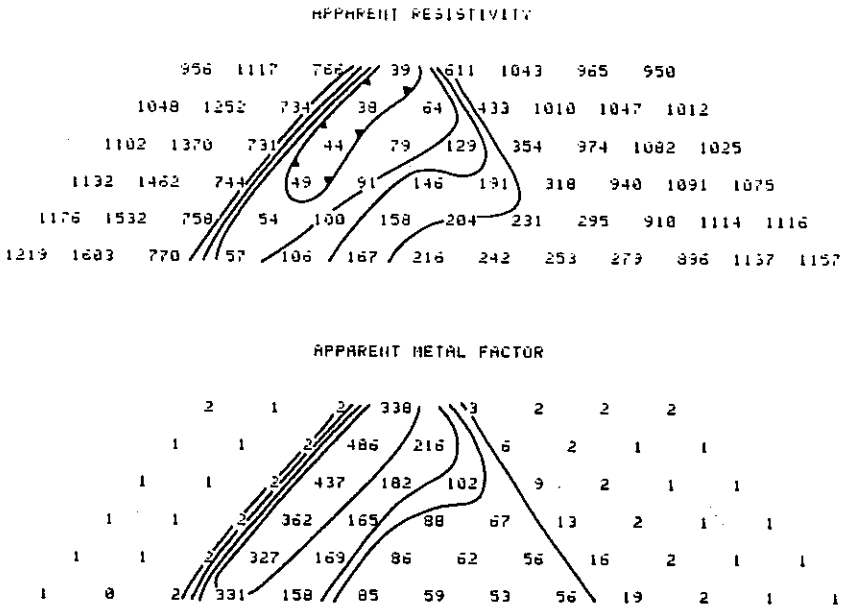
APPARENT RESISTIVITY
956 1117 766 39 611 1043 965 950
1048 1252 734 38 64 433 1010 1047 1012
1102 1370 731 44 79 129 354 974 1082 1025
1132 1462 744 49 91 146 191 318 940 1091 1075
1176 1532 758 54 100 158 204 231 295 918 1114 1116
1219 1603 770 57 106 167 216 242 253 279 836 1137 1157
APPARENT METAL FACTOR
2 1 3 338 3 2 2 2
1 1 2 486 216 6 2 1 1
1 1 2 437 182 102 9 2 1 1
1 1 2 362 165 88 67 13 2 1 1
1 1 3 327 169 86 62 56 16 2 1 1
1 0 2 331 158 85 59 53 56 19 2 1 1
APPARENT PFE
2.0 2.0 2.1 12.9 2.2 2.1 2.0 2.1
1.9 1.9 2.1 18.0 13.9 2.9 2.0 1.9 2.0
1.9 1.7 2.1 18.8 14.4 13.1 3.4 2.0 1.9 1.8
1.8 1.6 2.1 17.8 15.0 13.0 12.8 4.1 1.9 1.8 1.8
1.7 1.5 1.9 17.7 16.8 13.7 12.7 13.8 4.7 1.9 1.7 1.6
1.6 1.3 1.7 18.9 16.8 14.3 12.9 12.9 14.4 5.3 1.9 1.6 1.6
6W 4W 2W 0 2E 4E 6E
ρ1 = 1000
(f.e.)1 = 2%
(m.f.)1 = 2
ρ3 = 2
(f.e.)3 = 25%
(m.f.)3 = 1250

FIG. 28

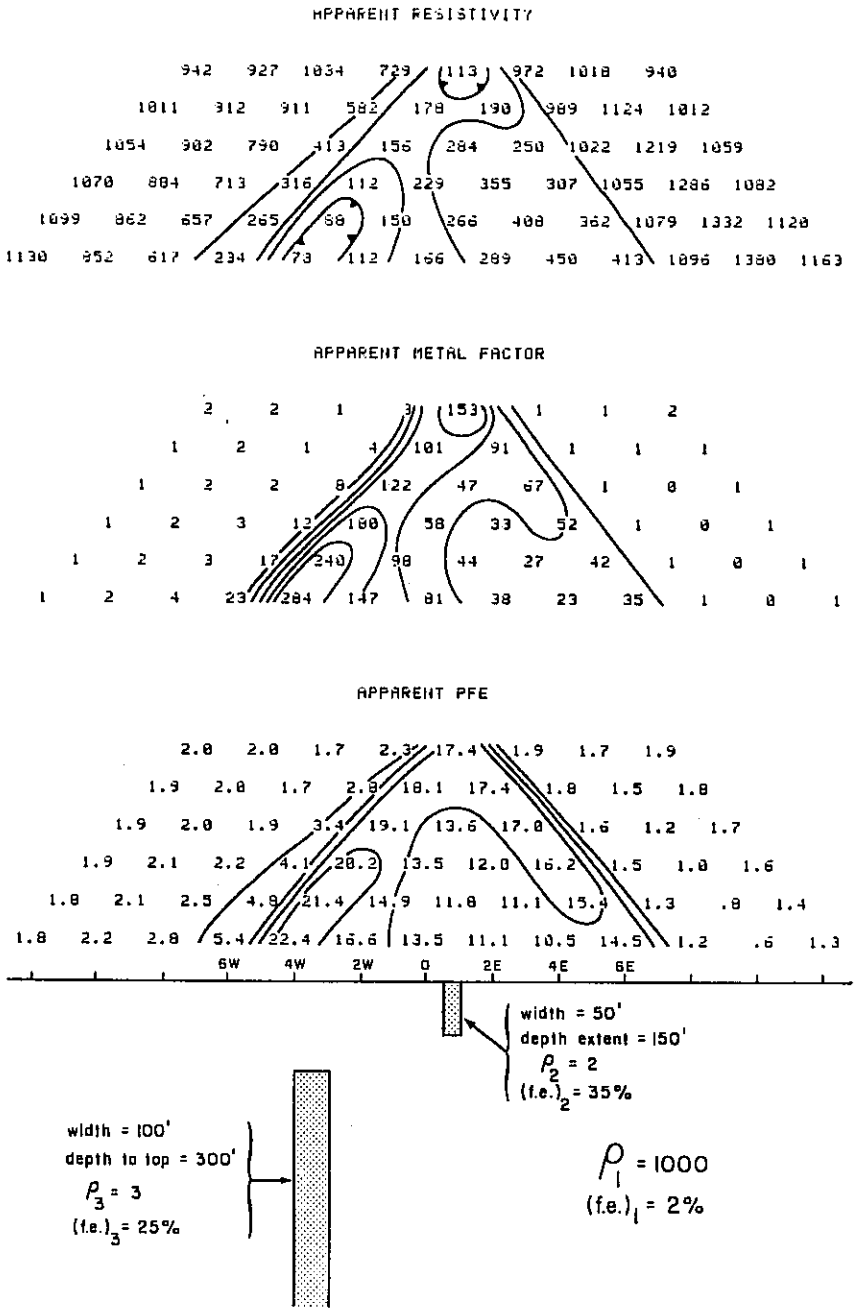
APPARENT RESISTIVITY
942 927 1034 729 113 972 1018 940
1011 912 911 582 178 190 989 1124 1012
1054 902 790 413 156 284 250 1022 1219 1059
1070 884 713 316 112 229 355 307 1055 1286 1082
1099 862 657 265 88 150 266 408 362 1079 1332 1120
1130 852 617 234 73 112 166 289 450 413 1096 1380 1163
APPARENT METAL FACTOR
2 2 1 3 153 1 1 2
1 2 1 4 101 91 1 1 1
1 2 2 8 122 47 67 1 0 1
1 2 3 12 180 58 33 52 1 0 1
1 2 3 17 240 98 44 27 42 1 0 1
1 2 4 23 284 147 81 38 23 35 1 0 1
APPARENT PFE
2.0 2.0 1.7 2.3 17.4 1.9 1.7 1.9
1.9 2.0 1.7 2.0 18.1 17.4 1.8 1.5 1.8
1.9 2.0 1.9 3.4 19.1 13.6 17.0 1.6 1.2 1.7
1.9 2.1 2.2 4.1 28.2 13.5 12.0 16.2 1.5 1.0 1.6
1.8 2.1 2.5 4.8 21.4 14.9 11.8 11.1 15.4 1.3 .8 1.4
1.8 2.2 2.8 5.4 22.4 16.6 13.5 11.1 10.5 14.5 1.2 .6 1.3
6W 4W 2W 0 2E 4E 6E
width = 50'
depth extent = 150'
ρ2 = 2
(f.e.)2 = 35%
width = 100'
depth to top = 300'
ρ3 = 3
(f.e.)3 = 25%
ρ1 = 1000
(f.e.)1 = 2%

FIG. 29

Recently however, we had occasion to try to interpret a field anomaly that was very similar to that shown in Figure 29. The presence of the shallow, limited depth extent source was known from previous drilling. By the trial and error method, we were able to show that the pattern (which is very similar to that in Figure 28) need not have originated from a dipping source.

By limiting the solutions somewhat, it is possible to create computer programs to do the inverse problem. That is, the computer accepts the field data as input and as output gives the vertical, tabular source that gives the best "least square fit" to that data. For comparison, the computer also outputs the pseudo-section data that would be measured for the source it has chosen.

The simplest problem is for resistivity data alone. The results shown in Figure 30 are from a geothermal exploration program in which the resistivity survey was completed using X = 250 meters. The large, deep resistivity low was measured on the side of an extinct volcano, under recent lava flows. The computer inversion gives a major, poorly determined, conductor (with a high conductivity times width product) at a depth of 350 to 400 meters. This data was used to show the geologist that the source of the resistivity anomaly could be a good geothermal target.

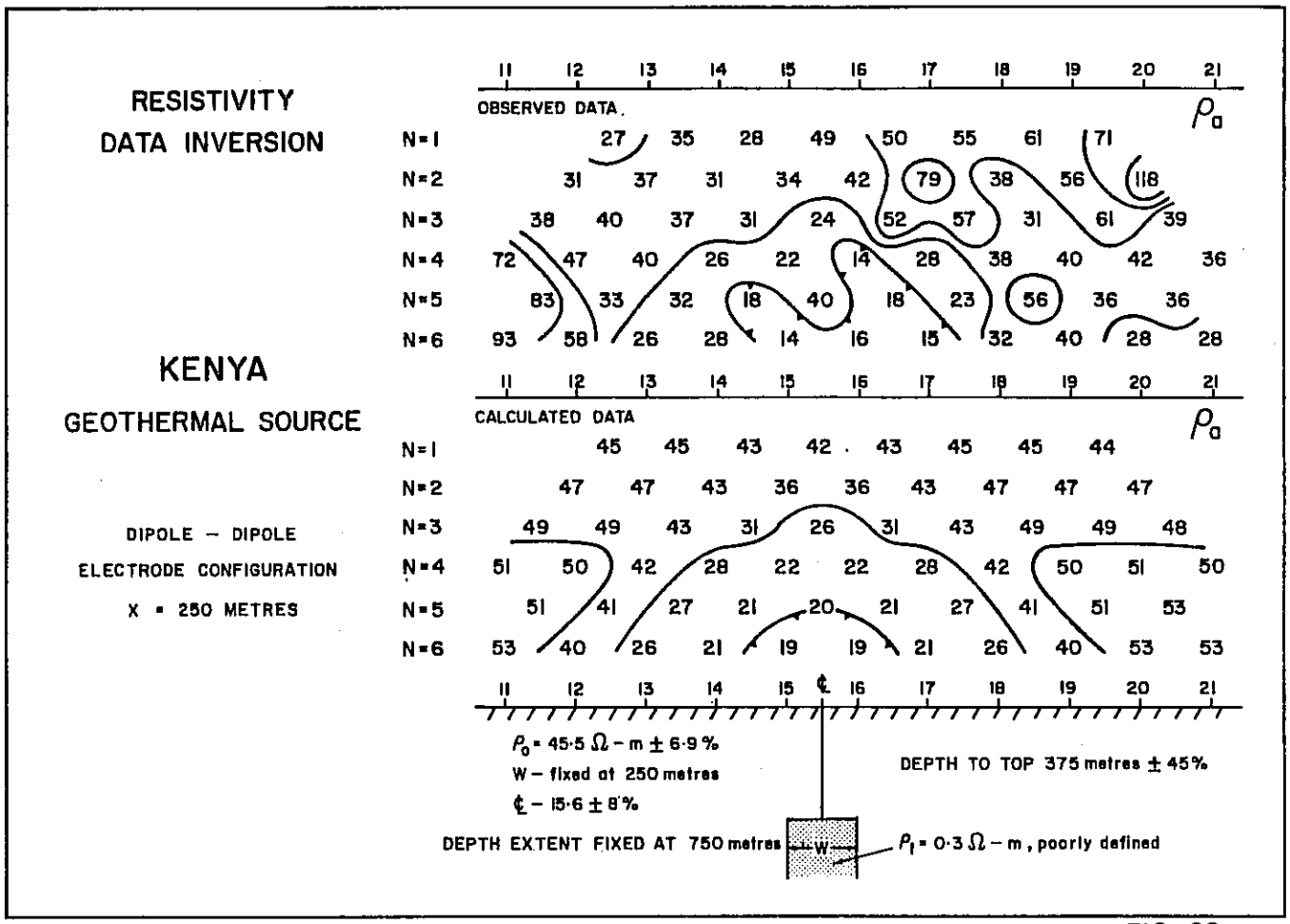

FIG. 30

The example shown in Figure 31 and Figure 32 is from the Pine Point Area. The computer inversion shows that in this case the source has a poor resistivity contrast with the surrounding limestones. However, the IP effect is quite anomalous.

If there is conductive overburden present, and the source itself is conductive, the inversions will be more complex. The data shown on Figure 33 and Figure 34 were measured with X = 100 feet, in an area where the depth of overburden was determined to be about fifty feet. The calculated results give a "good fit" to the measured data, and the source described by this inversion is a typical Canadian Shield, massive sulphide deposit.

The inversion program can also be used to show that two dissimilar anomalies can in fact be due to the same type of source. The inversions of the IP data shown in Figure 35 and Figure 36 are those for the field data previously shown in Figure 17 and Figure 18. The background resistivities are very different, and the depths to the top of the sources are different by a factor of three. However, the indicated source parameters are much the same. As we saw previously, the spectral characteristics of the IP anomaly from the two sources are quite different.

The use of the computer inversion techniques make it possible to obtain an estimate of the source parameters, even in situations in which an unusual geologic environment would make it difficult to interpret the data. The field results shown in Figure 37 are from a deeply buried source in a highly conductive environment. The rocks in which the survey was completed were porous, and filled with saline water. However, the inversion output on Figure 38 shows the source is not unlike that determined in Figure 34.

WHAT OF THE FUTURE?

There seems to be almost no limit to the future development of the induced polarization method. As the orebodies for which we search become deeper, and more difficult to detect, we will need all of the help we can get.

A simple extension of what we are now doing should lead to the following examples in the next twelve to twenty-four months.

a) The computer can be used to store parameters obtained by the computer inversions of spectral IP data. Therefore, it will be possible to correlate the electrical parameters (m, τ, c) of all sources known in a given geographical area or a certain geologic environment. For a new, unknown source, the computer could be asked to output the probability that the unknown source will be due to metallic mineralization of a certain type.

The data shown in Figure 39 was a first attempt at such a correlation. On the plot are shown the IP effect vs. Time-Constant (m, vs.τ) coordinates for a few massive sulphide

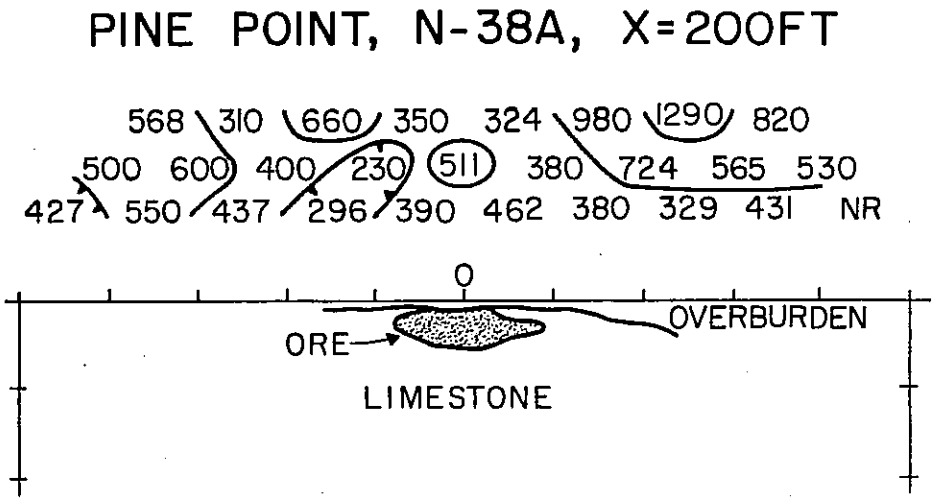
PINE POINT, N-38A, X=200FT
568 310 660 350 324 980 1290 820
500 600 400 230 511 380 724 565 530
427 550 437 296 390 462 380 329 431 NR
0
ORE
OVERBURDEN
LIMESTONE

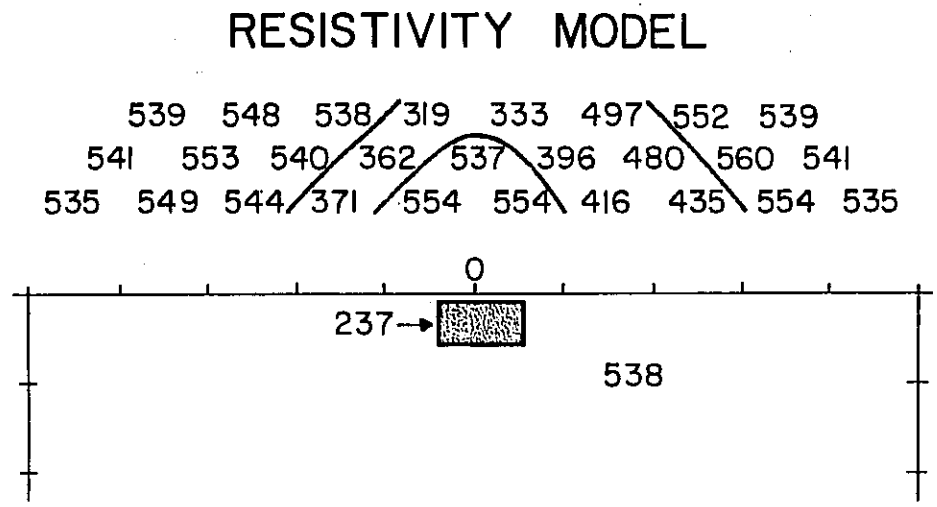
RESISTIVITY MODEL
539 548 538 319 333 497 552 539
541 553 540 362 537 396 480 560 541
535 549 544 371 554 554 416 435 554 535
0
237
538

FIG. 31

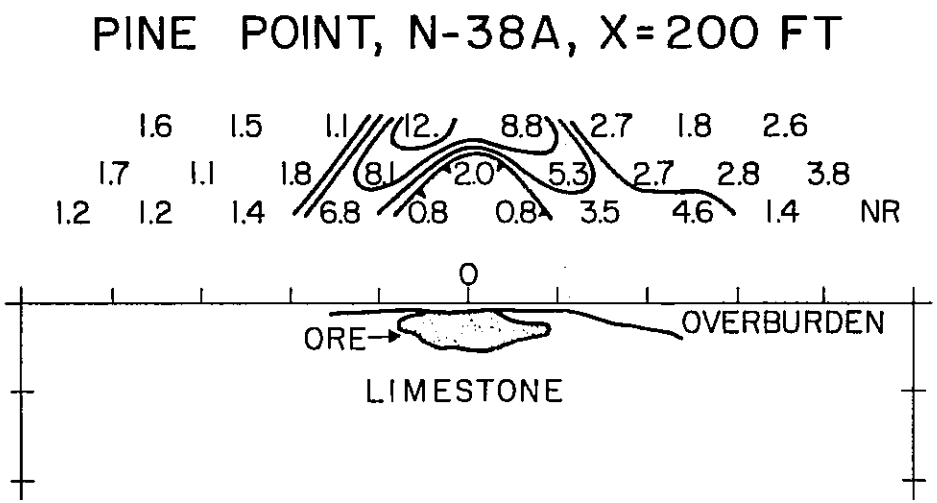
PINE POINT, N-38A, X=200 FT
1.6 1.5 1.1 12. 8.8 2.7 1.8 2.6
1.7 1.1 1.8 8.1 2.0 5.3 2.7 2.8 3.8
1.2 1.2 1.4 6.8 0.8 0.8 3.5 4.6 1.4 NR
0
ORE
OVERBURDEN
LIMESTONE

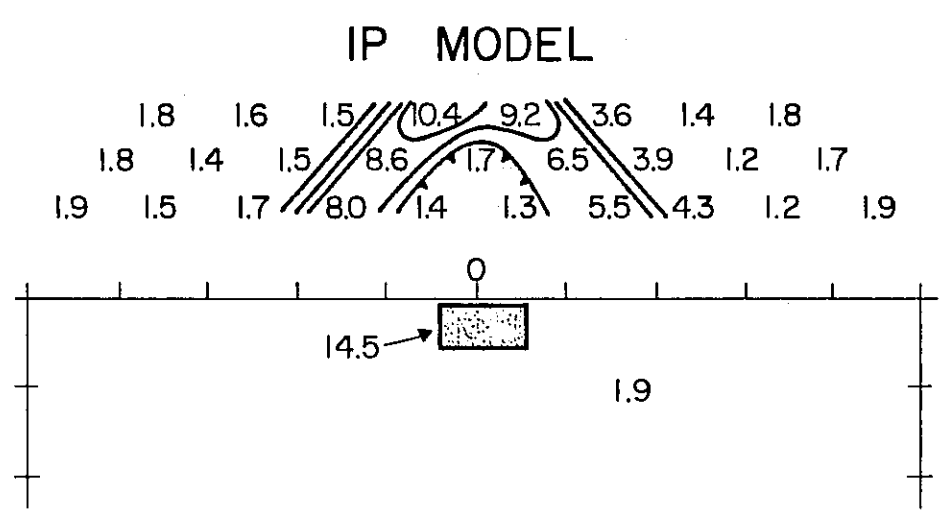
IP MODEL
1.8 1.6 1.5 10.4 9.2 3.6 1.4 1.8
1.8 1.4 1.5 8.6 1.7 6.5 3.9 1.2 1.7
1.9 1.5 1.7 8.0 1.4 1.3 5.5 4.3 1.2 1.9
0
14.5
1.9

FIG. 32

COMPUTER INTERPRETATION

OF GEOPHYSICAL DATA

INDUCED POLARIZATION AND RESISTIVITY

CANADIAN SHIELD MASSIVE SULPHIDE DEPOSIT, OVERLAIN BY CONDUCTIVE OVERBURDEN
ISO - COPPERFIELDS LINE 0+00

DETERMINE: HORIZONTAL POSITION
DEPTH TO TOP
MIDTH
RES OF SOURCE
RES OF OVERBURDEN
IP OF SOURCE

DIPOLE-DIPOLE ARRAY X = 100 FEET 100FT

RESISTIVITY DATA - OBSERVED (OHM-METERS)

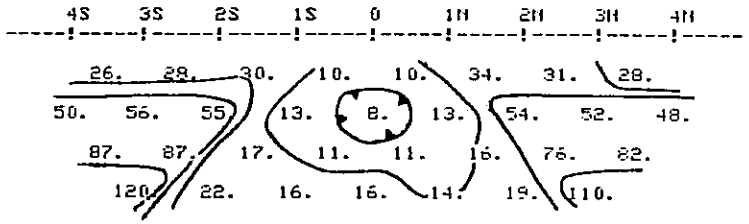

INDUCED POLARIZATION DATA - OBSERVED (PFE)

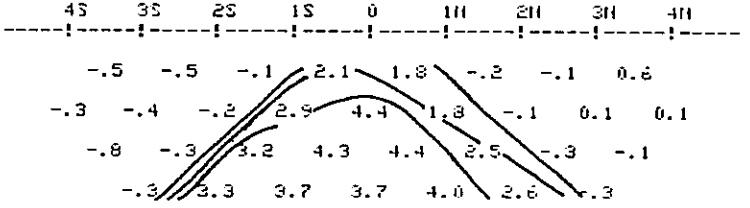

FIG. 33

RESISTIVITY DATA - CALCULATED (OHM-METERS)

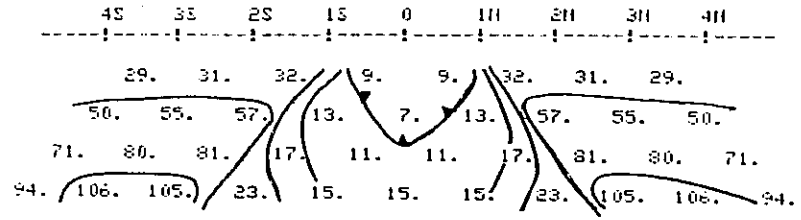

INDUCED POLARIZATION DATA - CALCULATED (PFE)

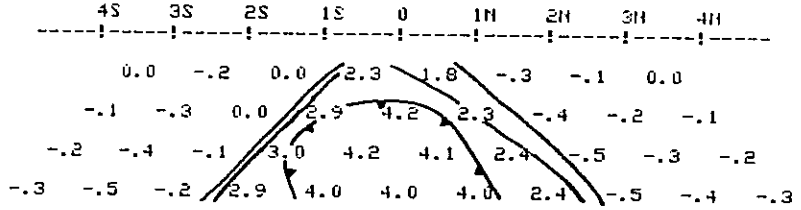

PARAMETERS OF THE CALCULATED SOURCE

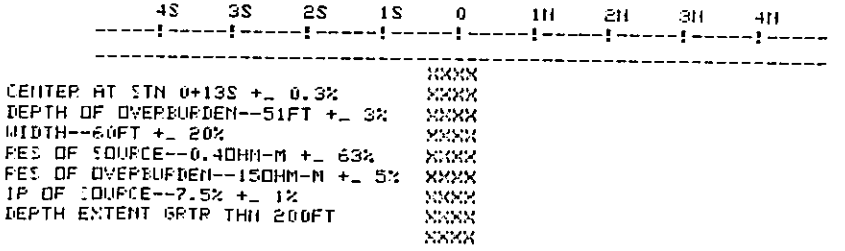

FIG. 34

LINE-18E

FINAL MODEL FOR DATA SET 1

OBSERVED DATA

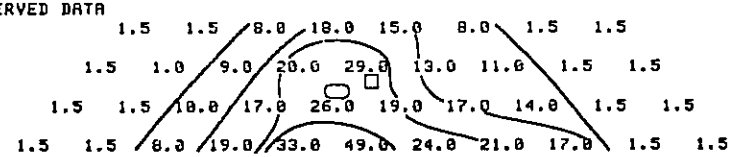

100*DIAGONAL OF INFORMATION DENSITY MATRIX

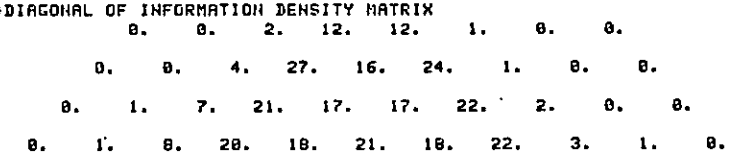

CALCULATED DATA

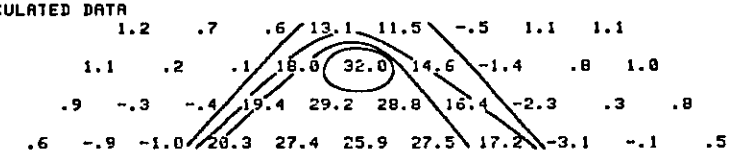

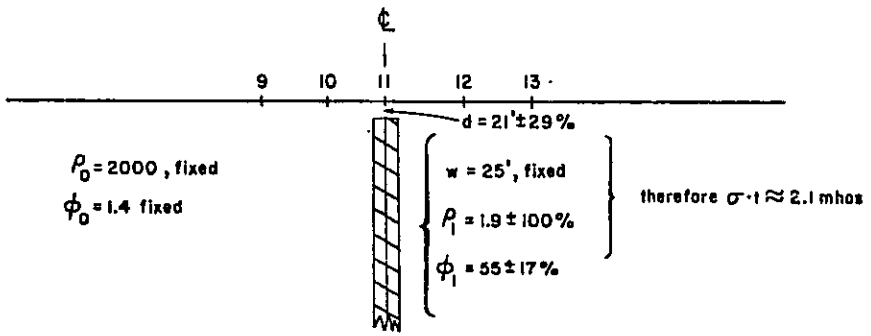

FIG. 35

LINE-15E

graphite source, with some pyrite

LINE-15E

phase at 0.3 Hz.

FINAL MODEL FOR DATA SET 1

OBSERVED DATA

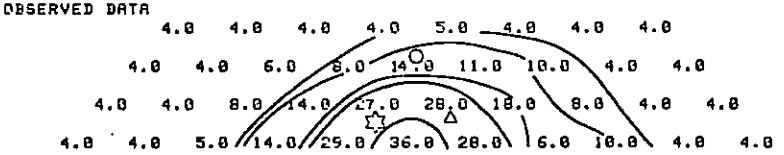

100*DIAGONAL OF INFORMATION DENSITY MATRIX

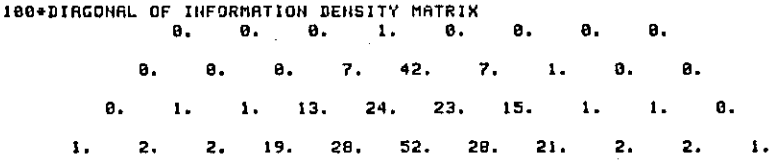

CALCULATED DATA

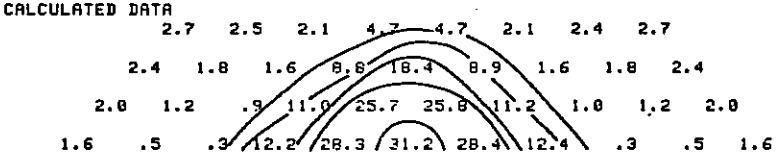

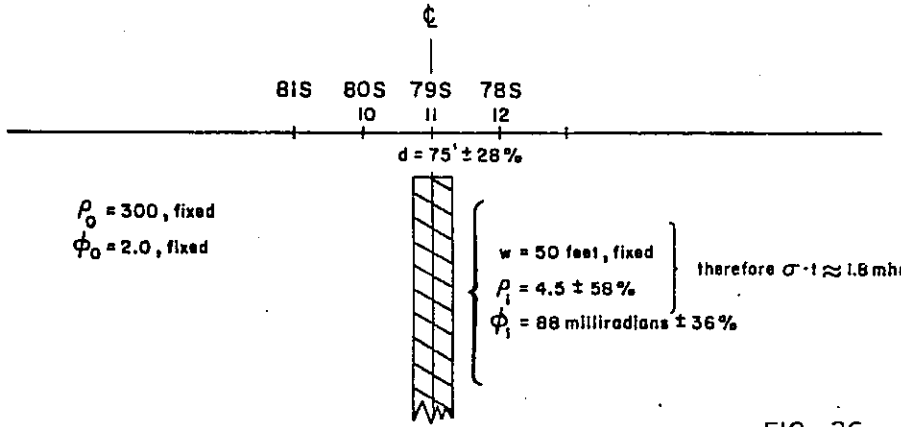

FIG. 36

COMPUTER INTERPRETATION

OF GEOPHYSICAL DATA

INDUCED POLARIZATION AND RESISTIVITY

DEEPLY BURIED SOURCE IN VERY CONDUCTIVE ENVIRONMENT – DETERMINE POSITION, DEPTH, AND PHYSICAL PROPERTIES OF SOURCE

DIPOLE-DIPOLE ARRAY X = 25 METERS 25M.

RESISTIVITY DATA – OBSERVED (OHM-METERS)

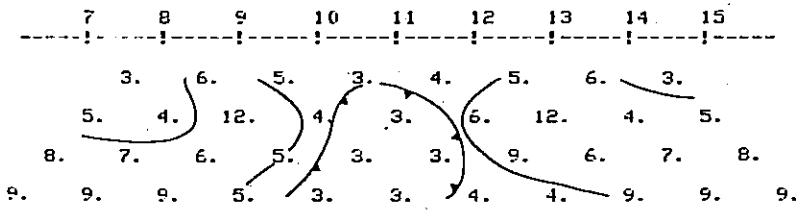

INDUCED POLARIZATION DATA – OBSERVED (PFE)

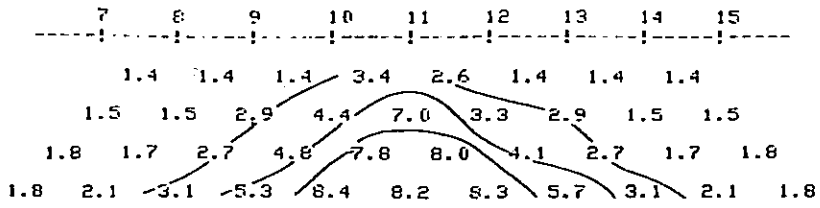

FIG. 37

RESISTIVITY DATA – CALCULATED (OHM-METERS)

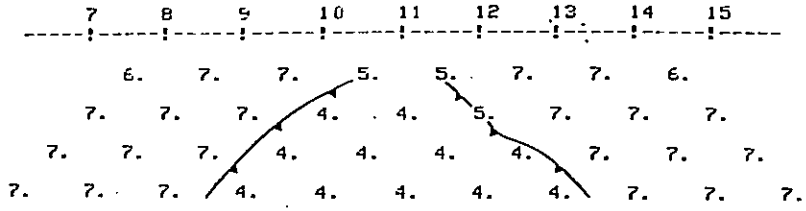

INDUCED POLARIZATION DATA – CALCULATED (PFE)

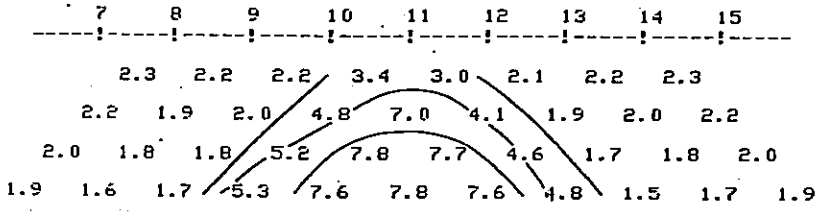

PARAMETERS OF THE CALCULATED SOURCE

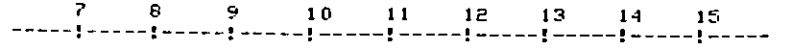

DEPTH TO TOP--23M +_ 11%
RES OF SOURCE--0.30HM-M +_ 45%
RES OF HOST--6.50HM-M +_ 5%
IP OF SOURCE--23 +_ 16%
IP OF HOST--2.3 +_ 11%
CENTER AT STN 10+90 +_ 1%

+++++
+++++
+++++
+++++
+++++
+++++
+++++

DEPTH EXTENT FIXED AT >50M
WIDTH FIXED AT 25M

FIG. 38

sources and massive graphite sources in Canada. More recent determinations have not been added to the plot, although additional field work in North America and Australia has shown the same grouping.

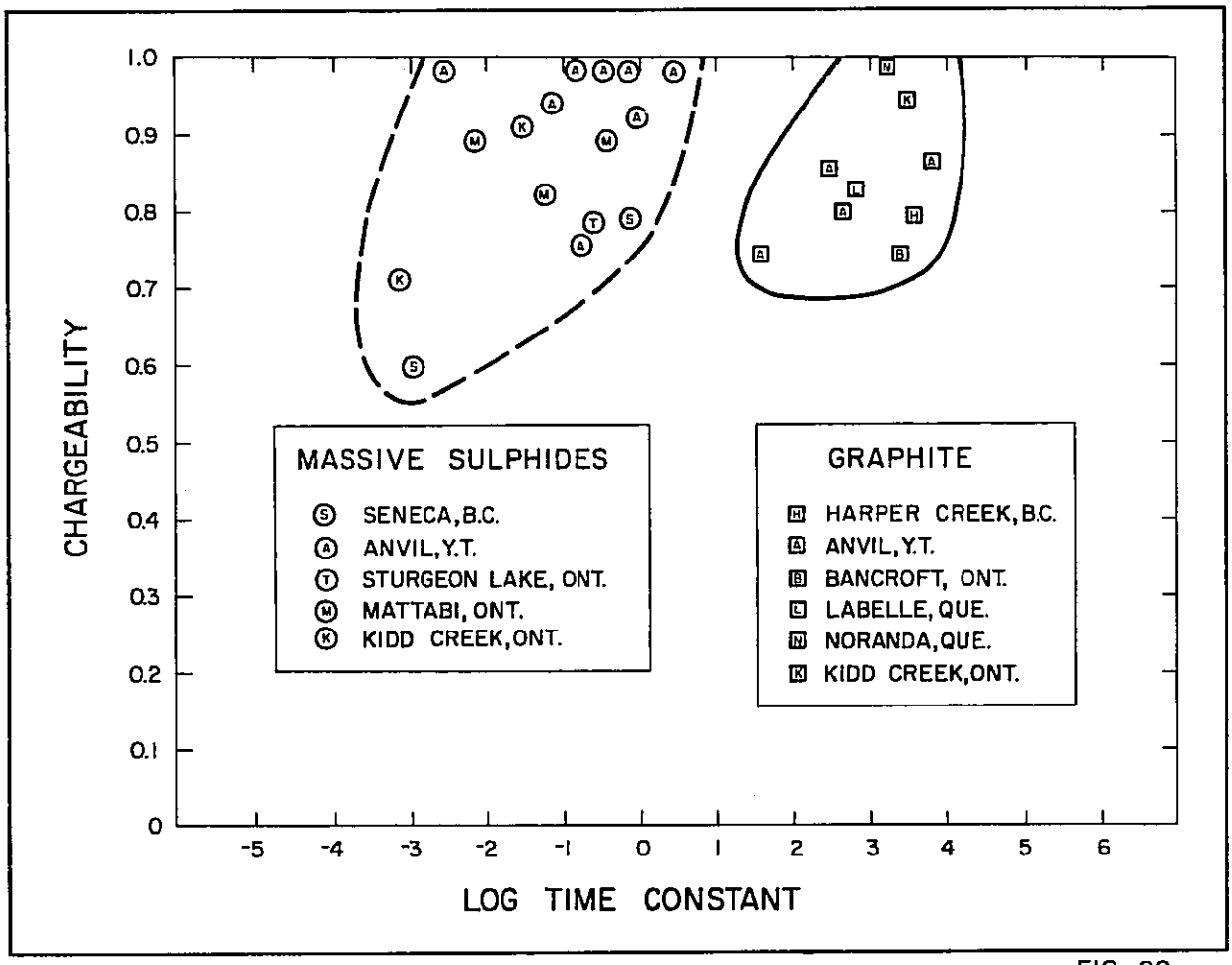

FIG. 39

b) The frequency range of spectral IP measurements with the IPV-3 System extends well up into the range that is normally used for electromagnetic prospecting. Indeed, as we have shown previously, the inductive coupling (EM) effects must be removed from the spectral IP plot before the electrical parameters of the source can be determined. In the near future, it should be possible to use this electromagnetic coupling information to gain further insight about the source.

The induced polarization and resistivity results in Figure 40 are from an area in South Australia. There is a known

pyrrhotite zone at Station 4 to Station 3, and a narrow Pb-Zn-Ag zone at about Station 0. The resistivity data shows a low over the conductive pyrrhotite zone. The raw phase data at 9.0 Hz and 0.11 Hz shows that IP effects are present, but the measurements (particularly at 9.0 Hz) are distorted by inductive coupling (EM) effects. When the inductive effects are removed, there is a definite IP anomaly from the pyrrhotite zone and a weak IP anomaly from the Pb-Zn-Ag zone. (see Figure 41).

The pseudo-sections shown in Figure 42 are a first attempt to use the inductive effects that have been removed from the dipole-dipole IP data. The M3 parameter is the electromagnetic component that has been removed from the measurement with each dipole pair.

The source centered at Station 4 to Station 3 gives a resistivity low, an IP high, and also a very large electromagnetic component. The source centered at Station 0 gives a weak, but definite IP anomaly. This source is not large enough to give a resistivity low using X = 25 meters. However, the electromagnetic coupling between the IP survey wires and the source is different from the resistive coupling between the electrodes and the source. There definitely is an electromagnetic component due to the Pb-Zn-Ag source.

c) With small desk-top computers, the calculation of a single forward IP problem can require five to ten hours. However, recent advances in small computers and new, interaction interfaces between CRT Displays and light-stylus hardware, will soon give the exploration geophysicist almost instantaneous interpretation capability.

For instance, the geometry shown on Figure 43 could be the first guess at the source of an IP anomaly. The geometry would be drawn upon the CRT Display by the geophysicist using an active light-stylus. At the push of a key, the computer would almost instantly display the pseudo-section shown. The computer would then print a "hard copy" of the field data, the calculated data and the geometry and parameters of the source.

The geophysicist could then use the light-stylus to alter the geometry to that shown in Figure 44. A push of the "operate" key would produce the pseudo-section shown in Figure 44. The pattern is only slightly different, but if it has greater similarity to the field data pattern, the geophysicist knows that he is on the right track.

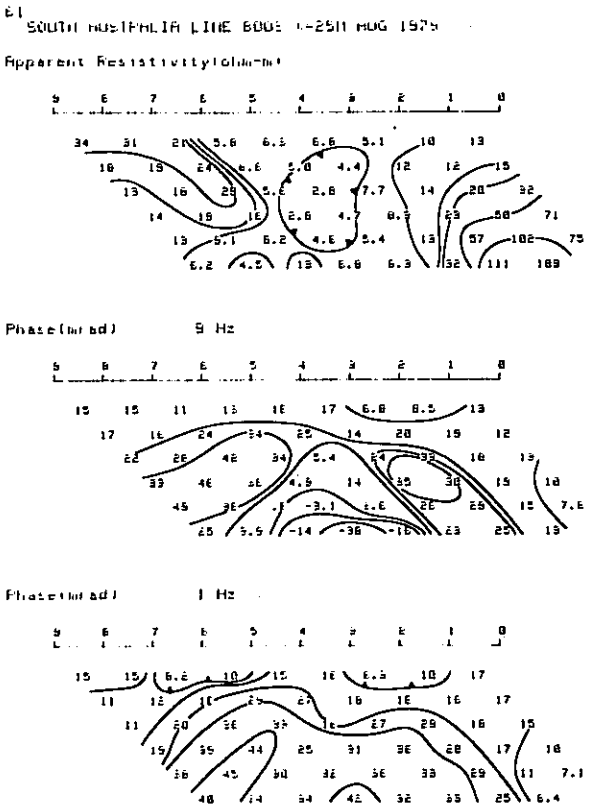

FIG. 40

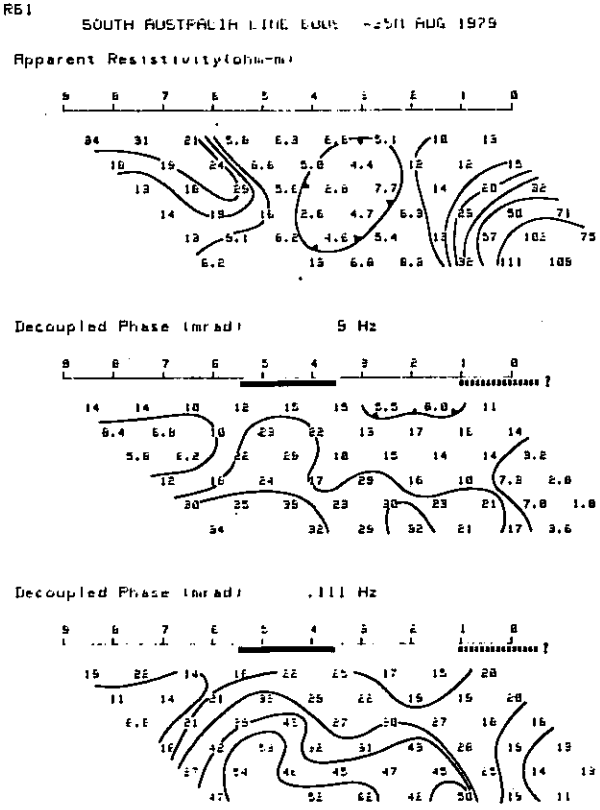

FIG. 41

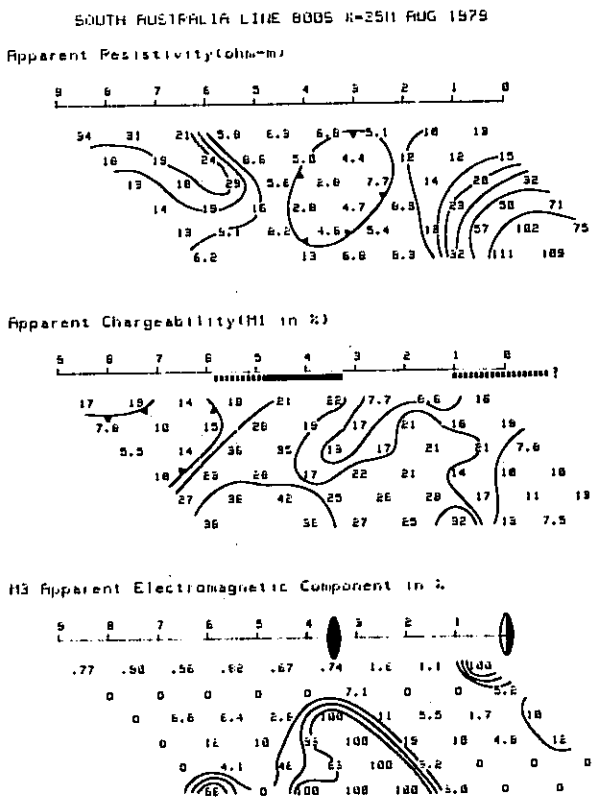

FIG. 42

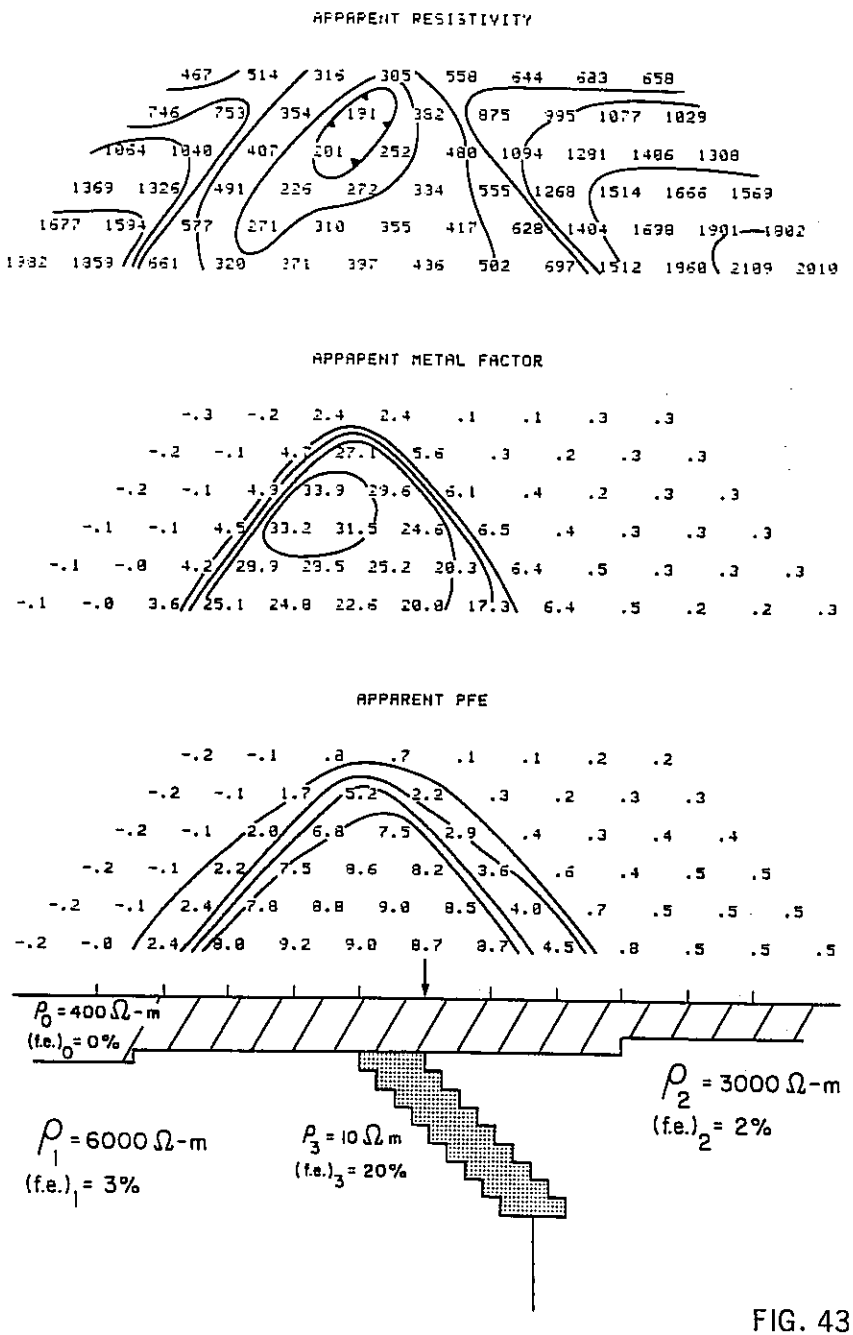
APPARENT RESISTIVITY
APPARENT METAL FACTOR
APPARENT PFE
ρ_0 = 400 Ω-m
(f.e.)$_0$ = 0%
ρ_1 = 6000 Ω-m
(f.e.)$_1$ = 3%
ρ_3 = 10 Ω m
(f.e.)$_3$ = 20%
ρ_2 = 3000 Ω-m
(f.e.)$_2$ = 2%

FIG. 43

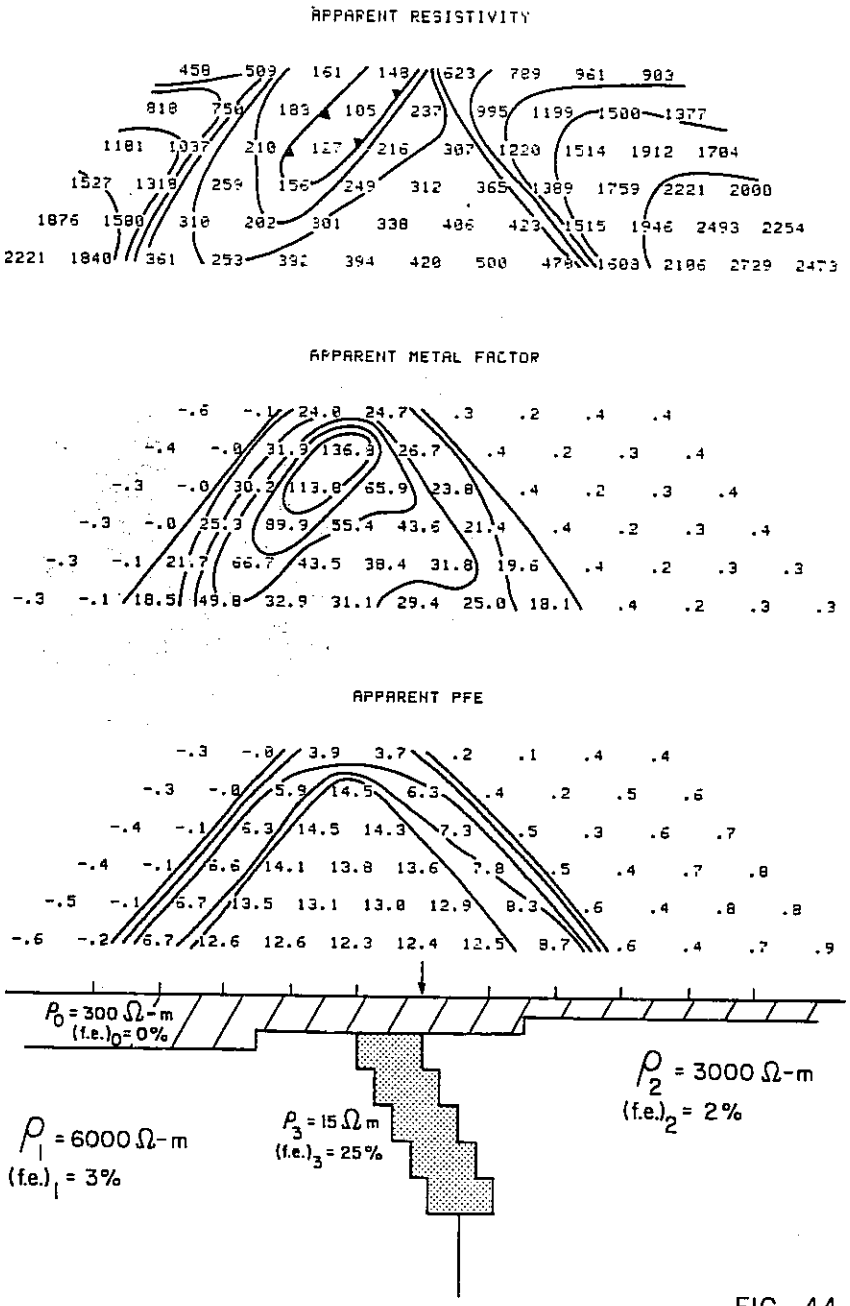
APPARENT RESISTIVITY
APPARENT METAL FACTOR
APPARENT PFE
ρ_0 = 300 Ω-m
(f.e.)$_0$ = 0%
ρ_1 = 6000 Ω-m
(f.e.)$_1$ = 3%
ρ_3 = 15 Ω m
(f.e.)$_3$ = 25%
ρ_2 = 3000 Ω-m
(f.e.)$_2$ = 2%

FIG. 44

Toronto Office: 200 Yorkland Blvd., Willowdale, Ont. M2J 1R5
Vancouver Office: 310 - 885 Dunsmuir St., British Columbia, V6C 1N5
Denver Office: 4690 Ironton St., Colorado, 80239, U.S.A.